TECHNISCHE UNIVERSITÄT WIEN
Vienna University of Technology

DIPLOMARBEIT

A COMPARATIVE STUDY OF STRATEGIES FOR VOLTAGE CONTROL IN MEDIUM VOLTAGE POWER DISTRIBUTION NETWORKS WITH DISTRIBUTED GENERATION

betreut von

PROF. DR. HERBERT STÖRI

INSTITUT FÜR ANGEWANDTE PHYSIK
TECHNISCHE UNIVERSITÄT WIEN

DIPL. ING. MATTHIAS STIFTER

ENERGY DEPARTMENT
AIT AUSTRIAN INSTITUTE OF TECHNOLOGY

von

ROMAN SCHWALBE

Senfgasse 1/8/6
1100 Wien

Wien, März 2013

Abstract

To increase the share of renewable energy sources in electricity production renewable energy generation is nowadays integrated decentralised into existing distribution grids. Especially in rural distribution grids a high share of generation can lead to an unacceptable voltage rise at the generation's feeding branch and limit the amount of generation hosting capacity. Therefore the central transformer's tap-change capability and the capability of distributed generation to contribute reactive power are used for voltage control in distribution grids. Existing voltage control concepts operate in a local scope, which means that the transformer's tap position and the generation's reactive power is controlled independently based on local measurement data. While the distributed generation hosting capacity of distribution grids is limited with local voltage control, coordinated voltage control concepts enable a maximum of generation connected to distribution systems by optimally utilising the existing infrastructure. Coordinated voltage control concepts that are centrally operated and depend on actual grid measurement data are able to improve the grid's power flow and reduce grid losses beside their primary task of voltage control.

In this work the effects that lead to voltage rise in distribution systems with distributed generation as well as the technical capabilities to influence grid voltage are described and analytically investigated. The 'contribution matrix' approach for the quantitative characterisation of voltage sensitivities of grid nodes is derived and analytically and numerically analysed. Based on the contribution matrix approach a natural control objective that minimises voltage violations from nominal voltage is derived and discussed. With the help of the insights gained during the investigation of this control strategy, the control strategy that was developed during the project 'DG DemoNet Validation' is derived and analysed. Four further coordinated voltage control strategies are proposed that follow different control objectives in addition to voltage control.

Together with six local voltage control strategies the proposed coordinated control strategies were simulated in two Austrian medium voltage distribution grids based on one-year load-profiles. These grids were simulated in the actual construction state and in a probable growth scenario with additional generation integrated. This makes an evaluation of the necessity and the technical capabilities and limitations of different voltage control concepts possible. The simulation results of the local and coordinated voltage control concepts are analysed and their influence to grid voltages, grid losses and the number of tap-changes are compared.

The simulation results show that coordinated voltage control concepts are able to maintain voltage quality in both grids in their actual constitution and in the probable growth scenario during the whole year. This could not be achieved with local voltage control concepts except running all DGs at a constant power-factor, which significantly increases grid losses. In general, grid losses of coordinated voltage control concepts that utilise the whole available voltage band are smaller than grid losses of local control concepts. With coordinated voltage control concepts it is possible to significantly reduce the number of necessary tap-changes. In some cases it is even possible to reduce grid losses compared to the uncontrolled reference scenario. Especially for the growth scenario of both grids, coordinated voltage control concepts seem to be very reasonable to maintain voltage quality.

Kurzfassung

Um den Anteil erneuerbarer Energieträger in der Elektrizitätserzeugung zu erhöhen werden heutzutage Erzeugungsanlagen dezentral in existierende Verteilnetze integriert. Speziell in ländlichen Verteilnetzen kann eine starke Rückspeisung zu einer unzulässigen Spannungsanhebung in Netzabschnitten mit hoher Erzeugung führen. Um dies zu vermeiden kann der Stufensteller des zentralen Transformators und die Blindleistung der einspeisenden Generatoren zur Spannungsregelung verwendet werden. Existierende Spannungsregelungen arbeiten unabhängig voneinander in einem lokalen Kontext, was bedeutet, dass sowohl die Position des Transformator-Stufenstellers als auch die Blindleistung der Kraftwerke nur anhand von lokalen Messwerten geregelt wird. Während die Aufnahmefähigkeit des Netzes für dezentrale Erzeuger mit solchen lokalen Spannungsregelungskonzepten begrenzt ist, können koordinierte Spannungsregelungskonzepte ein Maximum an verteilten Erzeugern im Netz ermöglichen, sodass die existierende Infrastruktur bestmöglich genutzt werden kann. Koordinierte Spannungsregelungen, die zentral betrieben werden und auf aktuellen Messwerten aus dem Netz basieren, können zusätzlich zu Ihrer primären Funktion der Spannungsregelung den Leistungsfluss im Netz optimieren und die Netzverluste reduzieren.

In dieser Arbeit wurden Effekte untersucht, welche zu Spannungsanhebungen durch dezentrale Erzeuger in Verteilnetzen führen, und die technischen Möglichkeiten zur Beeinflussung der Spannungen im Netz analysiert. Als Basis für koordinierte Spannungsregelungen wurde der Ansatz der "Beitragsmatrix" zur quantitativen Charakterisierung der Spannungssensitivitäten von Netzknoten hergeleitet und analytisch und numerisch untersucht. Damit wurde ein natürliches Regelungsziel hergeleitet und diskutiert, welches alle Netzspannungen so gut wie möglich auf Nennspannung hält. Die daraus resultierenden Erkenntnisse wurden verwendet um die Regelungsstrategie, die im Projekt "DG DemoNetz Validierung" entwickelt wurde, herzuleiten und zu analysieren. Anschließend wurden vier weitere koordinierte Spannungsregelungskonzepte vorgestellt, welche neben dem Primärziel der Spannungshaltung unterschiedliche Regelungsziele verfolgen.

Zusammen mit sechs lokalen Spannungsregelungskonzepten wurden die vorgestellten koordinierten Regelungskonzepte in zwei österreichischen Mittelspannungs-Verteilnetzen auf Basis von Jahres-Lastprofilen simuliert. Diese Netze wurden in ihrem aktuellen Zustand und in einem wahrscheinlichen Ausbauzustand mit zusätzlichen dezentralen Erzeugern simuliert, was eine Bewertung der Notwendigkeit und der technischen Möglichkeiten der verschiedenen Spannungsregelungen ermöglicht. Die Simulationsergebnisse der lokalen und koordinierten Regelungsstrategien wurden anhand ihrer Auswirkungen auf Netzspannungen, Netzverluste und der Anzahl der notwendigen Stufenstellungen verglichen.

Die Simulationsergebnisse zeigen, dass die koordinierten Spannungsregelungskonzepte die Spannungsqualität in beiden Netzen sowohl im aktuellen als auch im ausgebauten Zustand das ganze Jahr über sicherstellen können. Das kann mit lokalen Spannungsregelungskonzepten nicht immer erreicht werden, außer durch den Betrieb aller Kraftwerke mit konstantem Leistungsfaktor, was die Netzverluste signifikant erhöht. Generell sind die Netzverluste von koordinierten Regelungskonzepten niedriger als die Netzverluste von lokalen Regelungskonzepten. Mit koordinierten Konzepten kann die Anzahl erforderlicher Stufenstellungen signifikant reduziert werden und in manchen Fällen können die Netzverluste sogar niedriger als im unkontrollierten Referenzszenario gehalten werden. Speziell in den Ausbauzuständen beider Netze erscheinen koordinierte Spannungsregelungskonzepte zur Sicherstellung der Spannungsqualität sinnvoll.

Acknowledgement

I want to thank my advisor Dr. Herbert Störi for guiding me through the whole project. He was widening my view on the subject and was always available whenever I needed him.

Special thanks go to Matthias Stifter who advised me during the whole work and willingly managed proofreading in a short time period. So it is for my colleagues Benoît Bletterie and Helfried Brunner for their support and input.

This work would have been hardly realisable without the possibility to occupy multiple PowerFactory-licences in parallel for executing the simulations on the department's simulation-server. In addition I have to salute all my colleagues who accepted my working on this system claiming also their technical resources at that time.

Furthermore I want to honour the colleagues in my team and the external colleagues at *Salzburg Netz GmbH* and *Vorarlberger Energienetze GmbH* for the elaboration of the grid models I used in the simulations.

Finally I want to point out the insightfully acceptance by my fiancée Barbara that this work was in my focus for so many days, evenings and weekends.

Contents

Nomenclature

AVC	Automated Voltage Controller
CM	Contribution Matrix
CN	Critical Node
DG	Distributed Generation
DS	Distribution System
DSO	Distribution System Operator
HV	High Voltage
LL	Lower Limit
MV	Medium Voltage
OLTC	On-Load-Tap-Changer
OPF	Optimal Power Flow
pu	Per Unit
SS	SubStation
TF	Transformer
UL	Upper Limit

Chapter 1

Introduction

1.1 Historical Evolution of Distribution Grids

The original structure of the electric power system assigned decided tasks to the different voltage levels: The function of the high voltage network (transmission system) was to provide a large-scale meshed power system where few big plants supply their power while at the same time controlling the stability of the whole grid. The medium voltage network (distribution system) is a radial network with the aim to distribute the power generated in the high voltage network to the local area low voltage distribution grids or to the industrial customers who need a high connected rating. Since no generation was integrated into the distribution system (DS), the voltage profile was strictly monotonic decreasing radially from the central medium voltage (MV) transformer, which made power system planning and operation easy.

The need of a more sustainable electric energy production leads to a raising demand on renewable generation to be connected to the electric power system. While conventional electric generation supplies power from typically 10MW to 1GW (coal, gas, water, nuclear, ...) to the high voltage network, renewable electric generation emerges decentralised and supplies typically 100kW to 10MW (water, wind, solar, biomass, ...), which makes the integration into existing distribution grids technically and economically reasonable.

Integrating distributed generation (DG) into existing distribution networks can reduce grid losses, because energy demand is covered locally. But in cases of high production and low consumption it can also lead to an unacceptable voltage rise especially in rural DS since the voltage at the feeding branch can rise higher than the central transformer (TF) busbar voltage, which was impossible without DG. [1]

1.2 Scope of Work

Voltage control in distribution systems enables a high share of renewables integrated in existing distribution networks while it avoids (uneconomic) grid reinforcement. [2, 3]

While in the past voltage control was simply achieved by local voltage control of the MV transformer busbar voltage utilising the transformers on-load-tap-changer (OLTC), this approach is not sufficient in presence of DG. Different voltage control approaches exist with different amount of information of the grid necessary. Voltage control approaches which are based on voltage measurements at the grid nodes seem convenient for an effective and precise controlling, but they require communication infrastructure, which is actually not available in most DS and therefore has to be retrofitted.

This work examines voltage control strategies which depend on network node voltage measurements and use the capability of the DG to contribute to voltage control by providing reactive power. Therefore a control strategy arising naturally from the aim to keep all grid voltage as near as possible at nominal voltage is proposed. This control strategy will be compared with the control strategy developed in the DG DemoNet project, which utilises the whole available voltage band instead of trying to bring all grid node voltages to nominal value [4]. The reference criteria for comparison are the amount of needed

transformer tap-changes, the amount of needed DG reactive power and the DS losses as well as the robustness of the control strategy.

Based on the control objective to use as little reactive power from the DGs as possible, which is applied in the DG DemoNet project, further reactive power objectives with the aim of loss minimisation are proposed in this work and compared with the other control strategies.

The control strategies are validated by simulations based on network models of two Austrian distribution grids and historical and synthetic one-year-load-profiles of these grids. The simulations are carried out with the power system analysis and engineering tool DIgSILENT PowerFactory. The two distribution grids are the substation (SS) 'Lungau' in Salzburg and SS 'Nenzing' in Vorarlberg, where the field tests of the DG DemoNet Validation project were carried out in 2012.

Based on the simulation results the different voltage control concepts are evaluated concerning their impact on the grid and their effectiveness, and the ability of the DGs to reduce grid losses is stated.

1.3 Electrical Principles

1.3.1 Per Unit System

When investigating in MV grids, voltages appear in several ten thousand volts, but generally nominal MV grid voltages are not standardised to one fixed value. With a per unit transformation the grid voltages are expressed as fractions of the nominal grid voltage, so $u = \frac{U}{U_{Nominal}}$ (per unit variables are written in lower case with the unit [pu] , base unit variables are written in upper case). This has the advantage, that voltage states of different grids can be compared and analysed regardless of their nominal voltage level.

Powers, impedances and currents can also be transformed into a per unit system to be able to express quantities regardless their absolute size, but in the scope of this work only voltages were noted in pu.

1.3.2 Voltage Control Elements

This chapter describes the two techniques for influencing voltages in an electric supply network, which are utilised by the control strategies stated in this work. A more exhaustive list of voltage controlling elements in electric power systems can be found in [5, chap. 10].

1.3.2.1 Transformer

Within a SS transformer (TF), the voltage level from the high voltage (HV) side (primary side, e.g. 110kV) is transformed to the voltage level at the medium voltage (MV) side (secondary side, e.g. 27.5kV) depending on the transformers turn ratio (ratio between the number of primary windings to the number of secondary windings $\frac{N_{HV}}{N_{MV}}$, e.g. 4). However, in medium voltage transformers, this turn ratio can be varied because multiple tappings of the primary coil are lead through the transformer tank, so that the on-load-tap-changer (OLTC) can alter the number of primary windings without service interruption. The OLTC is placed at the HV side due to the fact that the switching currents are smaller than on the MV side. The number of available tap positions and the nominal step height of the voltage when performing a tap-change depends on the demand of the DS and can be individually designed. Typical are around thirty tap steps with a nominal voltage step height Δu_{Tap} of around $0,01$ to $0,015$pu. [6, chap. 6.2] [7, chap. 8.4]

Calculation of the variable tap-change voltage step height Because voltage level on the HV side U_{HV} can be considered as constant when performing a tap-change, the voltage step height on the MV side U_{MV} depends linear on the voltage level on the HV side and non-linear on the tap position: Bringing $U_{MV} = U_{HV}\frac{N_{MV}}{N_{HV}} = U_{HV}\frac{N_{MV}}{N_{HV}^{nominal}+k\Delta N_{tap}}$ with the actual tap position k and the change of the nominal number of windings ΔN_{tap} to a per unit base by dividing through $U_{MV}^{nominal} = U_{HV}^{nominal}\frac{N_{MV}}{N_{HV}^{nominal}}$ leads to $\frac{U_{MV}}{U_{MV}^{nominal}} = u_{MV} = \frac{U_{HV}}{U_{HV}^{nominal}}\frac{N_{MV}}{N_{HV}^{nominal}+k\Delta N_{Tap}}\frac{N_{HV}^{nominal}}{N_{MV}} = u_{HV}\frac{1}{1+k\cdot\Delta N_{Tap}/N_{HV}^{nominal}}$. The nominal tap-change voltage step height is

Symbol	Unit	Description
N_{HV}	-	number of actual primary coil windings on HV side depending on the tap position of the OLTC
$N_{HV}^{nominal}$	-	number of nominal primary coil windings on HV side at the default tap position of the OLTC
N_{MV}	-	number of secondary coil windings on medium voltage side
Δu_{tap}	pu	tap-change voltage step height
$\Delta u_{tap}^{nominal}$	pu	nominal tap-change voltage step height at default tap position (used as an important TF characteristic)
U_{HV}/u_{HV}	kV / pu	primary transformer voltage on high voltage
U_{MV} / u_{MV}	kV / pu	secondary transformer voltage on medium voltage side
k	-	tap position of the OLTC, default is $k = 0$
ΔN_{tap}	-	number of windings N_{HV} increases / decreases when performing a tap-change

Table 1.1: Symbol reference for the calculation of the MV tap-change step height

defined as the voltage change resulting at the HV side Δu_{HV} when increasing the tap position from the neutral tap position $k = 0$ to $k = 1$ by a constant and nominal MV voltage $u_{MV} = 1$pu, so it can be written as $\Delta u_{tap}^{nominal} := u_{HV}^{k=1} - u_{HV}^{k=0}\big|_{u_{MV}=1}$. With $u_{HV} = u_{MV}(1 + k\frac{\Delta N_{tap}}{N_{HV}^{nominal}})$ the nominal tap-change voltage step height becomes $\Delta u_{tap}^{nominal} = u_{MV}\frac{\Delta N_{tap}}{N_{HV}^{nominal}}\Big|_{u_{MV}=1} = \frac{\Delta N_{tap}}{N_{HV}^{nominal}}$ and therefore the dependency of the MV voltage of the HV voltage and the actual tap position is given as

$$u_{MV} = u_{HV}\frac{1}{1 + k\Delta u_{tap}^{nominal}} \tag{1.1}$$

Equation 1.1 is only valid in no-load operation, because a current flow over the transformer produces voltage drop on the MV side due to the transformer series resistance and the series inductance. Considering the voltage dependency of the loads as insignificant when performing a voltage change in the order of 0.01pu, this voltage drop will remain constant before and after the tap-change. Within this model the MV voltage tap-change step height of the transformer depending on the HV side and the actual tap position can be estimated as

$$\Delta u_{tap} \simeq u_{HV}\left(\frac{1}{1 + (k+1)\Delta u_{tap}^{nominal}} - \frac{1}{1 + k\Delta u_{tap}^{nominal}}\right) \tag{1.2}$$

This leads to the fact that the voltage change at the MV side resulting from a tap-change by a constantly assumed HV side depends on the actual tap position due to the fact that the OLTC is placed at the HV side and the number of windings changed at a tap-change is constant.

1.3.2.2 Synchronous Generators

In principle the three terminal voltages U_a, U_b and U_c of a synchronous generator resulting at the three stator coils a, b, c of the synchronous generator are induced by the excitation DC current I_e in the rotor coil e, see fig. 1.1. Considering the 120° phase difference of the terminal voltages due to the symmetrical arrangement of the stator coils around the rotor, the three terminal voltages can be summarised to the terminal voltage phasor[1] $\underline{U_K}$. In this way, voltages and currents of the three phase generator can be described by a single phase generator with voltage and current phasors, see fig. 1.2 a).

In engine idling, no current flows in the stator coils, so the terminal voltage phasor at the stator coils $\underline{U_K}$ is equal to the synchronous generated voltage $\underline{U_E}$. A constant mechanical moment on the rotor in rotating direction causes the synchronous generated voltage $\underline{U_E}$ to lead to the terminal voltage phasor $\underline{U_K}$ (the grid voltage), which leads to a current $\underline{I}$ through the stator coils. The angle between $\underline{U_E}$ and $\underline{U_K}$ is called the polar wheel angle θ, which is $\theta > 0$ in generator operation and $\theta < 0$ in motor operation. In

[1] A phasor, or phase vector, represents a harmonic oscillation with constant amplitude and frequency and variable phase angle, often represented as a complex number or vector in two dimensions. It is represented underlined.

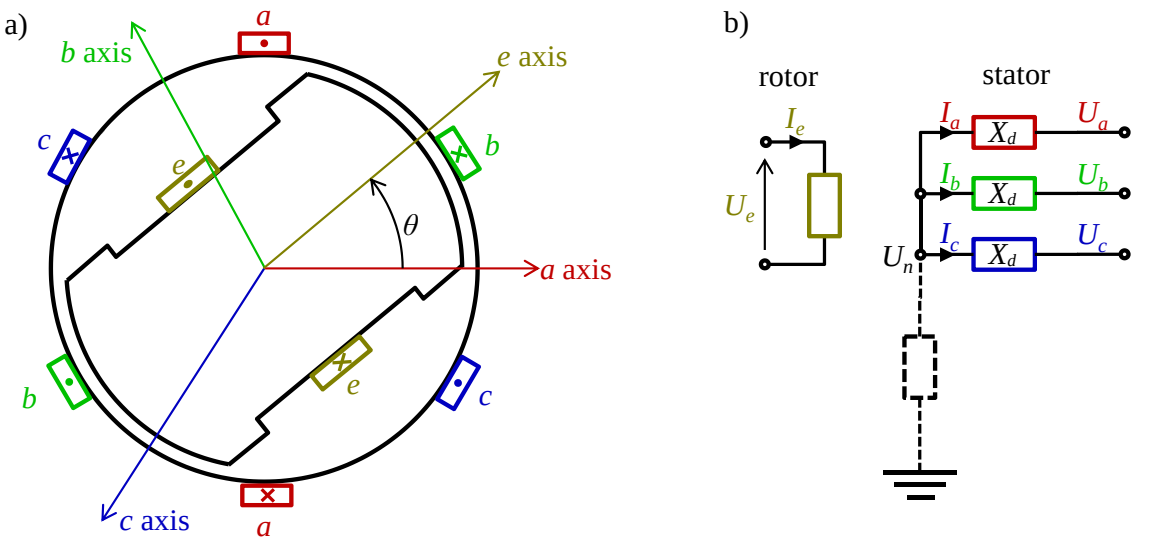

Figure 1.1: Schematic representation of a bipolar synchronous machine with three “phase” stator circuits (indices a, b, c) and one “excitation” rotor circuit (index e). [8, chap. 4]

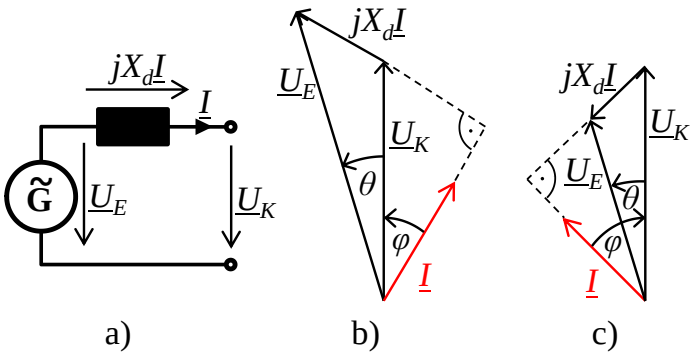

Figure 1.2: a) Simplified equivalent circuit diagram of a synchronous generator, b) vector diagram for resistive-inductive load (inductive operation), c) vector diagram for resistive-capacitive load (capacitive operation) [5]

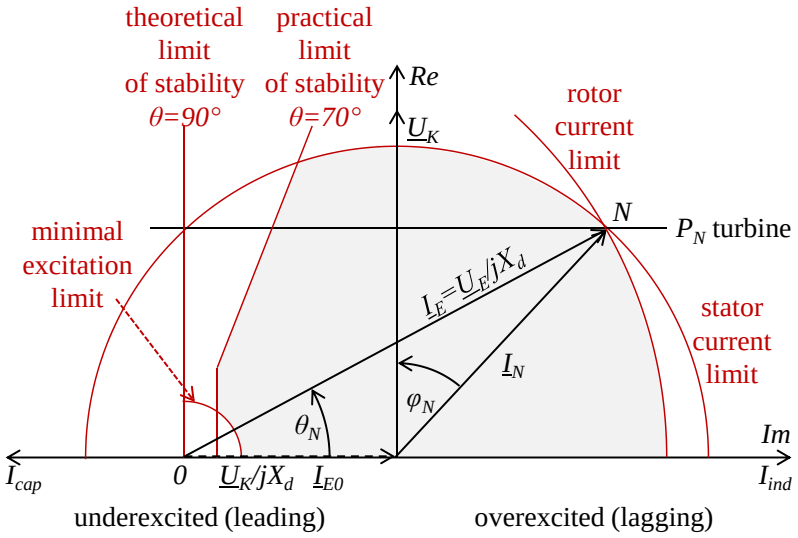

Figure 1.3: Operation diagram of a synchronous generator [5]

theory, the maximum mechanical power can be converted into electrical power at $\theta = 90°$, but $\theta > 90°$ leads to operation instability, so in practice generator operation will be in a range $0 < \theta < 70°$.

By controlling the amount of excitation current I_e in the rotor coil, the amplitude of $\underline{U_E}$ can be adjusted, which can be used to control the phase angle φ between $\underline{U_K}$ and the stator current $\underline{I}$. The stator current $\underline{I}$ is limited by the thermal limit of the stator coils.

Operating the synchronous generator overexcited (lagging) means to run a higher current through the rotor coil, leading to $\varphi > 0$ or to an inductive behaviour[2], see fig. 1.2 b). This operation mode is limited by the thermal limit of the rotor coil, leading to a rotor current limit.

Operating the synchronous generator under-excited (leading) means to run a lower current through the rotor coil, leading to $\varphi < 0$ or to a capacitive behaviour, see fig. 1.2 c). This operation mode is limited by the minimal excitation current for stable operation, which is around ten percent of the maximum rotor current.

Synchronous generators can operate in pure phase shift operation mode, which means that only reactive power and no active power is produced, $\varphi \simeq \pm 90°$.

Considering these facts, the operation diagram (P/Q diagram) of the generator can be defined as shown in fig. 1.3, where the stable operation is marked by the highlighted area within the limits. [5, chap. 8]

The influence of the reactive power of generators to the grid voltages is described in chapter 1.3.3.

1.3.3 Voltage Calculations in MV Grids

In this chapter the contribution of reactive power produced at a grid feeding point to the voltages in the grid will be analysed and different kinds of calculation models will be introduced.

1.3.3.1 Simplification of the Grid Model

A schematic model of a radial distribution grid is shown in fig. 1.4.

As the scope of the work is the analysis of MV control strategies, the influence of the HV grid to the MV grid will be omitted. Therefore the voltage reference point for the calculations (also called the slack) is set to the HV side of the transformer. In practice DS can be considered as symmetric because the phase load variability is balanced by the high amount of loads connected to the grid. This leads to the model

[2]This is the generators perspective, in grid perspective, the generator has capacitive behaviour, because it produces the reactive power the connected load consumes (an inductance has $Q > 0$, so it consumes reactive power). The change from generator's perspective to grid perspective can be done by inverting the sign of active and reactive power.

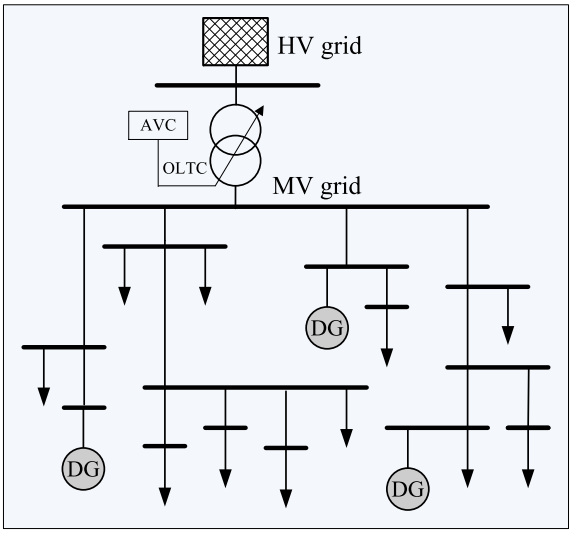

Figure 1.4: Schematic model of a radial distribution grid

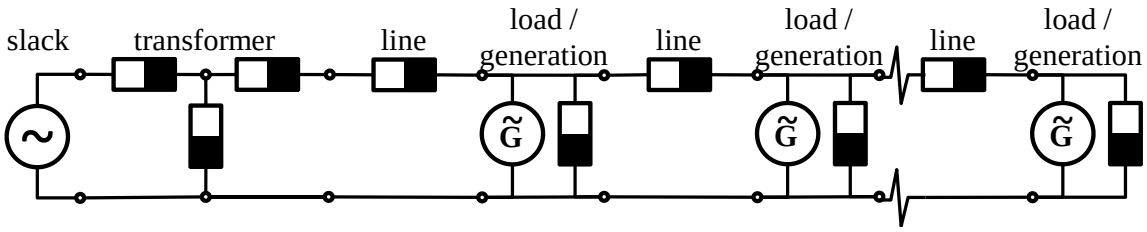

Figure 1.5: Simplified model of a distribution grid branch

displayed in fig. 1.5 of the grid where only one transformer branch is shown and other intra-branches are summarised by the loads and generators in between the line.

From this perspective it can be easily seen that the voltage level will strictly monotonic decrease if there is no generation in the grid, and in the opposite situation - no load and only generation - the voltage level will strictly monotonic rise in the grid seen from the transformers perspective. Situations where there will be a local maximum due to high generation or a local minimum due to high load are the general case[3].

1.3.3.2 The feeding Generator at the non-ideal Voltage Source

To take a look at the voltage control impact of reactive power produced by DG the model will be further simplified by neglecting the transformer's parallel impedance and all loads and all other generations, leading to a single generator connected to an ideal voltage source over a series impedance (which is the sum of the line impedance and the transformer's series impedance), see fig. 1.6

[3]From this point of view it is clear that only knowing the voltage at the end of the branch is not sufficient for voltage control.

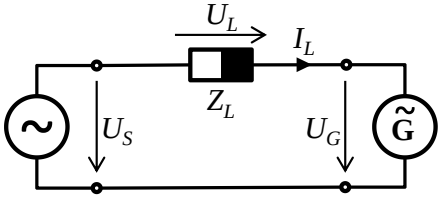

Figure 1.6: Schematic model of a feeding DG into the grid

Modelling the generator as an impedance $\underline{Z_G}$ with $Re\{\underline{Z_G}\} < 0$, which feeds the active power $P_G < 0$ into the grid[4] at nominal voltage is easy to calculate, but leads to a wrong behaviour of the DG, because $P_G(U_G) = \frac{U_G^2}{Z_G}$. The voltage controller of the synchronous generator will control the excitation current so that the whole mechanical rotor moment can be converted into active power. This leads to the fact that DGs have to be modelled as non-linear constant-power elements, making the voltage calculation more sophisticated:

When the slack voltage $\underline{U_S} = U_S^{re} = U_S \angle 0° = U_S$, the complex line series impedance $\underline{Z_L} = R_L + jX_L$ and the complex apparent power of the generator $\underline{S_G} = P_G + jQ_G$ are given, the current $\underline{I} = I^{re} + jI^{im}$, the complex generator voltage $\underline{U_G} = U_G^{re} + jU_G^{im}$, the line drop voltage $\underline{U_L} = U_L^{re} + jU_L^{im}$, the line losses $\underline{S_L} = P_L^{loss} + jQ_L$ and the apparent power provided by the slack $\underline{S_S} = P_S + jQ_S$ can be calculated: By utilising the power conservation in the grid with $P_S = P_L^{loss} + P_G$ and $Q_S = Q_L + Q_G$, the squared apparent power at the slack becomes $S_S^2 = (U_S I)^2 = P_S^2 + Q_S^2 = \left(P_L^{loss} + P_G\right)^2 + (Q_L + Q_G)^2 = \left(I^2 R_L + P_G\right)^2 + \left(I^2 X_L + Q_G\right)^2$. This defines a quadratic equation for the square of the magnitude of the current running through the system $I^4 Z_L^2 + I^2\left(P_G R_L + Q_G X_L - U_S^2\right) + S_G^2 = 0$, where only the solution with the negative root sign makes sense:

$$I^2 = \frac{U_S^2/2 - P_G R_L - Q_G X_L}{Z_L^2}\left(1 - \sqrt{1 - \frac{Z_L^2 S_G^2}{\left(U_S^2/2 - P_G R_L - Q_G X_L\right)^2}}\right) \tag{1.3}$$

Now the magnitude of the current the real and the imaginary part can be calculated from the complex power conservation equations: Solving $\underline{S_S} = \underline{U_S} \cdot \underline{I_S^*} = U_S I^{re} - jU_S I^{im} = P_S + jQ_S = P_L^{loss} + P_G + j(Q_L + Q_G)$ for the real and the imaginary part[5] leads to $I^{re} = \frac{I^2 R_L + P_G}{U_S}$ and $I^{im} = -\frac{I^2 X_L + Q_G}{U_S}$. Now the line voltage drop and the voltage at the generator can be calculated straight forward: $\underline{U_L} = \underline{Z_L} \cdot \underline{I}$, and $\underline{U_G} = \underline{U_S} - \underline{U_L} = \frac{S_G \cdot I}{I^2}$, and the magnitude of the generator voltage becomes $U_G = \frac{S_G}{I}$. Substituting the root of eq. (1.3) for I and $\sqrt{P_G^2 + Q_G^2}$ for S_G leads to the power sensitivities of the generator voltage $\frac{\delta U_G}{\delta Q_G}$ and $\frac{\delta U_G}{\delta P_G}$. The analytical terms describing these derivations are hardly readable and don't lead to new insights compared to the approximated terms, which describe the accurate terms very well in a wide range: Because of the fact that in practice the line impedance is small compared to the generator impedance, the second term in the root of eq. 1.3 is small compared to one, so with $\frac{Z_L^2 S_G^2}{\left(U_S^2/2 - P_G R_L - Q_G X_L\right)^2} \ll 1$ the root can be approximated by $\sqrt{1 - \frac{Z_L^2 S_G^2}{\left(U_S^2/2 - P_G R_L - Q_G X_L\right)^2}} \approx 1 - \frac{1}{2}\frac{Z_L^2 S_G^2}{\left(U_S^2/2 - P_G R_L - Q_G X_L\right)^2}$ which leads to the approximated current:

$$I \approx \sqrt{\frac{S_G^2}{U_S^2 - 2(P_G R_L + Q_G X_L)}} = \frac{S_G}{U_S}\frac{1}{\sqrt{1 - 2(P_G R_L + Q_G X_L)/U_S^2}}$$

This simplifies the calculation of the generator voltage magnitude, leading to $U_G = \frac{S_G}{I} = U_S\sqrt{1 - \frac{2(P_G R_L + Q_G X_L)}{U_S^2}}$. Because of $\frac{2(P_G R_L + Q_G X_L)}{U_S} \ll 1$ (same reason as mentioned above), the root can be approximated again by $\sqrt{1 - \frac{2(P_G R_L + Q_G X_L)}{U_S^2}} \approx 1 - \frac{P_G R_L + Q_G X_L}{U_S^2}$ so that the voltage magnitude at the generator becomes

$$U_G \approx U_S - \frac{P_G R_L + Q_G X_L}{U_S} \tag{1.4}$$

leading to the approximated voltage sensitivities $\frac{\delta U_G}{\delta Q_G} \approx -\frac{X_L}{U_S}$ and $\frac{\delta U_G}{\delta P_G} \approx -\frac{R_L}{U_S}$.

[4] It is more practical to analyse this situation in the "grid perspective", which means that load has positive active power and generation has negative active power.

[5] At this point it is necessary to have the phase angle of the slack voltage defined - in this case the slack voltage is pure real.

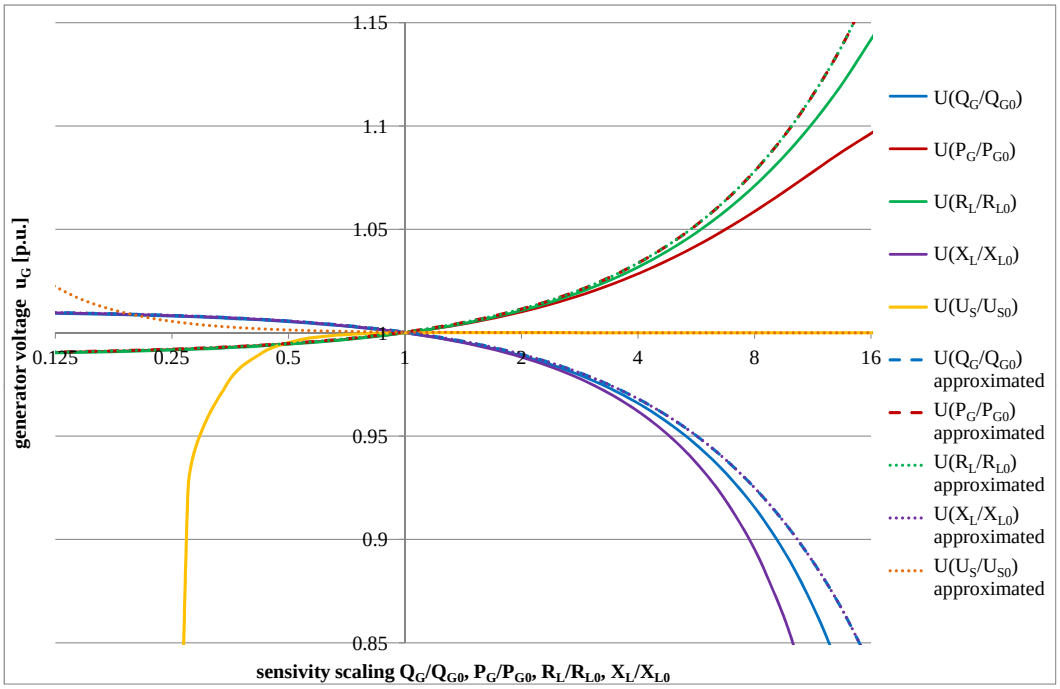

Figure 1.7: Generator voltage magnitude sensitivity analysis with typical reference values $U_{nominal} =$ 30kV, $U_{S0} = 1$pu, $R_{L0} = 10\Omega$, $X_{L0} = 20\Omega$, $P_{G0} = -2$MV and $Q_{G0} = 0.969$MVAr

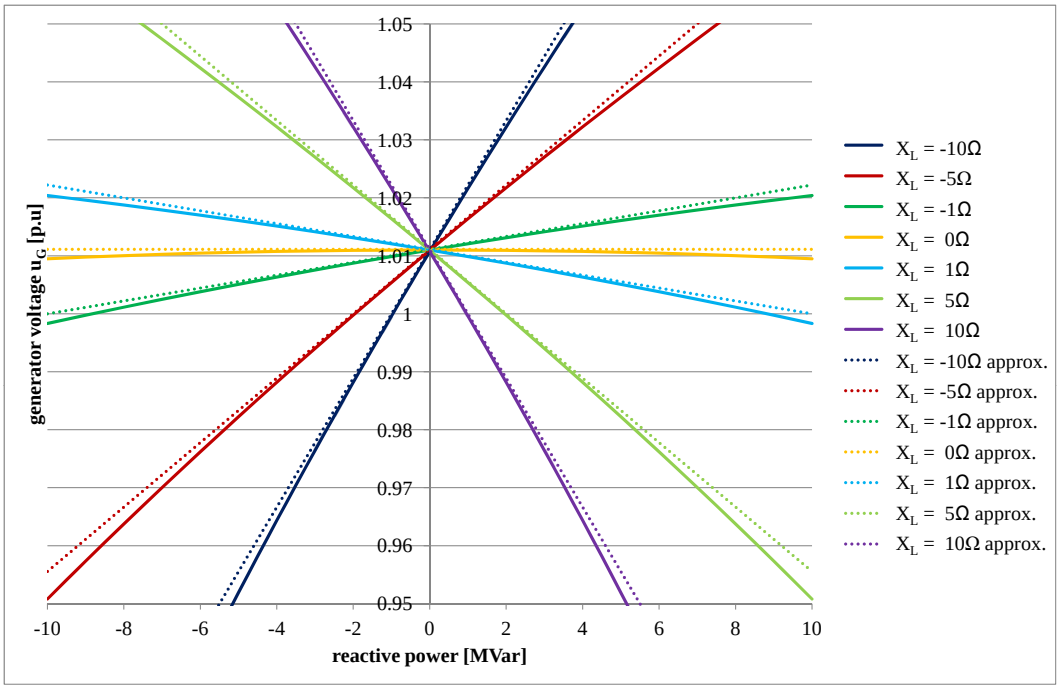

Figure 1.8: Dependency of generator voltage magnitude on generator's reactive power at typical reference values $U_{nominal} = 30\text{kV}$, $U_{S0} = 1\text{pu}$, $R_{L0} = 10\Omega$, $X_{L0} = 20\Omega$ and $P_{G0} = -2\text{MV}$

Verification of the approximations In fig. 1.7 a voltage sensitivity analysis is shown with typical reference values $U_{nominal} = 30\text{kV}$, $u_S = 1\text{pu}$, $R_L = 10\Omega$, $X_L = 20\Omega$, $P_G = -2\text{MV}$ where the generator's reactive power was set to $Q_G = 0.969\text{MVAr}$ leading to a reference generator voltage $u_G = 1\text{pu}$ which means that the voltage rise because of the generator feeding active power was balanced by the generator's reactive power. As seen in fig. 1.7, the two approximations made don't reduce the accuracy of the approximated results, because deviations from the exact values are not significant until the relative values are far away from one.

The side effect of the additional reactive power leading to $U_G = 1\text{pu}$ is that the voltage angle θ rises compared to $Q_G = 0$.

To take a closer look at the voltage sensitivity on reactive power, fig. 1.8 shows the voltage dependency of the generator's reactive power in an interval from -10MVAr to +10MVAr. Again, the deviation between the exactly calculated voltage and the approximated voltage is very small in a range between -2MVAr to +2MVAr, which is the interesting interval for voltage control in distribution grids.

1.3.3.3 Power Flow Calculation

As discussed in chapter 1.3.3.2, the analytical calculation of current and voltage in a simple grid consisting of a generator connected to a non-ideal voltage source (or in case of generation voltage drain) is surprisingly complex when modelling the generator as a non-linear constant P/Q element instead of a constant impedance element. Calculating more complex topologies with this approach becomes very inefficient or even impossible as the number of lines and nodes grows. Nevertheless this task is easy in radial grids compared to power flow calculations in meshed networks, where the way power flows and definition of a slack node is not unique. A very comfortable, fast and robust way to calculate the state of a grid is the power flow calculation, which is an iterative method for calculating voltages and

currents in a grid. Several algorithms for performing power flow calculations exist, which are based either on solving the current balance equation or the power balance equation in each node. In modern power flow calculation systems mainly the Newton-Raphson method [7, chap. 14.3.3] [6, chap. 6.2.3] is used, which is based on the power balance equation and it needs even in big grids only three to six iteration steps to converge[6]. Prior to the Newton-Raphson method, mainly the Gauss-Seidel method [7, chap. 14.3.2] [6, 6.4.2] was used, which is based on the current balance equation and has inferior convergence behaviour. At the beginning of the iterations, initial values for voltages and currents have to be assumed. The Gauß-Seidel method has the advantage that it is able to converge, even if the starting point is not ideally chosen, whereas the Newton-Raphson method can cause problems in such cases. In practise some initial iterations can be done with the Gauß-Seidel method resulting in a proper starting point for the Newton-Raphson method [5, chap. 18] [6, chap. 6.4.5].

1.3.3.4 Optimal Power Flow Calculation

Leaving some values for active power and / or reactive power undefined in an power flow calculation leads to an under-determined problem, where several aspects like voltage level limits or line current limits can be additionally taken into consideration for optimising the power flow. This leads to the optimal power flow calculation, which is performed for example in the power station resource scheduling, where the overall power grid state is optimised so that a maximum of economy and security is achieved. [5, chap. 18]

[6] Converging in this context means that the numerical calculated results for the voltages and currents are near by the exact values so that the resulting errors are small enough.

Chapter 2

State of the Art

2.1 Voltage Control in High Voltage Transport Networks

In past, monitoring and controlling of the whole electric power system was done primary in the transport network. Because of the fact, that energy can't be conserved in electric energy networks, the active power production has to be permanently controlled to fit the actual active power demand, as well as the reactive power production has to be controlled to fit the actual reactive power demand. When there is a lack of active power in the system, the missing active power is taken from the rotational energy of the generators leading to a deceleration of the generators and to a decrease in grid frequency. Contrariwise an excess of active power leads to an acceleration of the generators and to an increase in grid frequency. Therefore, active power control can be accomplished by frequency control, whereas voltage control can be achieved with reactive power control. The fact that adjacent transport networks are interconnected leads to a robust grid, because sudden generation dropout or load-throw-off can be balanced in a wider scope than in an isolated operated transport network. To assure stability in such big grids, grid control is operated in three stages: The primary, secondary and tertiary control for frequency / active power and the primary, secondary and tertiary control for voltage / reactive power. [5, chap. 15]

2.1.1 Frequency / Active Power Control

Because of the fact that the active power generation has to cover the active power demand, a significant amount of generation units has to be able to vary their feeding power according to the demand of the grid. Therefore it is necessary to adjust the feeding power within a few seconds to immediately stabilise generation dropout or load-throw-off. In contrast to grid voltage levels that vary from node to node, the grid frequency is constant in the whole grid (quasi-static view). Therefore the information of how much active power has to be fed into the grid globally can be easily measured by measuring the grid frequency locally, turning active power control into frequency control. [5, chap. 15.1]

2.1.1.1 Primary Control

To control sudden load variations, frequency control has to be performed individually by every participating generation station in parallel, leading to a response to the changed grid situation within a few seconds. This task has to be done in a way that grid stability is guaranteed all the time. The ability of the generators to rise power production within seconds is given by the so called active power seconds reserve. This means that the turbine input is in normal operation permanently slightly throttled (e.g. closing some turbine inlet valves) so that the turbine can produce a greater drive torque within seconds when releasing the throttling. For reasons of stability primary control is implemented as a proportional controller, leading to a defined and stable load apportionment of the compensation power to the controlling generators.

2.1.1.2 Secondary Control

Because of the permanent frequency deviation from nominal frequency resulting from the proportional control behaviour in primary control, a secondary control authority is needed. It automatically adjust the operation points of some generation units to bring grid frequency back to nominal value within a time span of a few minutes. Therefore a centralized operated grid frequency controller calculates active power set values for one or more generators, so that the load apportionment is relocated from all generators participating primary control to the secondarily controlled generators decidedly. Here storage power stations, pumped storage power stations and modern gas power stations are preferred. For secondary control communication infrastructure is necessary (eq. power line communication). The aim of the secondary controller is also to keep the long term frequency average at nominal frequency. This means that the grid frequency is set slightly above nominal frequency if there was a longer time span with a frequency lower nominal value. Through the task of secondary control, the primary control reserve is released so that it will be available for further primary controlling.

2.1.1.3 Tertiary Control

Within tertiary control, generation and operation costs are taken into account to operate the whole grid cost-effective. This long term control considers load and generation forecasts and generation schedules are created on base of negotiated agreements. At this level load throw-off and relocation of power production are taken into account to operate the grid in an optimised state, most times utilising an optimal power flow algorithm. At this control level the compliance of the power flow arrangements with the interconnected HV networks (adjacent control zones) is arranged. Tertiary control can partly be automatically carried out, but in general human interaction and input is necessary at this level.

2.1.2 Voltage / Reactive Power Control

Voltage levels in HV networks are in principle less critical than in MV or low voltage networks, because hardly any customer (who would make demands on voltage level) is directly connected to the HV grid. The MV grids are connected through transformers with OLTC balancing voltage level changes on HV side. Therefore voltage limits in HV grids can deviate up to $\pm 15\%$ from nominal value, depending on the individual grid.

A generator blackout results in a slightly lowered global grid frequency, but in strongly lowered local voltage levels. So reactive power has to be provided locally to control the voltages in the grid, in contrast to frequency control, where every generator in the grid contributes to the active power control. [5, chap. 15.2]

2.1.2.1 Primary Control

In contrast to active power control, primary voltage control has nothing to do with reactive power. Primary voltage control is performed by the automated voltage controllers of the transformers, which locally control the OLTC based on the measurement of the local busbar voltage, see 2.2.1.1.

2.1.2.2 Secondary Control

Secondary voltage control is - similar to secondary frequency control - operated by a centralized controller, which sends out set values for generators or other reactive power controlling devices (phase changer, series and parallel reactors, series and parallel capacitors, ...).

2.1.2.3 Tertiary Control

Tertiary voltage / reactive power control is part of the tertiary frequency / active power control, where the state of the grid is optimised based on measurements describing the state of the whole grid. Op-

timal power flow (OPF) algorithms are used to find an optimised grid state which fulfils the operational constraints of voltage level, line current and generator operation limitations, described by

$$U_{node}^{min} < U_{node} < U_{node}^{max}$$
$$I_{line} < I_{line}^{max}$$
$$P_{generator}^{min} < P_{generator} < P_{generator}^{max}$$
$$Q_{generator}^{min} < Q_{generator} < Q_{generator}^{max}$$

The objective function can consider multiple aspects, for example operation efficiency (minimising grid losses by reactive power compensation or relocation of generation to minimise line currents), generation cost effectiveness (costs of power generation in different stations) and operation security aspects (operating the grid centred within voltage limits or generator operation points). Since the possibilities for controlling the network state increased as well as the electricity demand, grid control became more complex, not only due to the deregulation of the energy markets. As a consequence, many different approaches performing complex optimal power flow calculations were developed. Solving the OPF problem can be done with linear programming methods, Newton-Raphson methods, quadratic programming methods, non-linear programming methods or interior point methods. In future, even artificial intelligence methods like neural networks, fuzzy logic, genetic algorithm, evolutionary programming, ant colony optimisation and particle swarm optimisation might be used [9].

2.2 Voltage Control in Medium Voltage Distribution Networks

As distribution networks are usually passively operated without meshes, voltage control is far less complex compared to voltage control in actively operated transport systems. The line length of DS is small compared to transport systems, which makes the use of reactive power compensation in general unnecessary. Since the share of DG integrated in DS was low compared to the supplied loads, the operation of DS was possible without having much information about the actual state of the grid, which means that DS controlling and planning was done offline by utilising grid models and historical load profiles. Therefore, DS had to be designed robust so that operating the grid without actual measurements from the grid was possible. Since the grid topology is radial, there is no possibility to optimise the power flow, because in fact there is only one way for power to flow. Line current limitations are therefore only considered by DS planning and designing, and not in operation.

In rural DS line current limits don't restrict the DG integration, because voltage limits are violated prior to current limits. Therefore in practise a necessary criterion for integrating new DG is the compliance of the voltage levels in high-load non-generation and in high-generation low-load situations. [1]

2.2.1 Local Voltage Control

In local voltage control, all voltage control measurements are performed individually with local measurements, so no communication infrastructure is needed. The two voltage control elements in DS are the transformer and the DGs.

2.2.1.1 Transformer

The primary device for voltage control in DS is the central MV transformer, which is the single connection point to the transmission system in radially operated DS. By assuming constant-current loads, the grid load is constant when performing a tap-change (see chap. 1.3.2.1), leading to a constant voltage step at all supplied nodes[1].

[1] Assuming a constant-power model for grid loads leads to a decreased current when performing a tap-change to the next higher voltage step and to the fact that the voltage step gets higher the farer the node is away from the transformer. In contrast, a constant-impedance model for grid nodes leads to a decreased voltage step height at nodes far away from the transformer because of the increased current in the lines.

Since tap-changers are mechanically constructed, the change of tap position under load without service interruption will produce an electric arc during switching operation, which leads to deterioration of the tap-changer. So it is necessary to minimise tap-changes during network operation.

Voltage Control with an Automated Voltage Controller (AVC) The tap position of the OLTC is controlled from the automated voltage controller, which decides whether if it's time to tap up or down based on the local voltage measurement of the MV transformer secondary busbar and a configurable voltage set value. Several vendor-specific implementations of AVC's exist, whereat in this work the behaviour of the A-Eberle REG-D™ [10] will be described, because it is used in the two distribution grids examined in the DG DemoNet project [4].

A-Eberle REG-D™ Beside the local voltage measurement U_{meas} of the MV transformer secondary busbar, the A-Eberle REG-D™ needs three main parameters to be specified for performing automated voltage control: The voltage set value U_{set}, a voltage deadband U_{DB}, and a time factor. The deadband specifies the tolerance range around the voltage set value where no tap-change is performed, so when $|U_{meas} - U_{set}| < U_{DB}/2$. When the deviation of the measurement to the set value becomes higher, a tap-change is taken into consideration, and is performed depending on an inverse time characteristic based on the time factor. This means that a small violation of the $U_{DB}/2$ limit will lead to a delayed tap-change, whereas a high difference will immediately lead to a tap-change. [10]

The voltage deadband U_{DB} has to be at least 20% higher than the TF's nominal tap-change-height $\Delta U_{tap}^{nominal}$, so $U_{DB} \geq 1.2\Delta U_{tap}^{nominal}$. This is necessary because otherwise the so called phenomenon "hunting" will occur, where shortly after a tap-change the tap-change will be reversed by introducing another tap-change in the other direction[2]. To assure stable grid operation it's reasonable to set the deadband twice as high as the nominal tap-change-height, so $1.4\Delta U_{tap}^{nominal} \lesssim U_{DB} \lesssim 2\Delta U_{tap}^{nominal}$.

This control technique compensates voltage variations on the HV side as well as voltage variations due to load variations leading to a voltage drop variation of the transformers series impedance.

Line Drop Compensation (LDC) When there is a high load in the grid, it can be assumed that voltage levels far away from the feeding MV transformer are low or even near at the allowed voltage lower limit in a branch without generation. To avoid undervoltage, raising the AVC's set value could be a solution, based on the assumption that a higher voltage set value won't bring transformer branches with high generation into overvoltage. On the other hand, more generation than load in the grid leads to voltages above the transformer's busbar voltage. In this case it could make sense to lower the AVC's set value, so that overvoltage in the feeding branches will be avoided, assuming that a load dominated branch won't get into undervoltage.

To achieve such an extended voltage control, the current through the transformer can be measured (or the current of a single and critical branch) and transformed into a voltage setpoint correction. This control approach needs some additional parameters from the grid (or the measured branch) to convert the current measurement into an voltage adjustment for the AVC's voltage set value. [11]

LDC can significantly improve the voltage situation in distribution grids by only using local measurements, although control accuracy can relatively easily be improved by involving multiple feeder current measurements, leading to a "multiple line drop compensation". [12]

[2]This will be illustrated with a small example: Consider a TF with a $\Delta U_{nominal}^{tap} = 0.01$pu, $U_{DB} = 0.01$pu, $U_{set} = 1$pu and $U_{meas} = 1.005$pu: Here $|U_{meas} - U_{set}| = 0.005 \leq U_{DB}/2 = 0.005$, so a down-tapping will be performed. Afterwards, $U_{meas}^{new} = U_{meas} - \Delta U_{nominal}^{tap} = 0.995$pu where again $|U_{meas} - U_{set}| = 0.005$, so an up-tapping will be performed - so the AVC "hunts", or "chases" the TF set value, without making improvements. The other extremum will be $U_{DB} = 0.02 = 2\Delta U_{nominal}^{tap}$, where at $U_{meas} = 1.01$pu down-tapping will be performed because $|U_{meas} - U_{set}| = 0.01 \leq U_{DB}/2 = 0.01$pu. Here, $U_{meas}^{new} = U_{meas} - \Delta U_{nominal}^{tap} = 1$pu, so the set value is exactly hit.

2.2.1.2 Distributed Generators

While the characteristics of TF's voltage control can be individually designed by the number of available taps and the tap-change voltage step height, the capability of DG contributing voltage control depends primarily on the line reactance between the transformer and the generator, and of course on the capability of the generator to produce reactive power. A DG with a low connection line reactance has the disadvantage of a low voltage control contribution (see chap. 1.3.3.2), but in practise a low line reactance means that the DG is placed near the transformer. This leads to a general voltage level close to the transformer's voltage level, which means that voltage control won't be necessary. On the other hand, a DG far away from the MV transformer probably has a high line reactance. Here reactive power production or consumption can make a significant contribution to the voltage level (see eq. 1.4) and the need of voltage control is also much higher due to the weaker feeding point (high line impedance).

The nominal power of older generators was designed to fit the turbine's nominal power. This makes a reactive power contribution impossible when operating at nominal active power, because producing reactive power means running a higher current through the generator's stator coils leading to an unacceptable heating at nominal power (see chap. 1.3.2.2). Newer generators are slightly overdimensioned so that at least an operation at power factor $PF = P_G/S_G = cos\varphi = 0.95_{inductive/capacitive}$ is possible at the whole active power operation range, leading to a reactive power contribution of minimal[3] $Q_G^{min/max} = \pm 0,329 P_G^{nominal}$.

Local voltage control is performed by the generators local controller, which can operate as a reactive power controller, a $cos\varphi$-controller or directly as a voltage controller (which means that a $Q(U)$ characteristic is used to determine the reactive power corresponding to the feed-point voltage). It is also possible to operate the generator with a constant $cos\varphi$, and if it comes to a voltage violation, operation can be switched to voltage control. [13, 14]

[3] These are only the minimal required limits, the exact borders can be determined from the generator's operation diagram, see fig. 1.3

Chapter 3

Related Work

A very comprehensive listing of relevant publications to the development of distribution system control strategies up to the year 2008 was done in [15, chap. 2]. Due to the fact this project deliverable was never published, the most important paragraphs will be cited here, with adapted reference indices to fit the framework of this work:

> ...
> *Coordinated control of substation voltage and reactive power of DG:*
> ...
> In [16] and [17] a two-stage continuous control algorithm that aims to keep the network voltages near their nominal value is proposed. The control can also be such that actions are taken only when either the minimum or the maximum voltage is approaching its limit. Algorithm proposed in [18] tries to restore the network voltages between acceptable limits by controlling the on-load-tap-changer (OLTC) position and voltage regulation mode of the main transformer and the generators reactive power output. In [19][1] the OLTC of the main transformer is controlled first. If the voltages cannot be restored to an acceptable level using the OLTC the reactive power of DGs is controlled according to a ranking table.
> ...
> *Methods using optimization:*
> ...
> Different optimization methods and objective functions have been proposed in publications. In [20] and [21] optimal power flow (OPF) is used to find the most favourable control options. In [20] OPF is used to minimise the active power curtailment and in [21] the OPF objective function was formulated to minimise the costs of transformer tap operation, reactive power absorption and the curtailed generation. The controllable variables are in both cases substation voltage (using main transformer OLTC) and reactive and active power of DG.
>
> In [22], [23] and [24] a genetic algorithm is used to determine the control options. In [22] the algorithm controls the main transformer OLTC, static VAr compensators (SVC), step voltage regulators (SVR) and shunt capacitors and reactors. Output of DG is not controlled. The objective function tries to keep the network voltages near the nominal value and, at the same time, reduce network losses. In [23] the main transformer OLTC, DG's reactive power and shunt capacitors are controlled using an algorithm that tries to minimise the difference of network voltages to nominal. In [24] the genetic algorithm is used to find a solution which minimises active power losses in the network.
>
> In [25] a local-learning algorithm in conjunction with multiobjective optimization and a supervisory process is used to determine the set points to voltage controlling devices.

[1] This paper describes the very beginning of the DG-DemoNet project in 2007, in the meantime, control algorithm completely changed as described in [4].

The objective function consists of active power losses, average voltage deviation, maximum voltage deviation and the reactive energy costs. The benefit of this approach is that using a local-learning algorithm reduces the solution time substantially and, therefore, this algorithm would be particularly suitable for online operating modes. [25]

In [26] the operation of the main transformer OLTC is modified and the position of the tap-changer determined using optimization that tries to keep the network maximum and minimum voltages as close to nominal as possible. In [27] SVCs are controlled using some kind of optimization.

Furthermore, in this paper ([15]) a control strategy is described, which uses a flowchart algorithm to determine the tap position for the transformer and the $cos\varphi$ set value for the only controllable DG in the grid. This makes the control algorithm simple because no optimisation approach is needed, with the disadvantage that no network optimisation can be performed.

In [28] grid voltages are optimised by calculating transformer, capacitor and DG set values based on one-day-ahead load forecasting without having voltage measurements. This is done firstly in uncoordinated (local) control with and without DG, and secondly in coordinated control with and without DG, where the objective was to minimise grid losses. Comparison of the simulation results showed that utilising DG for voltage control reduces grid losses and the amount of needed tap-changes, while the benefit of coordinated voltage control to uncoordinated voltage control is not very big.

As reactive power produced by DGs in DS can have a negative impact on a weak transport network, the use of DGs' reactive power is minimised in [29]. Therefore the operation mode with constant $cos\varphi$ is improved by raising the $cos\varphi$ if the grid situation allows it. This is calculated with an OPF method that minimises the reactive power produced by DGs. A comparison of a simulated offline passive approach based on predefined generator settings and an online active approach based on grid measurements shows that the active approach leads to less grid losses than the passive approach as expected, even if the saving is not significant.

In [30] again a passive approach is performed to control transformer voltage and DGs' reactive power. The optimisation is implemented as linear programming method with the objective function approaching optimal reactive power to comply with the voltage limits and fit the transport system reactive power demand. Therefore the concept of the contribution matrix is used like in [4], which gives the control approach presented in this paper a large analogy to the control strategy described here in this work, even if the control strategy examined here is designed to operate actively.

3.1 Categorization of DS Voltage Control Concepts

In the past thirty years, various control strategies for distribution grids to keep the grid voltages within their limits have been developed all over the world, which can be roughly separated by the following aspects:

- Real time control or generation of an operation schedule
  While some control strategies use historical load profiles calculating an operation schedule [28, 30], the most control strategies recently published mainly use real time measurements for distributed or coordinated voltage control [15, 16, 17, 18, 20, 21, 22, 23, 24, 25, 26, 29].

- Types of controlled elements
  While the tap-change capability of the MV transformer is used in all control strategies, the use of DG [15, 16, 17, 18, 20, 21, 23, 24, 25, 28, 29, 30], static VAr compensators [20, 22, 27], capacitor banks [28], switchable loads and other voltage controlling elements [22, 23, 24, 25, 27] depend on the individual framework requirements of the examined distribution grid.

- Amount of necessary grid information
  If real time measurement is used, some control strategies need only the transformer voltage and

the branch currents [17, 26], whereas other control strategies need decentralised measurements in the grid [15, 16, 18, 20, 21, 22, 23, 24, 25, 29].

- Type of underlying control algorithm
  While calculating set values for the controllable devices based on simple rules [15, 16, 17, 18] (e.g. flowchart) is sufficient for simple networks, most control strategies use a kind of optimisation approach [22, 23, 24, 25, 26, 27, 28, 30], where the most common approach is an optimal power flow algorithm [20, 21, 29], which is far from being the only solution, as described in [9].

- Additional control objectives
  Beside keeping voltage within limits, the controller can try to minimise active power curtailment [20, 21], minimise grid losses [22, 23, 24, 25, 28, 29], minimise the voltage deviation from nominal value [25, 26], minimise the amount of transformer tap-changes [21], minimise the amount switching operations of capacitor banks, or follow other approaches [25, 30].

3.2 Impact of Related Work to this Work

To enable a high share of renewables in DS, real time control methods using actual grid measurements are more effective than scheduled methods, because they know the actual state of the grid and can flexibly and immediately respond to grid changes. So the operational safety margins can be reduced to a minimum, and a maximum of DG can be integrated into existing DS. Due to the fact, that DS tend to become as highly equipped with measurements as transport systems in future, the control algorithm examined in this work, developed in [4], will be based on real time measurements.

The controlled elements of the algorithm stated in this work will be the central MV transformer's AVC and selected DGs in the grid, which offers a cost-efficient voltage control with comparably low complexity, because of the omission of planning, installing and maintaining additional voltage control devices.

Several control methods based on OPF methods were introduced, which have the drawback that they need to know (nearly) the complete state of the distribution grid with many load states and grid switch states. Either this leads to an enormous amount of necessary measurements and communication infrastructure, or it will require masses of historical load profiles, with have to be periodically updated, so that the OPF method can run. The control method of this work will only rely on voltage measurements of selected network nodes, and the active- and reactive power of selected controllable DGs, as well as on a rough topology information of the grid. If needed, the control method will be able to operate without topology information at the price of reduced effectiveness. Some of the extended control objectives stated in this work with the aim to reduce grid losses will also depend on TF and line current measurements similar to OPF methods.

As described in [15, chap. 2.2.3], optimisation algorithms are advantageous when controlling grids with many controllable elements, and flexibility, expandability and adaptability of the voltage control is necessary. In comparison with e.g. flowchart algorithms, the drawback of optimisation algorithms are a higher complexity, possibly no guaranty for convergence, potentially a higher computation time (which is relevant in real time control), and maybe the optimisation result could radically deviate from the current network's operation point. Nevertheless the advantages of optimisation algorithm predominate and convergence behaviour and computation complexity will be analysed for the control algorithm stated in this work.

Although it is a good idea, to use a control strategy which minimises the intervention into the uncontrolled grid state when firstly introducing a new voltage control concept (as it was done in the DG DemoNet project [4]), the use of further control objectives for minimising losses or costs is reasonable (as it is used in many other papers described above). Since the measurements used in the control algorithm stated in this work are not sufficient for knowing the complete state of the grid, loss optimisation can only be based on estimations. Within this work, the capability of different control objectives to help to reduce losses and operation costs is examined. Therefore, only stateless optimisation techniques will be used,

where the control solution will only depend on the actual state of the grid, without any dependencies of past grid states or possible future grid states. Since there is too little information to perform a power flow calculation, no statement can be made whether grid losses will be reduced when e.g. tapping up, or not. As operating experience show, that operating grids at the upper limit of the allowable voltage band leads to reduced grid losses, up-tapping might be generally reasonable. Maybe costs of up-tapping have to be taken in consideration, so cost reduction of a short period of higher grid voltage with less losses have to be compared with the costs of necessary tap-changes to reach this higher grid voltage - but this question won't be within the scope of this work. In this work the focus will be on different control strategies for utilising the DGs' reactive power and their influence to grid losses and transformer tap-changes.

Chapter 4

Coordinated Voltage Control with Contribution Matrix

Within this chapter, the fundamental concepts of coordinated voltage control with the contribution matrix approach will be introduced.

The voltage control approach stated in this work relies on actual voltage measurements from the grid. As it would be very uneconomical to equip every single node in the DS with voltage measurements, the voltage controller has to work with incomplete grid information. With systematic analysis of the DS and applying the techniques described in this chapter, voltage control can nevertheless be very accurate and reliable.

4.1 Concept of the Critical Nodes

To reduce the amount of necessary voltage measurements from the grid, the voltage interdependency of adjacent nodes can be used to omit redundant measurements and measurements, which will be very similar to the measurements of (electrically) near nodes. During this process attention must be paid on possible topology changes, which lead to changes in node adjacencies and therefore leads to changes in voltage interdependencies.

As the most important goal of voltage control is to keep all voltage in the grid within their specified voltage limits, the amount of necessary measurements can be further reduced by identifying the list of nodes, where voltage can be maximal or minimal in the whole grid. Having such a list of critical nodes (CN), it can be assumed that all other grid voltages are within the highest and the lowest voltage of the CNs. The list of CNs can be identified by examination of power flow calculations based on possible and realistic load- and generation situations, but topology changes have to be considered.

This approach has the drawback that the set of CNs can change, when new loads or new DGs are connected to the grid, if DS is rebuilt or extended. To prevent voltage violation, it will be necessary to operate voltage control with a safety margin to the specified voltage limits, because with the reduction of the number of voltage measurements voltage violation can no longer be ruled out with certainty.

In the DG-DemoNet project the list of CNs was determined by performing a power flow simulation with historical and synthetical annual load profiles of all nodes and generators in the grid. Based on the calculation results, the nodes with the highest or the lowest voltage at least once during the simulated year were identified. These nodes were aggregated if possible, so that adjacent nodes with similar voltages are represented by one CN. The resulting list of CNs was presented to the distribution system operator (DSO), who proved the feasibility of installing measurement and communication infrastructure. It has to be mentioned, that due to several reasons installing voltage measurements was not always possible, so a compromise had to be found together with the DSO.

4.2 Identification of the Controllable Distributed Generation

While for the optimisation of the grid losses it's optimal to have all existing DGs controllable, only a small number of DGs is necessary to keep grid voltages within their limits. These are typically DGs connected to a TF feeder with very high share of DGs, leading to voltages at this branch which are higher than the TF's busbar voltage.

The question of how many DGs should participate coordinated voltage control can be (like the number of CNs) an economical one, because installing active- and reactive power control equipment can be (especially at older generators) complicated, and installing communication infrastructure can be (depending on the position of the DG) expensive.

For involving existing DGs into voltage control, contracts between the DG operator and the DSO have to be adapted, which will depend on the benevolence of the DG operator.

As the existing DSs typically don't lead to voltage problems and voltage problems arise when integrating new DGs, it is reasonable to integrate these new DGs into coordinated voltage control to avoid problems with existing contracts or adaptations of old generator control modules.

The goal of the DG-DemoNet project was to enable of a high share of DG in DS and to avoid the resulting voltage violations, so the number of controllable DGs was kept minimal. The controllable DGs were selected from the TF branches with the highest voltage rises. These selected DGs are hydropower plants with nominal active powers from 600kW to 2,5MW, which are comparably easy to control because there are hardly generation fluctuations.

4.3 Concept of the Contribution Matrix

For voltage control of DS with DGs' reactive power, it is essential to know with which DGs the voltage magnitudes of the grid nodes can be influenced, and it is very practical to know how big the contribution from the DGs' reactive and active power on the voltage magnitudes is.

The information, which influence every DG has to every CN is given by the reactive power contribution matrix $A^{Q}_{CN,DG} = \frac{\delta U_{CN}}{\delta Q_{DG}}$ and the active power contribution matrix $A^{P}_{CN,DG} = \frac{\delta U_{CN}}{\delta P_{DG}}$. In practice, the contribution matrices will be calculated by performing a power flow sensitivity analysis, which means that a power flow calculation is performed twice with the same initial conditions, with a variation of active power δP_{DG} and reactive power δQ_{DG} respectively, and the differential quotient between the change in CNs' voltages and the change in DGs' active / reactive power fill the cells of the contribution matrices [1].

4.3.1 Variation of the Contribution Matrix Values

The slope of the curves in fig. 1.8 can be interpreted as the reactive power voltage sensitivity: The dotted lines indicate a constant voltage sensitivity because of the approximations lead to the linearised equation (1.4). The continuous lines show the exactly calculated voltage sensitivities, which slightly depend on the initial condition. This means that the values from the contribution matrix (CM) depend on the actual grid situation, as it shown in fig. 4.1, where the CM values were calculated based on one year load profiles. It can be seen, that the variation is negligible, because 50% of the annual CM values stick very close at their median, and the maximal relative deviation of the annual CM values from their mean value is in the order of 8% in average.

If a differential control strategy is used, small variations in the CM don't harm the functionality of the controller, because if the desired situation was not achieved within one control cycle, it can be accomplished in the next control cycle.

[1] With this approach, the accuracy of the CM values is slightly higher than calculating CM values from the line reactance and resistance (eq. (1.4), fig. 1.8), but the main advantage is that CM values for CNs located at other voltage levels connected via a transformer to the MV grid can be calculated in the same way like CM values of ordinary CNs, so no impedance transformation is necessary.

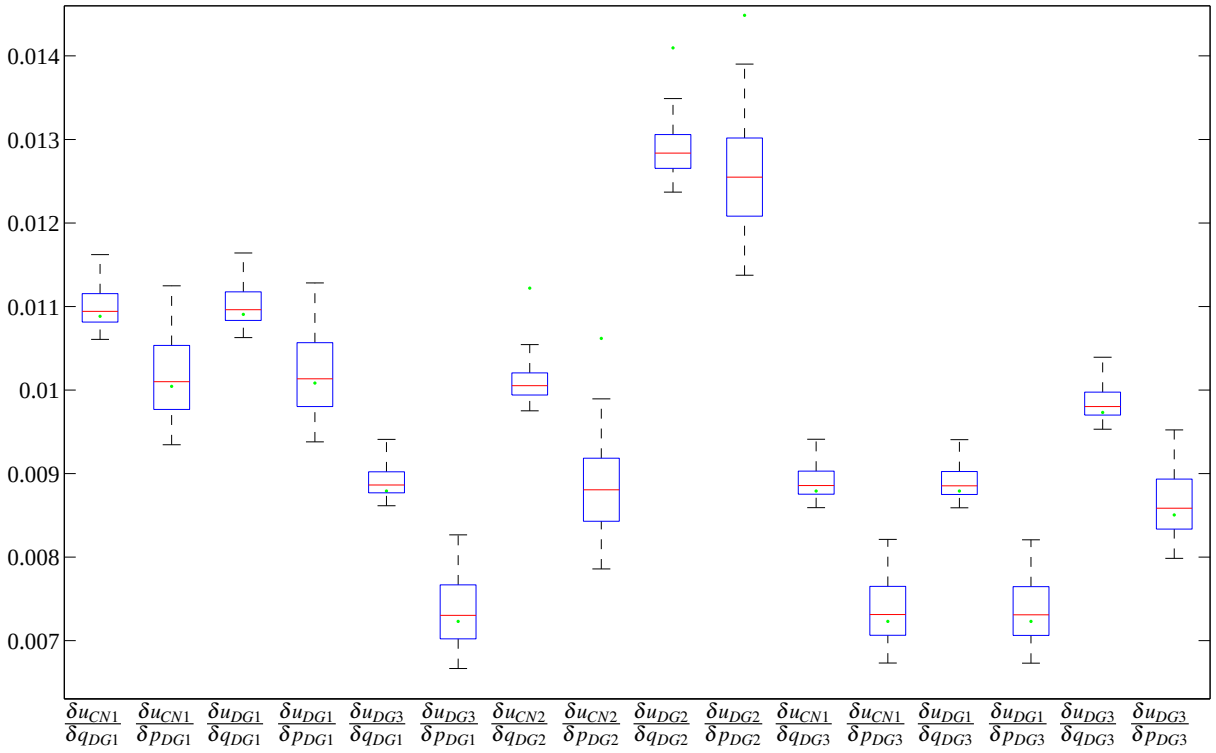

Figure 4.1: Boxplot of the time variation of contribution matrix values calculated by power flow sensitivity analyses based on one year load profiles in the Salzburg SS 'Lungau' (boxplots show the quartiles). The graph shows the analysis of the contribution of three DGs to their own feeding point and to selected other nodes. Voltages are in pu and active/reactive powers are in MW/MVAr, therefore the contribution matrix values are in the order of 10^{-2}. For this calculation, the slack was placed on the HV side of the TF, leading to non-zero values throughout. The green dot marks the CM values calculated with the approximation (4.1), which only considers the line impedance, see chap. 4.3.2.

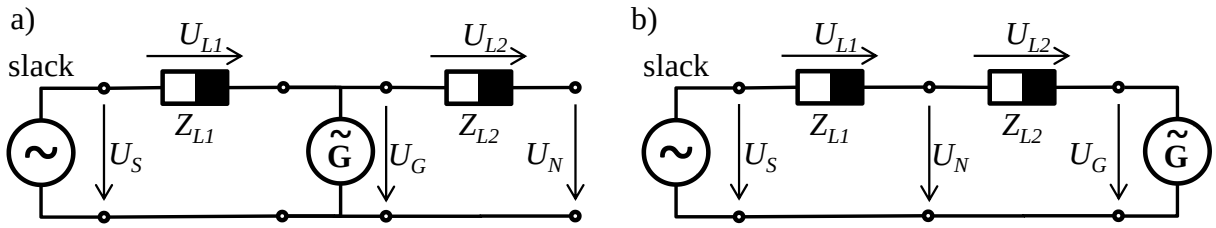

Figure 4.2: Schematic model of a feeding DG into the grid with a measurement node a) after and b) before the DG seen from the slack's point of view.

4.3.2 Deviation of an Analytical Approximation

In the model of elements with constant P and Q connected to a radial DS, a small change in (re-)active power at a node within the grid will be guided to the transformer into the HV grid, because all other network elements modelled as constant P/Q elements won't absorb this change, and changes in network losses are insignificant.

The linearised dependency of the voltage magnitude of a generator (feeding) node from the power flow between this generation node and the slack node was derived in chap. 1.3.3.2 with (1.4), which is valid not only for a feeding generator ($P < 0$) but also for a consuming load ($P > 0$).

In chap. 1.3.3.2 the reference Voltage (slack) U_S was assumed to be placed on the HV side of the TF, which means that the voltage sensitivities calculated contain TF's series impedance[2]. (1.4) stays valid if the slack U_S is placed on the MV side of the TF – then the calculated voltage sensitivities don't contain the TF's series impedance, leading to the fact that the resulting voltage rise is calculated relative to the TF's MV busbar voltage. The setting of the slack to the MV side is valid because according to the model there is no other way for power to flow than over the transformer, so the model of the line within slack and generation node keeps valid. The reference voltage (slack) can't be placed anywhere in the grid, because then it's not guaranteed that a change in (re-)active power will be forwarded to the slack, e.g. if the slack would be placed on another branch than the inspected grid node[3].

To derive an approximation for the contribution matrix values, (1.4) can only be used to calculate the contribution of any DG to any CN under the following modifications: The slack has to be at the transformer in any case (index *S*), the change of (re-)active power is done at the generator node (index *G*), but the node where the voltage sensitivity is analysed is an additional node placed somewhere else in the grid (index *N* for "node"), leading to the grid model displayed in fig. 4.2.

Altering the power flow with δP_G and δQ_G at the generator node leads to a change in generator node voltage δU_G, so (1.4) becomes $U_G + \delta U_G \approx U_S - \frac{1}{U_S}\left((P_G + \delta P_G)R_L + (Q_G + \delta Q_G)X_L\right)$. This leads to the approximated voltage sensitivities at the generator node $\frac{\delta U_G}{\delta Q_G} \approx -\frac{X_L}{U_S}$ and $\frac{\delta U_G}{\delta P_G} \approx -\frac{R_L}{U_S}$.

When analysing the voltage change at the measurement node δU_N, it is easy to see that it is the same as the generator voltage change δU_G when the measurement node is "behind" the generator node (fig. 4.2 a.), and it depends on the impedance Z_{L1} of the line between the slack and the measurement node, if the measurement node is "before" the generator node (fig. 4.2 b.). As the slack voltage is constant according to the model displayed in (fig. 4.2 b.), the measurement node can only "see" the voltage change caused through Z_{L1}, and Z_{L2} is only important for the voltage rise at the generation node. This leads to the conclusion that *the line impedance in (1.4) has to be interpreted as the impedance of the section of the path between the slack and the grid node, which is common with the path between the slack and the generation node*. This statement also holds for measurement nodes placed at an other feeder (here, the contribution would be zero if the slack is placed on the TF's MV busbar) or at an other branch within the same feeder (here, the contribution would be calculated with the line impedance of the line from the

[2]Of course, the slack voltage U_S as well as the TF's HV series impedance has to be transformed to the MV side of the TF to keep (1.4) valid ($U'_S = U_S \frac{n_{MV}}{n_{HV}}$, $Z'^{HV\,series}_{TF} = Z^{HV\,series}_{TF} \frac{n^2_{MV}}{n^2_{HV}}$).

[3]Furthermore the slack was assumed to be a strong node with a small voltage change compared to the node in grid.

slack to the branch point, where the paths divert).

Assuming HV voltage as constant as described in 1.3.3.1, it can be seen in fig. 1.5, that in principle every DG connected to the MV grid has an influence to the voltages of every node in the whole grid because of the TF impedance, which can be considered as significant compared to the line impedance in DS[4]. The placement of the slack on the MV side results in the fact that DGs only have a contribution to nodes located at their feeder.

4.3.3 Topology Changes

When grid topology changes, some nodes might be connected to an other feeder, which leads to a complete change of contribution matrix values. It is necessary to update the CM in such cases, because otherwise DGs would be utilised to influence a voltage of a CN which might not be influenceable any more by this DG, leading to an unpredictable behaviour.

If no topology information is available, the only information which will be certainly valid is the contribution of the DGs to their own feeding node (DGs' feeding nodes are very likely CNs), but the exact contribution value can vary depending on the connection path of the DG.

The most critical changes are DG and CN changeovers from one feeder to an other one. Topology changes within a feeder (branch changes) will probably lead to a change in CM values, but non-zero values won't become zero and vice versa (with the slack at the TF's MV side), which can be considered as less critical depending on the individual grid.

In the DG-DemoNet project topology information was provided by third-party topology extraction tools[5]. Based on the information which DG and which CN is connected to which TF (at which feeder) an appropriate contribution matrix is chosen from a set of contribution matrices. This set was prepared in offline calculation according to typical topology changes, which were provided by the DSO.

If an unknown topology occurs where no prepared contribution matrix matches, the voltage controller can operate with a minimal contribution matrix, where only the contribution matrix cells of the DGs to their own CN are non-zero.

4.3.4 Numerical Characteristics of the Contribution Matrix

4.3.4.1 Sign of CM Values

In chap. 4.3 the CM was introduced with $A^{Q}_{CN,DG} := \frac{\delta U_{CN}}{\delta Q_{DG}}$ and $A^{P}_{CN,DG} := \frac{\delta U_{CN}}{\delta P_{DG}}$ and in chap. 4.3.2 the voltage sensitivities were derived by the approximations $\frac{\delta U_G}{\delta Q_G} \approx -\frac{X_L}{U_S}$ and $\frac{\delta U_G}{\delta P_G} \approx -\frac{R_L}{U_S}$. Since $U_S > 0$, $R_L > 0$ and in rural DS $X_L > 0$ all CM values would be negative or zero in grid's perspective. Performing voltage control calculations with DGs is more common in the producers / generators perspective, because otherwise the P/Q operation diagram of the generators (see fig. 1.3) would have to be implemented upside down (turned for 180°), which would be confusing and error-prone. The change from grid perspective to generator perspective leads to a change of sign in P and Q, and therefore CM values become positive or zero:

$$A^{Q}_{CN,DG} := \frac{\delta U_{CN}}{\delta Q_{DG}} \approx \frac{X_L}{U_S} \qquad A^{P}_{CN,DG} := \frac{\delta U_{CN}}{\delta P_{DG}} \approx \frac{R_L}{U_S} \tag{4.1}$$

Consequently the contribution matrix in pu is defined as:

$$a^{q}_{CN,DG} := \frac{\delta u_{CN}}{\delta q_{DG}} = \frac{1\text{MVAr}}{U_{Nominal}} \frac{\delta U_{CN}}{\delta Q_{DG}} \approx \frac{1\text{MVAr}}{U_{Nominal}} \frac{X_L}{U_S}$$

[4]The TF's series reactance can be in the order of the line reactance between the DG and the TF, while the TF's series resistance is typically one to two orders of magnitude smaller than the line resistance.

[5]SS 'Lungau' (Salzburg) was operated with a Siemens power network process control system, which extracted the information which DG and which CN was is connected to which TF at which TF feeder into an xml file. This file was generated every time topology changed, and it was periodically read by the DG DemoNet voltage controller. In SS 'Nenzing' (Vorarlberg) topology information was provided by process variables that indicated which CN and which DG was connected to which TF (so the TF branch information was not given). These process variables could be read directly like other measurement variables.

$a^{q}_{CN,DG} \cdot 10^3$	DG^{a}_{820}	DG^{b}_{820}	DG_{840}	DG_{850}
CN_{208}	0	0	0	0
CN_{213}	6.885	6.885	0	4.972
CN_{313}	0	0	0	0
CN_{406}	0	0	6.120	0
CN_{602}	0	0	0	0
$DG^{a/b}_{820}$	6.906	6.906	0	4.971
DG_{840}	0	0	8.761	0
DG_{850}	4.963	4.963	0	5.833
TF_{MVbus}	0	0	0	0

$a^{p}_{CN,DG} \cdot 10^3$	DG^{a}_{820}	DG^{b}_{820}	DG_{840}	DG_{850}
CN_{208}	0	0	0	0
CN_{213}	9.159	9.159	0	6.571
CN_{313}	0	0	0	0
CN_{406}	0	0	8.248	0
CN_{602}	0	0	0	0
$DG^{a/b}_{820}$	9.193	9.193	0	6.570
DG_{840}	0	0	11.80	0
DG_{850}	6.572	6.572	0	7.737
TF_{MVbus}	0	0	0	0

Table 4.1: Contribution matrix example, based one the installed CNs and controllable DGs in default topology state in SS 'Lungau' in Salzburg. Reactive power CM (left) and active power CM (right) rescaled with 10^3 (calculated with reference voltage at TF MV busbar). Values are given in pu, where $U_{Nominal} = 30\text{kV}$ and powers are given in MW/MVAr.

$$a^{p}_{CN,DG} := \frac{\delta u_{CN}}{\delta p_{DG}} = \frac{1\text{MW}}{U_{Nominal}} \frac{\delta U_{CN}}{\delta P_{DG}} \approx \frac{1\text{MW}}{U_{Nominal}} \frac{R_L}{U_S}$$

4.3.4.2 Dependency of Slack Position

If CM is calculated having the slack on the TF's HV side, all CNs and DGs have the path through the TF in common, even if they are located on different feeders, leading to the fact that in this case CM values won't be zero. The influence of the TF impedance can be considered as constant to all CM values, so CM values calculated with a HV slack differ from CM values calculated with a MV slack by the TF's impedance ($A^{Q\,HV}_{CN,DG} = A^{Q\,LV}_{CN,DG} + \frac{X_{TF}}{U_S}$).

4.3.4.3 Typical CM Example

Table 4.1 shows the contribution matrix of the default topology state in SS 'Lungau' in Salzburg with five CNs somewhere in the grid (row 1 to 5), three CNs at each controllable DG node (row 6 to 8) and finally the CN at the TF's MV busbar (last row). DG^{a}_{820} and DG^{b}_{820} are connected to the same grid node, therefore they need only one voltage measurement and have the same contribution values in their columns. Conspicuously are the contribution values of DG_{850} which have a strong similarity with the ones from DG_{820} and in fact they are connected to the same feeder and nearly to the same branch (with only 8km line between them), so they have influence to the same CNs, while DG_{840} has influence to other CNs (see fig. 4.3).

The second remarkable thing are the three nodes where no DG has a contribution. This is in principle not surprising, because rural DSs have typically many feeder (depending on the size of the supplied area), leading to an apportionment of the CNs to these feeders. So it's clear that if controllable DGs are only placed on two feeders, as it is the case in this DS, only a part of CNs will be influenceable (see fig. 4.3).

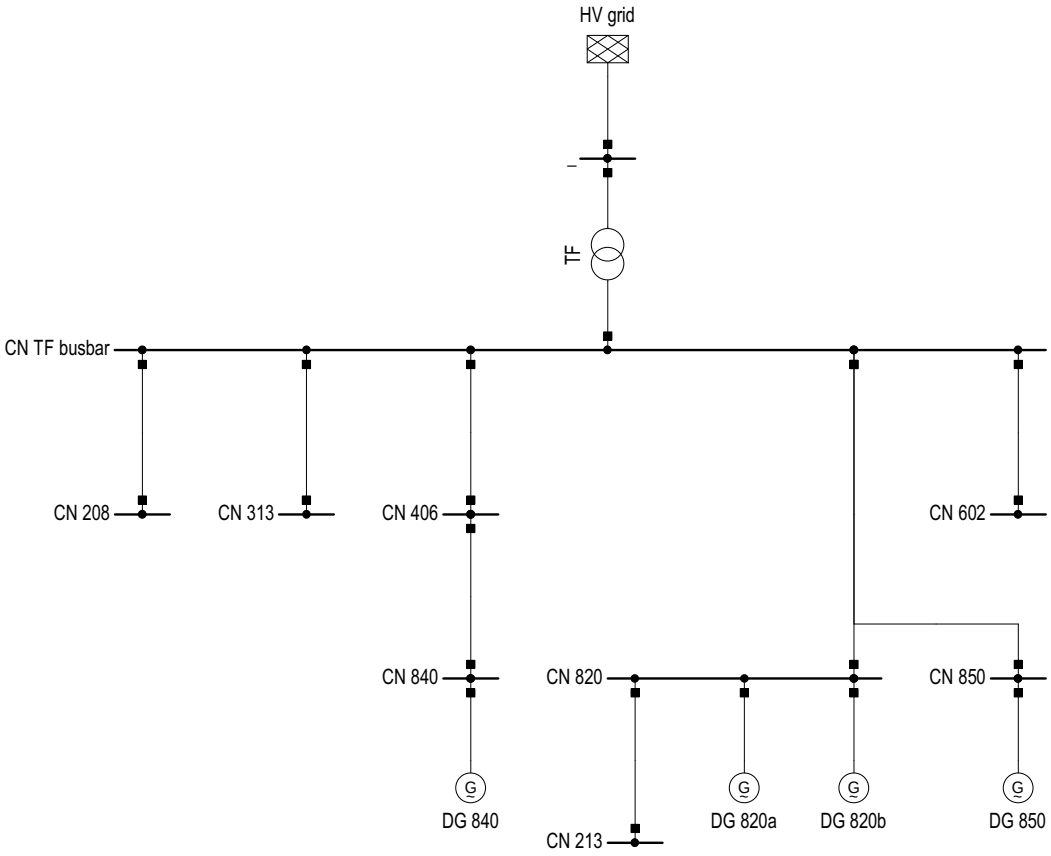

Figure 4.3: Schema of control-relevant network elements in SS 'Lungau' in Salzburg in normal switching state (only 9 of 500 network nodes and 4 of 15 DGs are shown).

Chapter 5

Coordinated Voltage Control Approaches

As discussed in chap. 3.2, the aim is to provide real-time voltage control for DS, where actual voltage measurements are taken from the grid and set values for the central TF and controllable DGs are calculated. Voltage control has to work without having complete grid information. Therefore the following information is assumed to be available:

actual grid data	offline data
topology information	contribution matrix
voltage of the CNs, both TF busbar voltages (MV and HV)	(configurable) voltage limits
(re-)active power of all controllable DGs (re-)active power flow over the TF (optional) reactive power flow at selected lines (optional)	controllable DGs P/Q diagrams
TF tap position	TF's neutral, min. and max. tap position TF's nominal tap-change height AVC's deadband

Since measurements are possibly spread over a big supply area, it should be mentioned that communication channels can be slow and unreliable. Voltage control strategies should be robust and be able to cope with measurement blackouts and long communication delays.

Within the following chapters, different control strategies are defined with different control objectives and their control behaviour is analysed. Simulation results to these control strategies are listed in chap. 6, where the control strategies and their ability to reduce operation costs will be compared.

5.1 Introduction of Level- and Range-Control

Within this chapter, the basic conditions for coordinated voltage control strategies are discussed: Starting at a straightforward ansatz, different aspects of coordinated voltage control strategies are discussed, gradually leading to a separation of voltage control strategies into a so called level controller and a range controller. The resulting problem is a constrained linear least square optimisation problem, whose solvability by an unconstrained linear least square approach will be analysed. The constrained problem will be solved in chap. 5.2.2.

5.1.1 Natural Control Objective: Nominal Voltage at all Nodes

It is desirable to have nominal voltage at all nodes in the grid, because this would maximise power quality and safety margins to the voltage limits . Of course this is not realistic, but it can make sense to formulate a control objective which always tries to restore network voltages to their nominal value as best as possible. This aim is stated as $\min \left| U_{CN} - U^{nominal} \right|$ for one node with voltage U_{CN} (indices

written inferior) and reference voltage $U^{nominal}$ (variable description written superior), but extending this for multiple nodes (CNs) to $\min \sum_{CNs} \left| U_{CN} - U^{nominal} \right|$ has a disadvantage: Maybe the control strategy finds the minimum in a way that all deviations from nominal value are very small for all nodes except for one node, where the voltage deviation is very high. This problem can be solved by weighting higher deviations more heavily, which can be done by replacing the absolute function by a quadratic function[1], leading to:

$$\min \sum_{CNs} \left(U_{CN} - U^{nominal} \right)^2$$

5.1.2 Problem Formulation

5.1.2.1 Straightforward Approach utilising DGs' (Re-)Active Power and the TF's OLTC

By utilising the voltage control elements (TF and DGs), the CNs' voltage can be influenced by (re-) active power with the linearised model of the contribution matrix and a change in tap position ΔN^{tap}, where ΔU^{tap} is approximated to be constant in the whole grid and can be calculated using (1.2):

$$U_{CN}^{new} = U_{CN} + A_{CN,DG}^{Q} \cdot \Delta Q_{DG} + A_{CN,DG}^{P} \cdot \Delta P_{DG} + \Delta N^{tap} \cdot \Delta U^{tap}$$

The control variables ΔQ_{DG} and ΔP_{DG} are continuous and ΔN^{tap} is in whole numbers.
This leads to the following optimisation problem:

$$\min_{\Delta Q_{DG}, \Delta P_{DG}, \Delta N^{tap}} \sum_{CNs} \left(U_{CN} + A_{CN,DG}^{Q} \cdot \Delta Q_{DG} + A_{CN,DG}^{P} \cdot \Delta P_{DG} + \Delta N^{tap} \cdot \Delta U^{tap} - U^{nominal} \right)^2$$

The limits for $\Delta N^{tap} = N^{tap,new} - N^{tap}$ is given by the minimal and the maximal tap position $N^{tap,min}$ and $N^{tap,max}$

$$N^{tap,min} \leq N^{tap} + \Delta N^{tap} \leq N^{tap,max}$$

The DGs' operation point resulting by applying $Q_{DG}^{new} = Q_{DG} + \Delta Q_{DG}$ and $P_{DG}^{new} = P_{DG} + \Delta P_{DG}$ has to be within the valid operational area in the PQ diagram which will look similar to the highlighted area in fig. 1.3. In a first draft the PQ diagram can be approximated with a simple rectangle, leading to the (re-)active power constraints

$$\begin{aligned} Q_{DG}^{min} < Q_{DG} + \Delta Q_{DG} < Q_{DG}^{max} \\ P_{DG}^{min} < P_{DG} + \Delta P_{DG} < P_{DG}^{max} \end{aligned}$$

5.1.2.2 Leave Active Power Control out

This formulation of the voltage control objective has a big disadvantage: Since the primary goal is the achievement of nominal voltage at each node, there is no room for maximising DGs' active power output (respectively avoiding active power curtailment). This control objective would lead to minimal power flow and minimal grid losses, because active power will be generated where it's needed, but it is not possible to give active power production priority. Because active power curtailment is related with financial penalties for the DG's operator and on the other hand the share of renewable energy shall be increased, the analysis of this control strategy will be continued without active power as a controllable variable and will be picked up in other control strategies in chap. 5.2.3. In the meanwhile active power will assumed to be accordant to the actual supply of primary energy.

[1] This doesn't prevent solutions leading to situations described above, but it they will be more unlikely.

5.1.2.3 Utilise the existing and proven TF's AVC

The second disadvantageous aspect is that the tap position is directly controlled. In DS sudden voltage changes can occur often, both at the TF's HV busbar (tap-changes in the HV grid, topology changes in the HV grid, load or generation throw-off, ...) and on the TF's MV busbar (topology changes, sudden load or generation changes, ...). Therefore, directly controlling the tap position would need a very good knowledge of the dynamics in transport and distribution system and a very reliably and fast communication channel between the voltage controller and the TF. Only in this case it would be possible to recognise sudden voltage changes and perform necessary control actions in time.

Relying on the existing and proven AVC (which is installed directly in the TF's substation) for controlling the OLTC has the benefit that knowledge about the grid's dynamic behaviour is not necessary. The AVC will automatically keep the voltage near at the voltage set value, leading to the fact that no interference is necessary at sudden voltage changes. So control actions can be performed in a longer cycle period, trusting the AVC that it will balance critical voltage changes automatically. This makes a reliable and fast communication channel unnecessary, because the TF's voltage measurement can be treated in the same way as all other CNs.

Calculating the AVC's voltage set value from the resulting ΔN^{tap} by $U^{set} = U^{TF} + \Delta N^{tap} \cdot \Delta U^{tap}$ would mean that the AVC's voltage control feature will be overruled, because an intended change of tap position is sent to the AVC via an adjusted voltage set value. This would be an adverse solution, because continuous changes in the grid (leading to continuous changes of measurement variables) would then produce a discontinuous controller output. For example, a change of one voltage measurement in the order of the measurement variable resolution (10^{-15} at double precision) could lead to a different optimum of the tap position and therefore a discontinuous change in voltage set value. To avoid the redundant re-implementation of an inverse time characteristic (hysteresis) and other timing and stability characteristics for performing tap-changes (as described in chap. 2.2.1.1), it is beneficial to use the features of the AVC to perform a smooth grid operation without unnecessary tap-changes. It is much more reliable to send continuous voltage set values to the AVC, which are calculated in a way that continuous changes in the grid lead to continuous changes in set values.

This leads to a significant change in the type of the problem, because the control of the discontinuous tap position will be replaced by the control of the continuous AVC's voltage set value, leading to the fact that the control of tap position is delegated to the AVC, so tap position is not relevant for the control strategy any more. As a consequence the control strategy has to cope with the fact that in the long run it can only be guaranteed that TF's busbar will be within the range specified by the AVC's deadband around the AVC's voltage set value. This could be seen as a drawback, but the rise in robustness and the reduction of control complexity are the more important advantages.

5.1.2.4 The resulting robust Control Strategy utilising DGs' Reactive Power and TF's AVC

Considering all the aspects dealt with in chap. 5.1.2.2 and 5.1.2.3 and introducing the continuous change of AVC's voltage set value as $\Delta U^{set} = U^{set} - U^{TF}$ as well as the CNs voltage deviation from nominal value $\Delta U_{CN} = U_{CN} - U^{nominal}$, the problem changes to the following:

$$\min_{\Delta Q_{DG}, \Delta U^{set}} \sum_{CNs} \left(\overbrace{\Delta U_{CN}}^{\text{measured}} + A^{Q}_{CN,DG} \cdot \overbrace{\Delta Q_{DG}}^{\text{to be determined}} + \overbrace{\Delta U^{set}}^{\text{to be determined}} \right)^2 \tag{5.1}$$

5.1.2.5 Separating the Calculation of the AVC's Set Value

The optimum for ΔU^{set} can be analytically derived by setting the first deviation zero, which leads to $2\sum_{CNs} \left(\Delta U_{CN} + A^{Q}_{CN,DG} \cdot \Delta Q_{DG} + \Delta U^{set} \right) = 0$, so with the number of CNs N^{CN} the change in AVC's

voltage set value becomes

$$\Delta U^{set} = -\frac{1}{N^{CN}} \sum_{CNs} \left(\Delta U_{CN} + A^{Q}_{CN,DG} \cdot \Delta Q_{DG} \right) \tag{5.2}$$

which is - not surprisingly - the negative mean value of the resulting voltages after the reactive power optimisation.

Eq. (5.2) shows that the calculated TF set value is influenced by DGs' reactive power changes and by CM values.This can be dangerous in practice, because it's not guaranteed that DGs will carry out the requested changes (due to the fact communication can be slow and unreliable in DS). And it's also not guaranteed that the selected CM describes the behaviour of the grid in its actual state accurately enough. Therefore it is not sure that the requested changes will really lead to the voltage changes calculated.

Beside sudden changes in load or generation , tap or topology , the grid's voltages will be continuous and steady with a low dynamic due to the fact that typically many customers are connected to the grid, so all power variations are balanced. Therefore, the difference in grid voltages from one control cycle to the next won't be very big when for example performing a controller cycle in the order of five minutes. This leads to the assumption that the required reactive power changes resulting from the optimisation won't be very big during normal operation. In combination with the already very small CM values, the second term in the sum of (5.2) can be neglected, leading to:

$$\Delta U^{set} \approx -\frac{1}{N^{CN}} \sum_{CNs} \Delta U_{CN} \tag{5.3}$$

In principle, the stability of this approach has to be proven, but the decoupling of TF voltage set value calculation and DG reactive power set value calculation described in the following paragraph makes the stability of this approach evident.

5.1.2.6 Introduction of Level- and Range-Controller

When analysing the nature of this problem a very important and useful insight can be found: Due to the assumption that the calculation of ΔU^{set} can be separated from the optimisation of ΔQ_{DG} and calculated independently (eq. (5.3)), ΔU^{set} is used to minimise the remaining voltage deviations from nominal voltage by trying to place the voltages as good as possible around nominal voltage, assuming that ΔU^{set} influences all grid voltages equally when the AVC decides to perform a tap-change. This leads to the insight that optimising the voltage *level* with reactive power is not necessary, because reactive power should only be used to optimise the relative differences of the voltages between each other and setting the voltage levels should be the task of the AVC.

The first advantage of this approach is the reduction of necessary reactive power, because an unnecessary high amount of reactive power would be needed to change voltages in the order of ΔU^{tap}, due to the fact that CM values are in practice relatively small. In other words: The control of the voltage level is much more efficiently performed by the TF than with DGs' reactive power.

A further advantage of this approach becomes apparent: Typically there are permanent voltage variations in the HV grid, which are of course transformed to the MV side of the TF and propagated in the whole MV grid. It would not make sense to control this voltage variations with reactive power from DGs, because therefore a permanent correction of reactive power set values would be necessary, which could weaken grid stability.

This leads to the important fact that it is reasonable to split the task of voltage control into two controllers, which can work independently from each other (assumed that the overall system stability is given):

The *level controller* calculates the voltage set value for the transformer to raise or lower all voltages in the grid in parallel, whereas the *range controller* calculates the reactive power set values (and possibly the active power set values) of the controllable DGs to change the voltage differences of the CNs among each other.

Therefore the level controller calculates voltage set values for the AVC in a very robust way with

$$U^{set} = U^{TF} - \frac{1}{N^{CN}} \sum_{CNs} \Delta U_{CN} \tag{5.4}$$

which only depend on actual measurement values and don't rely on the CM and the DGs' response to the requested reactive power set values. It can be performed without any topology information.

5.1.2.7 The remaining Problem of DGs' Reactive Power Calculation

In parallel to the level controller, the range controller solves the optimisation problem to calculate the DGs' reactive power , which results from inserting (5.2) in (5.1). But prior to this (5.2) will be further simplified:

$$\Delta U^{set} = -\frac{1}{N^{CN}} \sum_{CNs} \left(\Delta U_{CN} + A^{Q}_{CN,DG} \cdot \Delta Q_{DG} \right) = \underbrace{-\frac{1}{N^{CN}} \sum_{CNs} (\Delta U_{CN})}_{-\overline{\Delta U^{CNs}}} \underbrace{- \frac{1}{N^{CN}} \sum_{CNs} \left(A^{Q}_{CN,DG} \cdot \Delta Q_{DG} \right)}_{\frac{1}{N^{CN}} \sum_{CNs} \left(A^{Q}_{CN,DG} \right) \cdot \Delta Q_{DG}}$$

$$= -\overline{\Delta U^{CNs}} - \underbrace{\frac{1}{N^{CN}} \sum_{CNs} \left(A^{Q}_{CN,DG} \right)}_{A^{Q\,col\text{-}avg}_{DG}} \cdot \Delta Q_{DG} = -\overline{\Delta U^{CNs}} - A^{Q\,col\text{-}avg}_{DG} \cdot \Delta Q_{DG} \tag{5.5}$$

$\overline{\Delta U^{CNs}}$ is the mean voltage deviation of all nodes from nominal voltage, and $A^{Q\,col\text{-}avg}_{DG}$ is a line vector containing the average of the corresponding CM column in each column. Now, (5.5) can be inserted into (5.1) leading to:

$$\min_{\Delta Q_{DG}} \sum_{CNs} \left(\Delta U_{CN} + A^{Q}_{CN,DG} \cdot \Delta Q_{DG} - \overline{\Delta U^{CNs}} - A^{Q\,col\text{-}avg}_{DG} \cdot \Delta Q_{DG} \right)^2$$

As mentioned above, the aim of the range controller is not to keep all voltages at nominal voltage as good as possible, but to keep the deviations from their mean value as small as possible. If (5.3) would have been inserted into (5.1), the last term in the brackets would be missing. This term is responsible for adjusting the target voltage $\overline{\Delta U^{CNs}}$ (the CNs' mean value) according to the voltage changes $A^{Q}_{CN,DG} \cdot \Delta Q_{DG}$ caused by the change in DGs' reactive power, so that the "base" of range controllers objective keeps relative.

$\Delta U_{CN} - \overline{\Delta U^{CNs}} = (U_{CN} - U^{nominal}) - (\overline{U^{CNs}} - U^{nominal})$ can be written as the voltage difference from each CN to the mean voltage of all CNs $\overline{\Delta} U_{CN} = \Delta U_{CN} - \overline{\Delta U^{CNs}} = U_{CN} - \overline{U^{CNs}}$, and due to the fact that the index CN is fixed outside the sum, $A^{Q}_{CN,DG}$ is a line vector like $A^{Q\,col\text{-}avg}_{DG}$ which can be subtracted leading to the expression[2] $A_{CN,DG} = A^{Q}_{CN,DG} - A^{Q\,col\text{-}avg}_{DG}$ and to:

$$\begin{gathered} \min_{\Delta Q_{DG}} \sum_{CNs} \left(\overline{\Delta} U_{CN} + A_{CN,DG} \cdot \Delta Q_{DG} \right)^2 \\ Q^{min}_{DG} \leq Q_{DG} + \Delta Q_{DG} \leq Q^{max}_{DG} \end{gathered} \tag{5.6}$$

This is a quadratic optimisation problem under linear constraints and therefore classified as a convex optimisation problem. Convex optimisation problems of quadratic functions have the characteristics that an optimum always exists (provided that $Q^{min}_{DG} < Q^{max}_{DG}$), that the optimum is always unique and that this optimum is always the global optimum [31].

[2] $A^{Q}_{CN,DG} - A^{Q\,col\text{-}avg}_{DG}$ is the deviation of the CM from the corresponding column means, so it's irrelevant if the CM is calculated with the slack at the HV side or at the MV side of the TF, because the constant difference of the TF's impedance contribution will be averaged out.

5.1.3 Linear Least Square

In this chapter, the problem derived above will be solved with a linear least square approach, which is only possible by neglecting the reactive power constraints. This might be possible if the reactive powers resulting from the least square approach are small enough so that they will be likely to be within the constraints given in (5.6). This would bring the big advantage that the complex optimisation procedure can be replaced by a trivial matrix operation.

5.1.3.1 Problem formulation

The optimisation problem stated in (5.6) is converted into a least square problem by setting the resulting voltage deviations from average voltage to zero

$$\overline{\Delta}U_{CN} + A_{CN,DG} \cdot \Delta Q_{DG} = 0 \tag{5.7}$$

leading to a system of N^{CN} linear equations for the N^{DG} unknown changes in reactive power. In practice there will be more CNs than DGs in the grid, because every DG connected to the grid will probably cause a CN at the feeding point, so the assumption that the linear equation system is overdetermined is reasonable. Even if it is not possible to calculate the inverse of the CM in a conventional way, several concepts exist for inverting non-quadratic matrices A, where the Moore-Penrose pseudoinverse A^+ is the most common technique [32, chap. 1]. The calculation of the Moore-Penrose inverse can be performed with several approaches, where the most common one is the singular value decomposition approach [32, chap. 6]. In practice, many mathematics and matrix toolboxes (Matlab, Maple, Mathematica, ...) offer build-in-functions for the calculation of the Moore-Penrose pseudoinverse of non-quadratic matrices.

Thus, the linear least square problem (5.7) can be solved with the pseudoinverse $A^+_{DG,CN}$ of $A_{CN,DG}$ by

$$\Delta Q_{DG} = -A^+_{DG,CN} \cdot \overline{\Delta}U_{CN} \tag{5.8}$$

5.1.3.2 Calculation Results

This approach was tested in the SS 'Lungau' in a one year simulation based on historical load profiles. For this simulation, 29 nodes from about 500 nodes in the grid were selected as potential critical nodes (topology changes were considered), and all 15 available DGs were selected to participate in voltage control[3]. The deviation of voltages in the grid from their mean value in the uncontrolled simulation is shown in fig. 5.1. The influence of the snow melting in spring, the decline of available water in summer and the occasional rise in water availability due to heavy rain in autumn as well as the general shortage of water in winter can be easily identified in this diagram.

When applying the linear least square approach to this grid situation, an enormous amount of reactive power would be needed as it is shown in fig. 5.3. The least square approach demands reactive power in the order of several MVAr from the DGs, which is unrealistic. Not only because of the fact that typical DGs' apparent power in MV grids is in the order of one MVA and the lines and the TF can't transport the resulting currents, but also because in this range the linearised model of the grid will be wrong, so the contribution matrix approach would not be applicable. If the demanded reactive powers could be applied and the concept of the CM would keep valid within this grid state change, the voltages will get very close to nominal voltage as shown in fig. 5.2.

5.1.3.3 Analysis of the Calculation Results

A tree-shaped connection schema of the CNs and DGs is given in fig. 5.4, which helps to understand the three explanations that can be given for the high amount of necessary reactive power:

[3] During the DG-DemoNet project, nine CNs (including DGs and TF) were available, and only three DGs were controlled

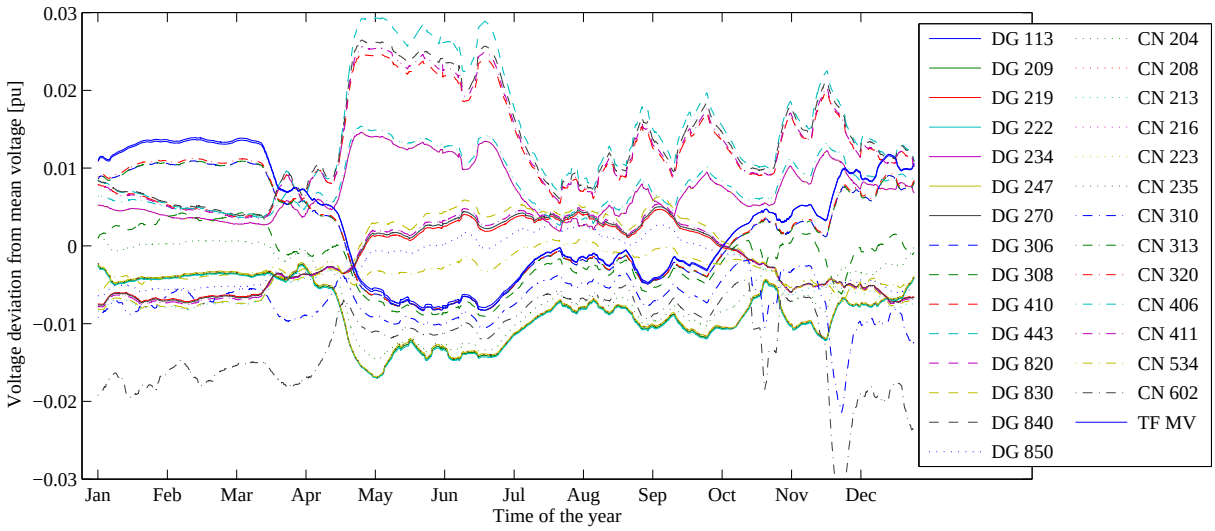

Figure 5.1: Deviations from mean voltage of SS 'Lungau' in a one year simulation without voltage control . A gliding average with a time frame of one week was performed to filter out daily and weekly oscillations. (The origin of the y-axis is the mean value of all grid voltages which varies in time, but this variation is not displayed since it can be effectively controlled by the tap-change capability of the TF)

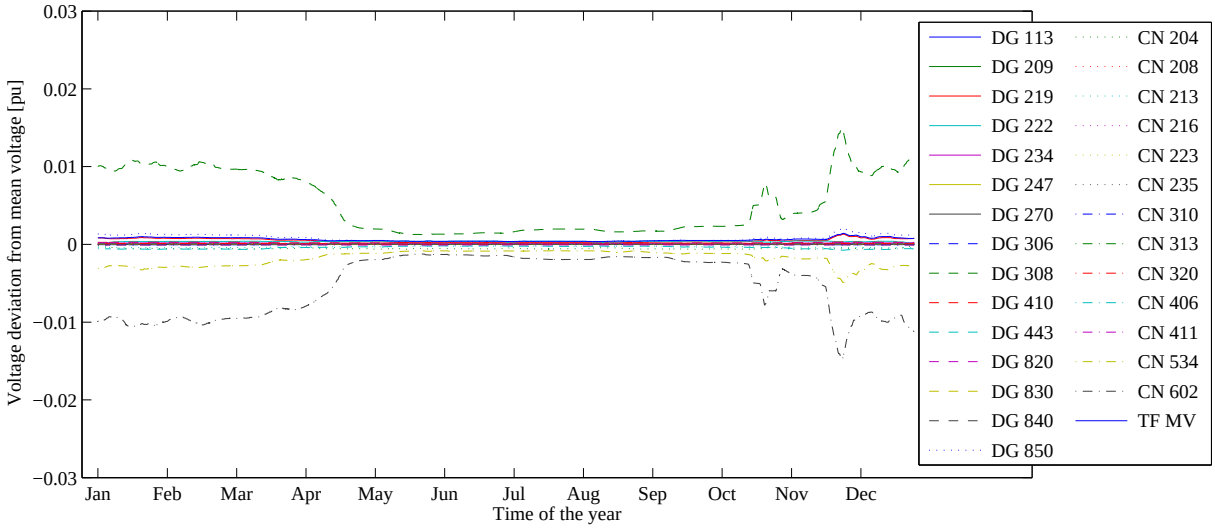

Figure 5.2: Deviations from mean voltage of SS 'Lungau' in a one year simulation with applied voltage control based on the unregularised least square approach. A gliding average with a time frame of one week was performed to filter out daily and weekly oscillations. (The origin of the y-axis is the mean value of all grid voltages, which varies in time, but this variation is not displayed since it can be effectively controlled by the tap-change capability of the TF)

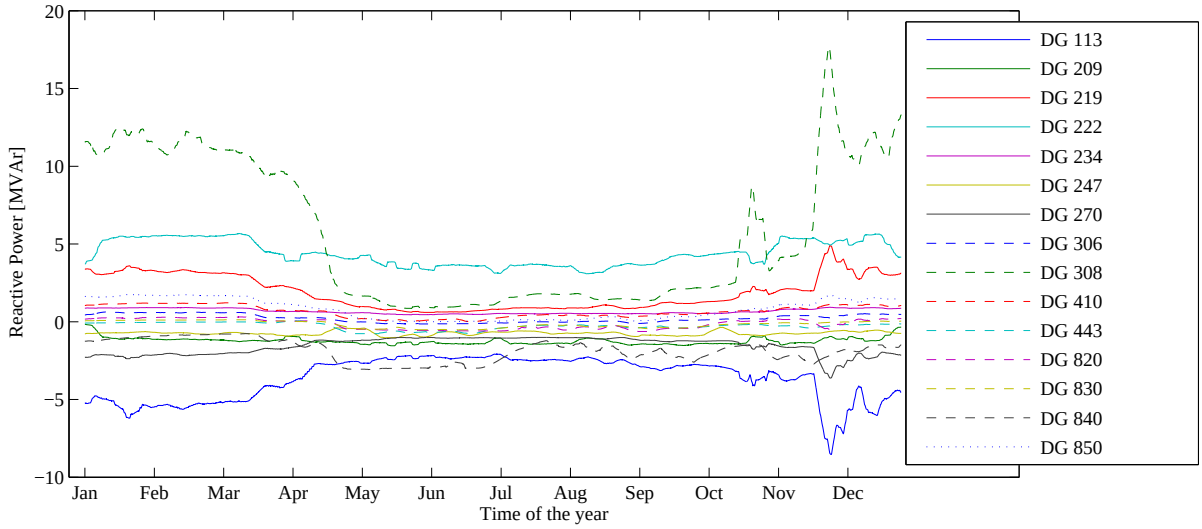

Figure 5.3: Linear least square solution for DGs' reactive power to keep voltages as good as possible at their mean voltage. For this one-year simulation in SS 'Lungau' all available DGs are utilised to participate voltage control. A gliding average with a time frame of one week was performed to filter out daily and weekly oscillations.

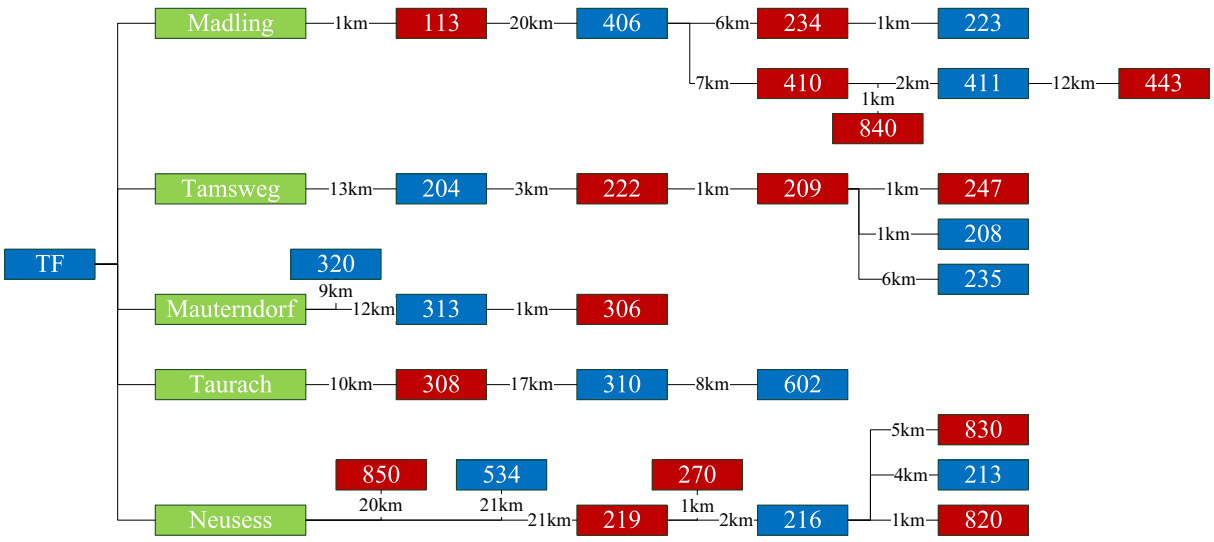

Figure 5.4: Tree-shaped connection model of the selected CNs and DGs in SS 'Lungau' in normal switching state. Since the connection point of every DG is a CN, only nodes are displayed in the model where blue nodes indicate CNs and red nodes indicate CNs with a connected DG. The green nodes specify the transformer branch names. Distances written on the connection lines specify the cable length (mostly aerial lines) between the adjacent CNs.

The extreme high amount of reactive power of DG_{308} (dashed green line) is due to the special topology of the TF branch 'Taurach', because here only one single DG is installed comparably close to the TF. In addition, ski lifts of a ski region are connected at the end of this branch (CN_{602}), making among other things voltage levels of this branch low in winter. Therefore the unregularised least square approach demands a lot of positive reactive power from the DG_{308} to rise voltage levels in this branch, leading to the situation shown in fig. 5.2, where voltage level of DG_{308} gets comparably high to lift voltage level of CN_{602}. This situation can also be interpreted as a kind of "ill conditioning" of the problem, because at the place where voltage levels are very low no DG is available to influence voltage levels. The only possibility to influence voltage is a DG comparably near at the TF, which has due to the small line impedance between TF and DG only a small contribution to the voltage at the end of the feeder. It can be modelled as shown in fig. 4.2 a) with $Z_{L1} \ll Z_{L2}$.

The second remarkable reason for the extreme high demand of positive reactive power on DG_{219}, which has a strong correlation to the negative reactive power demand on DG_{270}, can also be reasoned by the topology: DG_{219} and DG_{270} are placed at the same TF branch 'Neusess' only two kilometres away from each other. Because of this, a "voltage step" can be "build", if one DG produces masses of reactive power, which will be consumed by the other DG. In times of low generation (winter) the branch voltages are lower than TF busbar voltage, so the DGs next to the TF (DG_{219} and DG_{850}) will produce positive reactive power to lift voltage levels at CN_{534}, leading to a comparably high voltage level at DG_{219}, which will be compensated by the negative reactive power from the following DG (DG_{270}). This results in voltage levels at DG_{270} (and afterwards in the branch) are completely independent from their connection point and can be optimised "separately". This can also be seen as some kind of "ill conditioning" of the least square problem, because contribution matrix columns of DG_{219} and DG_{270} are very similar.

A similar reactive power correlation can be found between DG_{222} and DG_{209}, which are only half a kilometre away from each other.

The high reactive power demand on DG_{113} (solid blue line) is due to an adverse position for providing reactive power - it is placed only one kilometre away from the TF at the branch 'Madling', leading to the fact that it has hardly any contribution to the CNs. So the DG_{113}'s column in CM has very small entries, which leads to a line in the corresponding Moore-Penrose inverse CM with very big values. This can also be seen as an "ill conditioning" of the problem. For the voltage control approach of bringing all voltages as good as possible to nominal voltage, the DG could be excluded from voltage control without losing significant ability of voltage control.

5.1.3.4 Regularisation of the Problem

Even if it's possible to calculate optimal grid voltages very easily with the least square approach, the bad condition of the contribution matrix (this means a high linear dependency of the matrix columns) causes unrealistic high demands on reactive power. To avoid such high reactive power results the matrix can be regularised, where different regularisation approaches exist. In general, regularisation means bringing knowledge of the solution into the problem formulation. In this case the high linear dependency of the matrix columns cause a very flat minimum (many combinations of reactive power cause a similar voltage profile), which can be further classified. Due to the fact the DGs' reactive power is limited it makes sense to prefer solutions which are close to the origin in the multidimensional DG space. This means that the linear independency of the matrix columns can be increased by adding the square of every DGs' reactive power to the least square problem. This can be simply done by adding an identity matrix (scaled with a factor f) with the size of the problem (i.e. the number of DGs) at the bottom of the existing contribution matrix, so that (5.7) becomes

$$\begin{pmatrix} \overline{\Delta U}_{CN} \\ 0 \\ \vdots \\ 0 \end{pmatrix} + \begin{pmatrix} A_{CN,DG} \\ f \quad \dots \quad 0 \\ \vdots \quad \ddots \quad \vdots \\ 0 \quad \dots \quad f \end{pmatrix} \cdot \Delta Q_{DG} = 0$$

The underpart of the equation will penalize high amount of reactive power, so that the phenomenons described above will vanish.

With a penalty factor $f = 0.01$, reactive power demands decrease to 1MVAr in maximum as shown in 5.5. But the solution depends on f and no guaranteed limits for reactive power can be specified this way. Of course, grid voltage spreading will increase compared to the unregularised problem as it is shown in fig. 5.6.

5.1.3.5 Analysis of the regularised Results

In fig. 5.5 it can be seen that the highest difference to the unregularised approach is the treatment of DG_{113}, which has hardly any reactive power demand in the regularised approach. As mentioned before, it's placed very near to the TF and has therefore hardly any contribution to the CNs - in other words: The negative weighting of the DGs' reactive power is stronger than any positive effect this DG can contribute to a voltage improvement. To use this DG nevertheless, the factor f could be decreased only for this DG, but in fact this DG is not very important for this voltage control approach. In contrast to the unregularised reactive power results (fig. 5.3), the regularised reactive power results (fig. 5.5) show a typical behaviour depending on the season: The highest generation is in the late spring caused by the melting water, so nearly every DG needs negative reactive power to compensate the resulting voltage rise. The lowest generation is during winter, where many DGs need positive reactive power to compensate voltage drop.

The second remarkable thing at fig. 5.6 is that obviously voltage control is very effective in times of high generation (spring), because here the voltage rise due to active power feeding of the DGs can be easily balanced by reactive power. In winter voltage decrease due to high load can't be balanced as easily, because it typically occurs at places where no DG is nearby (in fig. 5.6 skiing lifts (among other things) cause a high load at CN_{602}, which leads to lower voltage at CN_{602} and CN_{310}, which can't be controlled because no DG is near). This shows a new aspect of coordinated voltage control, which was not mentioned before: If coordinated voltage control is performed, DGs' reactive power can not only be used for reducing voltage rise in times of high generation, but also to reduce voltage drop because of high load.

5.1.3.6 Conclusion

The stability of the unregularised problem suffers from the structure of the CM, leading to reactive power demands resulting from the least square approach which are in worst case around one order of magnitude too high. Therefore a regularization of the CM is necessary. The choice of the reactive power penalty factor $f = 0.01$ brings the reactive power demands in the right order of magnitude, but most times they are still too high for the DGs[4].

The resulting voltage *ranges* (the difference between maximal and minimal grid voltages) from the uncontrolled simulation, the least square approach and the regularised least square approach are shown in fig. 5.7: This is not a conventional boxplot, because the top edge of the boxes show the 95% percentile (and not the 75% percentile [=3. quartile] like in default boxplots) and the bottom edge of the boxes show the 5% percentile (and not the 25% percentile [1. quartile]). It is readily identifiable that with arbitrary reactive power an enormous amount of range can be freed for additional DGs, but with generator's

[4] eight from the fifteen DGs have a nominal apparent power from about 400kW and less - so the capability to deliver reactive power will be in the order of 200kVAr and less.

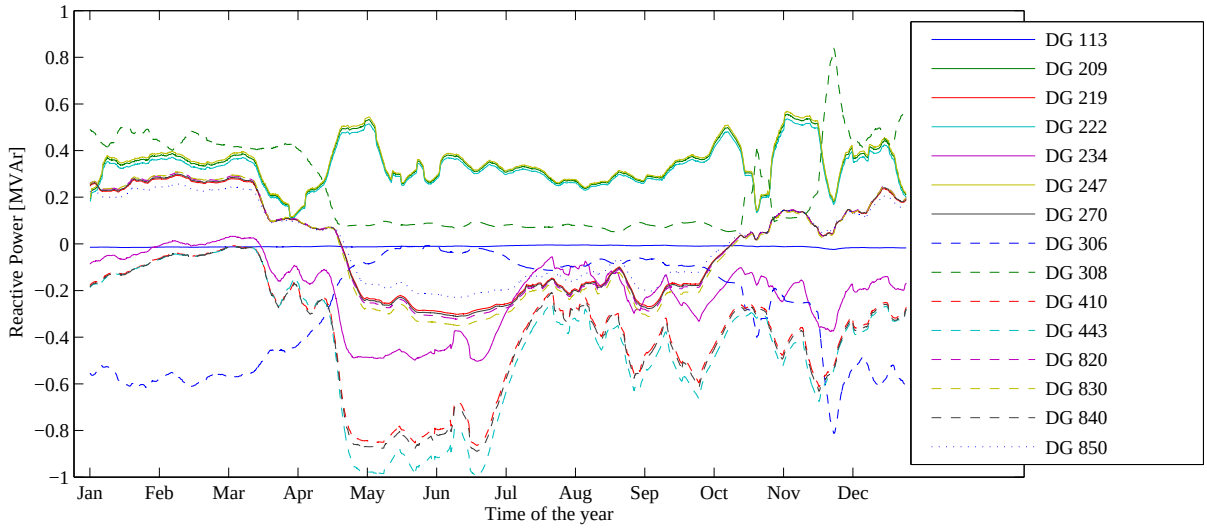

Figure 5.5: Regularised linear least square solution for DGs' reactive power to keep voltages as good as possible at their mean voltage. For this one-year simulation in SS 'Lungau' all available DGs are utilised to participate voltage control. A gliding average with a time frame of one week was performed to filter out daily and weekly oscillations.

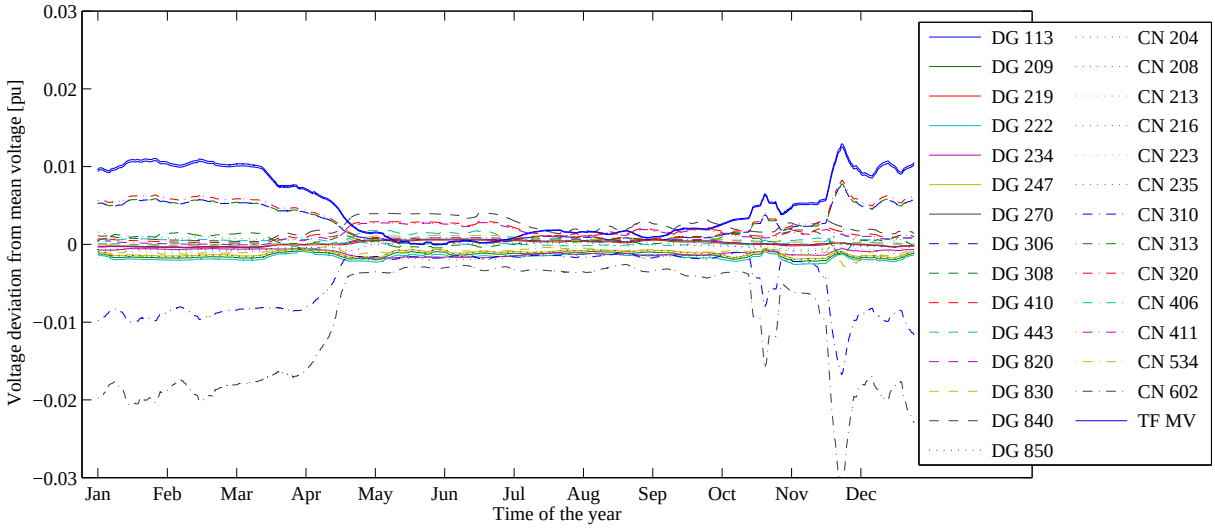

Figure 5.6: Deviations from mean voltage of SS 'Lungau' in a one year simulation with applied voltage control based on the regularised least square approach. A gliding average with a time frame of one week was performed to filter out daily and weekly oscillations. (The origin of the y-axis is the mean value of all grid voltages, which varies in time, but this variation is not displayed since it can be effectively controlled by the tap-change capability of the TF)

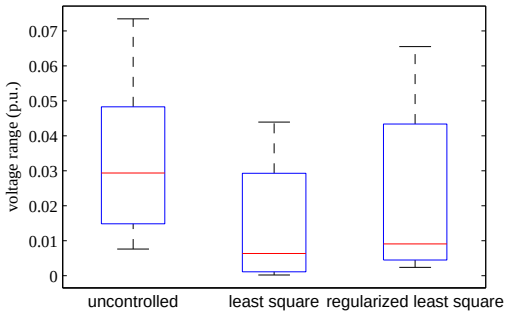

Figure 5.7: Voltage range of SS 'Lungau' in a one year simulation in comparison without voltage control, with applied voltage control based on the unregularised least square approach and based on the regularised least square approach. The top edge of the boxes show the 95% percentile, and the bottom edge of the boxes show the 5% percentile.

constraints of reactive power, the effect of range reduction is limited. Nevertheless the median of the voltage ranges can be controlled very effective, but the highest ranges occurred in the simulation cannot be controlled well with reactive power, as it can be seen in fig. 5.7.

An important characteristic of the least square approach is that every CNs' voltage violation is weighted equally (if no weighting was applied), so the number of CNs and their location in the grid can significantly alter resulting reactive powers. For example if there are several different topology changes concerning one branch, many CNs must be installed in this branch, because voltage levels have to be watched in any switching state. Supposed that these CNs are all connected to the same branch in default switching state, probably many of these CNs won't be critical in this switching state. Since the least square approach minimises the quadratic sum of all voltage deviations, the voltage deviations of these CNs will have a major share on this sum, if there are comparably less CNs in other branches. Without weighting this could lead to a result where the mentioned branch is perfectly optimised at the expense of voltage levels in other branches with only one CN for example. To solve this problem either unnecessary CNs have to be excluded or weighted depending on the topology, making the system of the least square approach unnecessarily complex.

In the next chapter voltage control concepts depending on an constrained optimisation approach are described, which are far less susceptible for unpredictable voltage violations and have no dependency on weighting parameters (this has the advantage that no further investigation has to be made to determine appropriate weighting parameter values).

5.2 Control Objectives utilising the available Voltage Band

For stable grid operation it is necessary to assure that all grid voltages are within specified limits. General limits for DS are given in [33] by $\pm 10\%$ of nominal voltage, but in practice these limits can't be utilised completely, because in [33] the general limits for low voltage grid voltages are also given by $\pm 10\%$ of nominal voltage. Since low voltage transformer typically don't have OLTC capability (the TF's transmission ratio is fixed), voltage line drop in low voltage DS has to be considered in the operation of the MV DS. Therefore, all voltages of DS nodes are kept within a range of typically 10% (e.g. $\pm 5\%$) so that 10% of range remains for voltage drop in the low voltage grid. In practice this 10%-range is further reduced to avoid operating the grid at its limits (e.g. 2%), where every unexpected deviation from scheduled operation could lead to voltage violation in the connected low voltage grid.

As described in chap. 4.1 not every DS node will be monitored, so a safety margin to the limits has to be maintained (e.g. 1%).

During the validation phase of the DG DemoNet project voltage limits were set to 0.99pu for lower-

Symbol	Unit	Description
U^{DB}/u^{DB}	kV / pu	Configured deadband of the AVC (see chap. 2.2.1.1)
U^{AVCset}	kV	Remotely configurable voltage set point for the AVC
U^{UL}/U^{LL}	kV	Voltage upper- and lower limit for voltage controller (set in agreement with the DSO)
VB	kV	Voltage band between voltage upper- and lower limit ($VB = U^{UL} - U^{LL}$)
EVB	kV	Effective Voltage Band - voltage band without the AVC's deadband ($EVB = VB - U^{DB}$)
ΔU^{tap}	kV	Voltage step height of the MV TF
U^{max}/U^{min}	kV	Actual maximal and minimal grid voltage ($U^{max} = max(U_{CN})$, $U^{min} = min(U_{CN})$)
S	kV	Actual range (spreading) between actual maximal and minimal grid voltage ($S = U^{max} - U^{min}$)
U^{TF}	kV	actual TF's MV busbar voltage
U^{set}	kV	resulting AVC's voltage set value

Table 5.1: Symbol reference for the calculation of the MV tap-change step height

and 1.05pu upper-limit in both grids 'Lungau' and 'Nenzing'.

As derived in chap. 5.1.2.6 it is reasonable to split the task of voltage control with TF and DGs into two separate controllers, which can work independently from each other. The so called *level controller* calculates the voltage set value for the TF's AVC to control voltage height in the whole DS. The so called *range controller* calculates the (re-)active power set values for the DGs to control the relative voltage difference between the nodes among each other. When having the freedom to operate the DS anywhere within the specified voltage limits, different control objectives can be pursued, which will be described in the following chapters. Simulation results of these concepts will be compared in chap. 6.

5.2.1 Voltage Level Control by utilising the MV Transformer

Depending on the relation between the actual range of all CN voltages and the given voltage limits, the AVC's voltage set value can be calculated according to different strategies. These strategies can only cause different tap positions, if there exists multiple tap positions where all grid voltages are kept within their limits. But it has to be considered that TF's tap position is not directly controlled, because controlling of the TF's OLTC is done by the AVC (see chap. 5.1.2).

5.2.1.1 The Effective Voltage Band (EVB)

In the calculation of AVC set values it has to be considered that the TF's busbar voltage can differ up to the half of the AVC's deadband $U^{DB}/2$ from the AVC voltage set value U^{set}, because the AVC will only perform a tap-change if the TF busbar voltage U^{TF} is outside the range of $U^{set} \pm U^{DB}/2$ (see chap. 2.2.1.1).

To assure that no grid voltage will violate the limits given by U^{UL} (UL ... upper limit) and U^{LL} (LL ... lower limit), U^{set} can't become higher than $U^{UL} - U^{DB}/2$ or lower than $U^{LL} + U^{DB}/2$, because then it's guaranteed that the AVC will tap down if $U^{TF} > U^{UL}$ and tap up if $U^{TF} < U^{LL}$. Therefore it is absolutely necessary that the spreading of all grid voltages $S = \max_{CNs}(U_{CN}) - \min_{CNs}(U_{CN})$ (including the TF as CN) has to be smaller than the given voltage band $VB = U^{UL} - U^{LL}$, so $S < VB$, because otherwise there will be no tap position where all nodes are within the given limits. Due to the fact voltage levels can only be altered in discrete voltage steps ΔU^{tap}, it is necessary that $S < VB - \Delta U^{Tap}$, so that theoretically there will be a tap position where no limits are exceeded. When considering the AVC's deadband it's clear that a permanently stable and robust grid operation will only be possible if $S < VB - U^{DB}$, because then it will be possible to maintain the deadband margin of $U^{DB}/2$ to U^{UL} and U^{LL} for every voltage set value. This introduces in addition to the voltage band VB the effective voltage band:

$$EVB = VB - U^{DB} = \left(U^{UL} - U^{LL}\right) - U^{DB}$$

5.2.1.2 Level Control Modes for Normal Grid Operation

When the actual grid situation allows a range of possible AVC set values, which is the case when $S < EVB$, different level control strategies can be operated:

Upper-Limit It can make sense to operate the DS with all voltages being as high as possible, so that the AVC will tap up as soon as it is risklessly possible without bringing one CN into overvoltage. This has the benefit to reduce line losses in grids with constant PQ-loads, because line current is reduced.

By knowing all actual CN voltages U_{CN} and the actual TF's busbar voltage U_{TF}, this can be accomplished by aligning the TF set value U^{set} at the highest possible voltage $U^{UL} - U^{DB}/2$ reduced by the voltage difference between the highest voltage of all CNs $U^{max} = \max_{CNs} U_{CN}$ and the TF busbar voltage U^{TF}:

$$U^{set}_{upper\text{-}limit} = U^{UL} - U^{DB}/2 - (U^{max} - U^{TF}) \tag{5.9}$$

Lower-Limit Contrariwise it can make sense to operate the DS with all voltages being as low as possible, so that the AVC will tap down as soon as risklessly possible without bringing a CN into undervoltage. This has the benefit to reduce line losses in grids with constant impedance-loads (which is typically not the case in practice), because line current is reduced. The voltage set value can be calculated like in (5.9) with the minimal voltage of all actual CN voltages $U^{min} = \min_{CNs} U_{CN}$:

$$U^{set}_{lower\text{-}limit} = U^{LL} + U^{DB}/2 + (U^{TF} - U^{min}) \tag{5.10}$$

Centered Furthermore it can make sense to maximise the safety margin of the highest and the lowest CNs to the voltage limits, which means that all CNs are placed centred in the available voltage band. This will maximise operation safety and power quality and it might be a good compromise in grids with constant-PQ loads (e.g. switching power supplies) and constant-impedance loads (e.g. all kinds of resistive heaters).

Here, both U^{max} and U^{min} have to be considered, which are contained in $S = U^{max} - U^{min}$:

$$U^{set}_{Centered} = U^{UL} - (VB - S)/2 - (U^{max} - U^{TF}) = \frac{U^{UL} + U^{LL}}{2} + \left(U^{TF} - \frac{U^{max} + U^{min}}{2} \right) \tag{5.11}$$

The difference between (5.11) and (5.4) consists in the fact that in (5.4) the mean voltage deviation is corrected, while in (5.11) only the boundary values are considered. If the CNs are reasonably uniformly distributed in the DS, so that every CN is an accumulation of nearly the same number of real grid nodes, (5.4) could be better suitable for performing a centred operation mode. In practice, every CN is a result of a different number of grid nodes, so (5.4) would have to be replaced by a weighted sum to keep the approach of considering all CNs for mean value calculation meaningful. (5.11) is independent from these considerations and it leads to an equal safety margin to lower- and upper-limit, which is more robust if voltage measurements are reliable. (5.4) has the big advantage that a blackout of one CN measurement won't produce a big voltage change in AVC's set value, but it has the big withdraw that voltage violation can't be ruled out with guaranty (imagine one single voltage outlier which has only a proportionate change to alter the sum). In general (5.11) can be considered as the more practical approach to run the grid voltages power-quality optimised.

Minimum-Tapping To save the amount of necessary tap-changes, it can also make sense to calculate AVC's set values in a way that it will only perform a tap-change if it's needed to avoid voltage violation. This strategy can significantly reduce the amount of necessary tap steps, while line losses won't be optimised.

If all grid nodes are far enough away from the voltage limits, so that under consideration of the AVC's deadband no voltage violation will occur, the voltage set value will be the actual TF's voltage measurement value, so the deadband is always centred around the measurement value. If the voltages

in the grid come near to a limit, the voltage set point is calculated like in level control mode upper-limit (5.9) or lower-limit (5.10):

$$U^{set}_{minimum\text{-}tapping} = \begin{cases} U^{set}_{upper\text{-}limit} & U^{max} > U^{UL} - U^{DB}/2 \\ U^{set}_{lower\text{-}limit} & U^{min} < U^{LL} + U^{DB}/2 \\ U^{TF} & \text{else} \end{cases} \tag{5.12}$$

5.2.1.3 Level Control Mode for Times with a high Voltage Spreading

When it comes to situations where $S > EVB$, continuing with the operation of the level control modes listed above could lead to voltage violations. Operation in upper-limit mode causes all grid nodes to be aligned at the voltage upper-limit, but when $S > EVB$ undervoltage can occur. This can be considered as less critical than operating in lower-limit, where $S > EVB$ could lead to overvoltage (overvoltage reduces the lifetime of the electrical infrastructure[5]). So if $S > EVB$, the level control mode should be set to upper-limit to avoid overvoltage, but a possible undervoltage has to be accepted.

Set value continuity The change in level control mode (when $S < EVB$ changes to $S > EVB$) must not lead to a discontinuous AVC set value, because as explained in chap. 5.1.2, continuous changes in grid measurements must not lead to discontinuous changes in controller set value outputs, which is more critical for the AVC set value than for the DGs. Set value continuity can be shown for evaluating (5.9) - (5.12) for $S = EVB$, where all four control modes must return the same voltage set value[6].

Upper-Limit-Extended When simply changing level control mode to upper-limit if $S > EVB$, it can easily happen that the grid gets into an undervoltage situation, where an up-tapping would be possible but won't be performed. This situation will be described by the following example:

Consider a spreading of grid voltages which is slightly bigger than the effective voltage band, so $\varepsilon > 0$ in $S = EVB + \varepsilon > EVB$: If in addition to this the maximum grid voltage is close before the value where an up-tapping would be performed, so $\Delta > 0$ in $U^{max} = U^{UL} - U^{DB} + \Delta$, then the voltage lower limit can be violated because $U^{max} - U^{min} = (U^{UL} - U^{LL}) - U^{DB} + \varepsilon$, so $(U^{UL} - U^{LL}) - U^{DB} + \varepsilon + U^{min} = U^{UL} - U^{DB} + \Delta$ which can be simplified to $U^{min} = U^{LL} + \Delta - \varepsilon$. The AVC will perform a tap-change if $\Delta \leq 0$, so if $0 < \Delta < \varepsilon$ undervoltage will occur. Depending on the relation between tap-change height ΔU^{tap} and the configured AVC's deadband U^{DB}, up-tapping will be possible if $U^{max} < U^{UL} - \Delta U^{tap}$ to avoid undervoltage.

This situation is illustrated in fig. 5.8 a) and b), where all possible grid situations (this means all possible values for U^{min} and U^{max} that fulfil $S = EVB + \varepsilon$) and their resulting TF set value (U^{set}) are shown. In fig. 5.8 a) $\varepsilon = 0$ (so $S = EVB$), therefore the voltage set point U^{set} is constant, as it is shown in the upper diagram. The AVC will perform a tap-change if the U^{TF} value crosses the U^{DB}-borders[7], leading to resulting grid voltages shown in the lower diagram (in this example $\Delta U^{Tap} = U^{DB}/2$ is assumed), so it's clear that no voltage violation will occur. In fig. 5.8 b) $\varepsilon > 0$, and if the conventional level control mode upper-limit would be operated, U^{set} would keep constant too. Again, the AVC will perform a tap-change at the crossing of U^{TF} with the U^{DB}-borders, but as it can be seen in the lower diagram that this is too late, because undervoltage occurs in the range between the two red dotted vertical

[5] Several items of protection equipment are installed in the grid to prevent overvoltages with their trigger point being significantly higher than the voltage limits given for voltage control.

[6] To show that lower-limit set value becomes the same as the upper-limit set value when $S = EVB$, inserting from $S = U^{max} - U^{min} = VB - U^{DB} = (U^{UL} - U^{LL}) - U^{DB}$ the minimal grid voltage $U^{min} = U^{max} + U^{DB} - (U^{UL} - U^{LL})$ into (5.10) leads to $U^{set}_{lower\text{-}limit} = U^{LL} + U^{DB}/2 + U^{TF} - U^{max} - U^{DB} + U^{UL} - U^{LL}$, which is the same as (5.9).

The same can be done for the centered operation mode by inserting $S = VB - U^{DB}$ into (5.11), which also produces the same value as (5.9).

For the minimum-tapping mode (5.12) nothing has to be done any more, because when $S = VB - U^{DB}$, either $U^{max} \geq U^{UL} - U^{DB}/2$ or $U^{min} \leq U^{LL} + U^{DB}/2$ (This can be proved by $U^{max} + U^{DB} - (U^{UL} - U^{LL}) = U^{min} \leq U^{LL} + U^{DB}/2$, which can be simplified to $U^{max} \leq U^{UL} - U^{DB}/2$, so in any case the "else"-case in (5.12) won't be chosen.)

[7] Here the inverse time characteristic of the AVC is neglected.

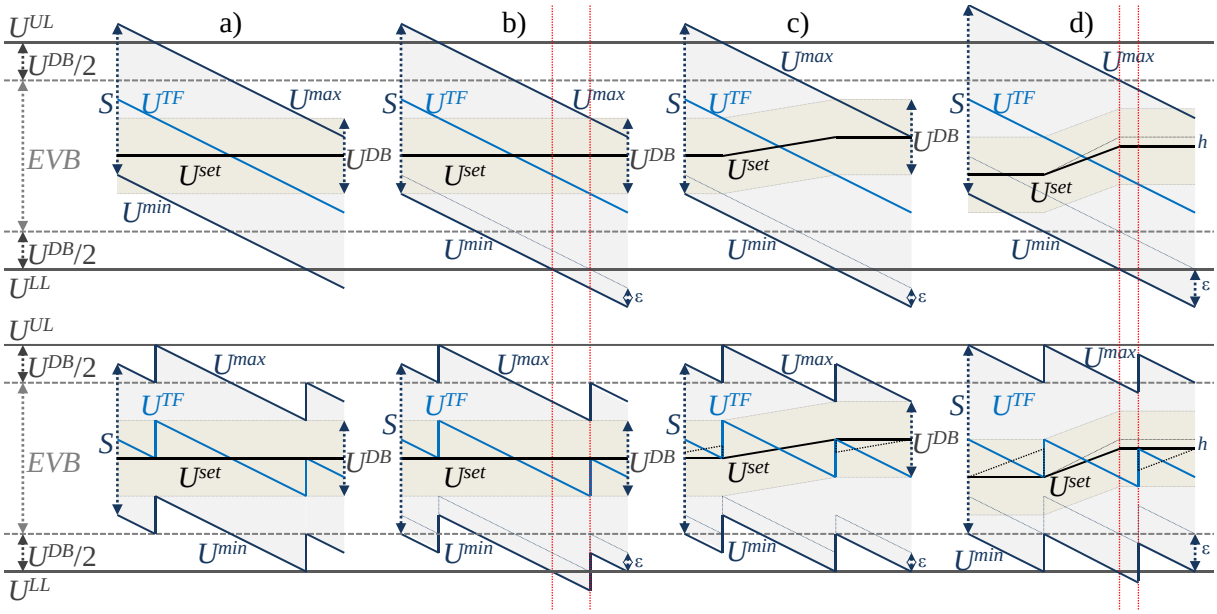

Figure 5.8: Different grid situations represented by different combinations of U^{min} and U^{max} with the correspondent voltage set values U^{set}: a) $S = EVB$ and level control mode upper-limit / lower-limit / centered / minimum-tapping; b) $EVB < S < VB - \Delta U^{tap} - h$ and level control mode upper-limit; c) Same spreading as in b) with level control mode upper-limit-extended; d) $S > VB - \Delta U^{tap} - h$ and level control mode upper-limit-alignment. The upper diagrams show the grid situation and the controller response, the lower diagram show the grid situation after application of the controller response (here $\Delta U^{tap} = U^{DB}/2$ is assumed). Detailed explanation is given in the text.

lines. This is because the upper-limit mode does only consider the maximum grid voltage and doesn't bother about the minimum grid voltage.

If ε is small enough in situations with $U^{min} < U^{LL}$ so that up-tapping would be possible without leading to overvoltage, up-tapping can be performed by calculating the AVC's set value according to (5.10) like in lower-limit – but only if the resulting maximal voltage after the tap-change is far enough away from the U^{UL}, so that hunting (see chap. 2.2.1.1) will be avoided. This will be done by introducing the hysteresis h, so up-tapping will be performed if $U^{min} < U^{LL}$ and $U^{max} + \Delta U^{tap} < U^{UL} - h$. Therefore, undervoltage can be avoided for ranges $S < VB - \Delta U^{tap} - h$ and therefore $0 < \varepsilon < U^{DB} - \Delta U^{tap} - h$.

Again, it is very important that static changes in grid voltages lead to static changes in controller output, so the set values of the normal upper-limit and the "lower-limit-extension" for $U^{min} < U^{LL}$ will be linearly interconnected as it is shown in fig. 5.8 c). This figure shows the same grid situations as fig. 5.8 b), but here U^{set} is not constant anymore and rises for lower grid voltages, so undervoltage can be avoided because up-tapping will be performed earlier as show in the lower diagram of fig. 5.8 c). The dotted U^{set}-lines in the lower diagram show the voltage set values which would result in the next control cycle after the tap-change was performed.

The set value in this upper-limit-extended mode is calculated in three cases:

$$U^{set}_{upper\text{-}limit\text{-}extended} = \begin{cases} U^{set}_{upper\text{-}limit} & U^{max} > U^{UL} \\ U^{set}_{lower\text{-}limit} & U^{min} < U^{LL} \\ U^{UL} - U^{DB}/2 + (S - EVB)\frac{U^{UL} - U^{max}}{VB - S} - (U^{max} - U^{TF}) & \text{else} \end{cases} \tag{5.13}$$

This function is continuous in its three cases[8] and continuous in the level control mode change at

[8]It can be easily proven that for $U^{max} = U^{UL}$ the third case of 5.13 will become the same as the first case, because the third summand of the third case vanishes due to $U^{UL} - U^{max} = 0$. On the other hand, if $U^{min} = U^{LL}$, the third case has to be

$S = EVB$[9].

Summing up, the level control mode upper-limit-extended was introduced to avoid undervoltage in situations where $EVB < S < VB - \Delta U^{tap} - h$ (h is the hysteresis to avoid hunting). This was done by combining the level control mode upper-limit for $U^{max} > U^{UL}$ with the control mode lower-limit for $U^{min} < U^{LL}$, and in between the set values of both level control strategies were linearly interconnected to assure continuous controller output in continuous grid situations.

Upper-Limit-Alignment If $S > VB - \Delta U^{tap} - h$, undervoltage can't be avoided anymore, because if $U^{min} = U^{LL}$ up-tapping would lift $U^{max} = U^{min} + S > U^{min} + VB - \Delta U^{tap} - h = U^{LL} + VB - \Delta U^{tap} - h = U^{UL} - \Delta U^{tap} - h$ too near to overvoltage, which could cause down-tapping in the next control cycle and could lead to hunting.

So when $S > VB - \Delta U^{tap} - h$, the only thing which can be done is watching the maximal grid voltage. If it becomes $U^{max} \leq U^{UL} - \Delta U^{tap} - h$, up-tapping can be performed, which means that in this situation the AVC's voltage set value has to be calculated in a way that $U^{set} = U^{TF} + U^{DB}/2$. On the other hand, overvoltage has to be avoided as it is done in (5.13) and (5.9), so both strategies can be again interconnected with a linear function, leading to

$$U^{set}_{ul\text{-}alignment} = \begin{cases} U^{set}_{upper\text{-}limit} & U_{max} > U_{UL} \\ U^{UL} - \Delta U^{tap} + U^{DB}/2 - h - (U^{max} - U^{TF}) & U_{max} < U_{UL} - (\Delta U^{tap} + h) \\ U^{UL} - U^{DB}/2 + (U^{DB} - \Delta U^{tap} - h)\frac{U^{UL} - U^{max}}{\Delta U^{tap} + h} - (U^{max} - U^{TF}) & else \end{cases} \tag{5.14}$$

This is also shown in fig. 5.8 d), which shows grid situations with a higher spreading than in 5.8 b) and c). The thin dotted U^{set}-line in the upper diagram shows the U^{set}-values for $h = 0$, so it can be seen that the set values without hysteresis are reduced by h to avoid hunting. In the lower diagram the dotted U^{set}-line shows the U^{set} values which would result in the next control cycle if the tap-change was performed. The decrease of h increases the difference of the dotted U^{set}-line to the solid U^{set}-line, which will lead to hunting if this difference gets close to ΔU^{tap}. The undervoltage marked by the red dotted vertical lines in fig. 5.8 d) cannot be prevented any more.

Of course (5.14) has to become the same as (5.13) when $S = VB - \Delta U^{tap} - h$[10].

Summing up, the level control mode upper-limit-alignment was introduced to avoid overvoltage and hunting when operating upper-limit-extended in times of very high voltage ranges. While the range S in upper-limit-extended is small enough so that this level control mode can keep all voltages within their limits, upper-limit-alignment has to cope with voltage ranges that are too big to fit into the given voltage band in any case. Whether the range can be hold within the limits or not does not only depend on the voltage range S, but also on the nominal tap-change height ΔU^{tap} (the smaller the tap-change height is, the easier it is to keep all voltages within their limits).

Finally, the improvement in voltage control is directly shown in fig. 5.9, which shows a comparison of grid simulation with and without the extension for high voltage ranges. In the upper diagram grid voltages

---

rearranged:
$U^{UL} - U^{DB}/2 + (S - EVB)(U^{UL} - U^{max})/(VB - S) - (U^{max} - U^{TF}) =$
$U^{UL} - U^{DB}/2 + (S - (VB - U^{DB}))(U^{LL} + VB - U^{min} - S)/(VB - S) - (U^{max} - U^{TF}) =$
$U^{UL} - U^{DB}/2 + S - VB + U^{DB} - U^{max} + U^{meas} = U^{LL} + U^{DB}/2 + (U^{TF} - U^{min}) = U^{set}_{lower\text{-}limit}$,
so also in this case the third case of (5.13) becomes the same as the second case.

[9] For $S = EVB$ (5.13) becomes the same as (5.9) - (5.12), which can be easily seen as the third summand in the third case vanishes again due to $S - EVB = 0$.

[10] The second case can be rearranged with $U^{UL} = U^{LL} + VB$ and $U^{max} = U^{min} + S$ to
$U^{LL} + VB - \Delta U^{tap} + U^{DB}/2 - h - (U^{min} + S - U^{TF}) =$
$U^{LL} + VB - \Delta U^{tap} + U^{DB}/2 - h - U^{min} - VB + \Delta U^{tap} + h + U^{TF} = U^{set}_{lower\text{-}limit}$.
The third case in (5.14) can also be easily matched to the third case in (5.13) by simply replacing the first bracket $U^{DB} - \Delta U^{tap} - h = S - VB + U^{DB} = S - EVB$ and the denominator $\Delta U^{tap} + h = S - VB$.
The third case in (5.14) is continuous with the first case at $U^{max} = U^{UL}$ because the numerator in the third case vanishes at $U^{max} = U^{UL}$, and the third case is continuous with the second case at $U^{max} = U^{UL} - (\Delta U^{tap} + h)$, which can be simply calculated by replacing the U^{max} in the numerator with the boundary value.

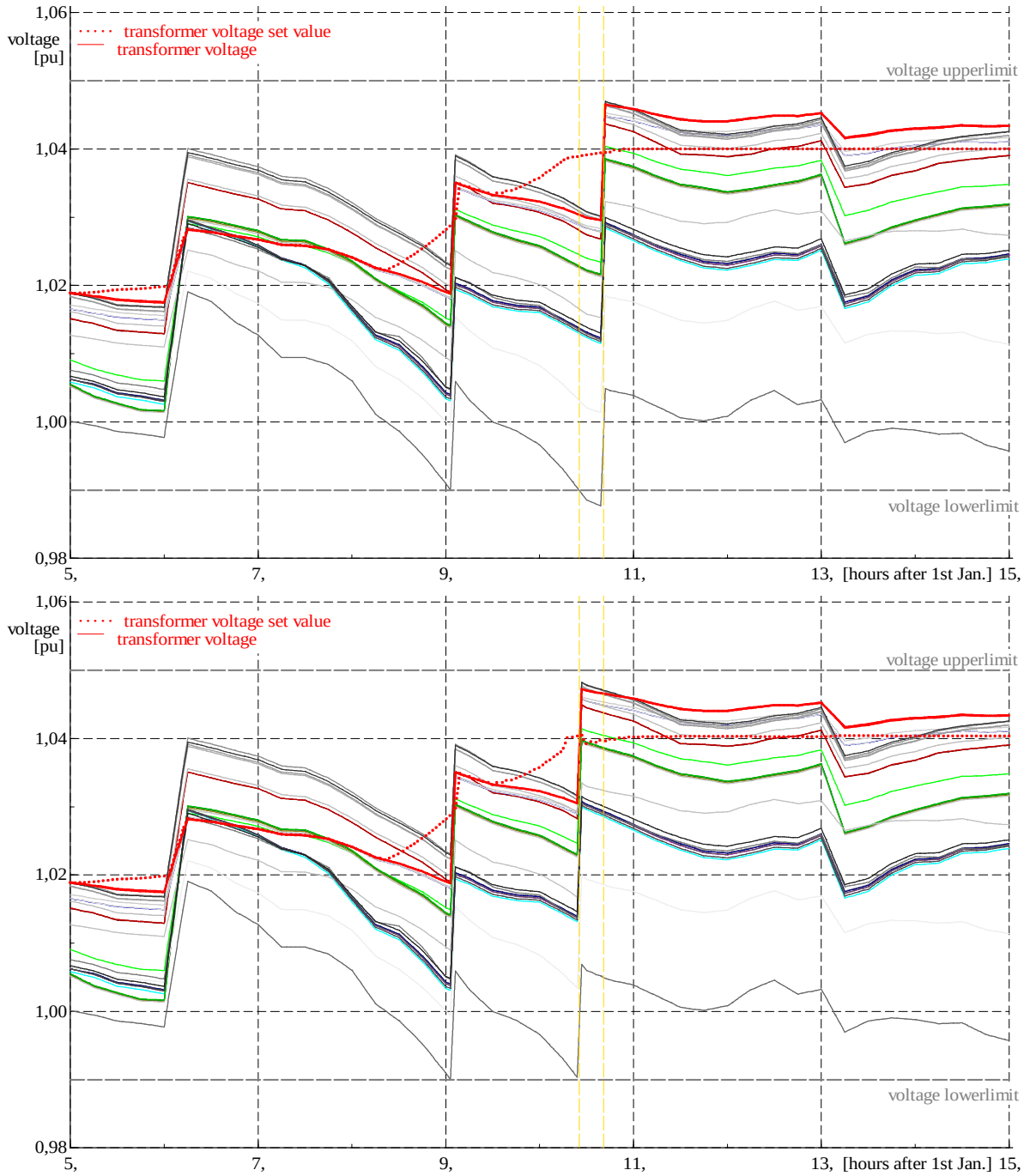

Figure 5.9: Comparison of a grid situation controlled by level control mode upper-limit (above) and controlled by level control mode upper-limit-extended (below) without having any DG controlled. The main difference in set point calculation can be seen shortly before undervoltage occurs (marked by the yellow lines). Voltage limits dashed grey, TF's busbar voltage red, voltage setpoint dotted red.

Symbol	Unit	Description
Q_{DG}	MVAr	Actual reactive power of the DG with the index *DG*
ΔQ_{DG}	MVAr	Change in reactive power of the DG with the index *DG* (parameter for the optimisation problem)
$Q_{DG}^{min/max}$	MVAr	Minimal / Maximal reactive power the DG with the index *DG* can provide.
$A_{CN,DG}^{Q}$	kV/MVAr	Reactive power contribution matrix
EVB	kV	Effective Voltage Band - voltage band without the AVC's deadband ($EVB = VB - U^{DB}$)
U_{CN}	kV	Actual Voltage at the CN with the index *CN*
$A_{CN,DG}^{P}$	kV/MW	Active power contribution matrix
Q^{TF}	MVAr	Actual reactive power flow over the TF
$Q^{desired}$	MVAr	Desired value of reactive power as the target value of the optimisation process
$B_{line,DG}^{Q}$	1	Adjacency matrix that contains information which DG is connected behind which line
$Q_{line}^{desired}$	MVAr	Desired value of reactive power at the line with the index *line*
Q_{line}^{meas}	MVAr	Actual reactive power flow over the line with the index *line*

Table 5.2: Symbol reference for the formulation of the reactive power objective functions

violate the given voltage limits because the conventional upper-limit "does not recognise" that up-tapping would be possible without coming into overvoltage. In the lower diagram the voltage violation can be improved by setting a slightly increased voltage set value in times of low grid voltage, leading to an earlier up-tapping and to the prevention of undervoltage.

5.2.2 Voltage Range Control by utilising the controllable DGs

In contrast to the voltage control algorithm based on the linear least square approach, which always minimises the voltage deviation to the voltage mean value, the voltage control approaches proposed in this chapter will use the whole available EVB (defined in chap. 5.2.1.1) to follow different objectives[11]. These objectives are of different complexity and require different information from the grid. They all have in common that they try to restrict the voltage range to values smaller than the EVB, so that the TF will always find a tap position to keep all voltages within the given voltage band. If it is not possible to keep all grid voltages within a range smaller than the EVB, all control algorithm have to find the minimal range that is possible in the actual grid situation within the available DGs' reactive power contributions.

5.2.2.1 Mathematical Analysis of the upcoming Problem

The controllable reactive power of n_{DG} DGs form a n_{DG}-dimensional Euclidean space, where the reactive power limitations of the generator limit every single dimension by a maximum and a minimum. Therefore the n_{DG}-dimensional form of the set of possible operation points is a hyper-rectangle.

The grid voltages of n_{CN} grid voltages measurements also form a n_{CN}-dimensional Euclidean space, where the valid operation range of the grid limit every single dimension by the grids voltage lower- and upper-limit. Therefore the n_{CN}-dimensional form of the set of valid grid states is a hypercube (supposed that grid voltage requirements are equal at every CN in the grid - otherwise it is a hyper-rectangle too).

The linear transformation between this two spaces is given by the reactive power contribution matrix, which transforms changes in the n_{DG}-dimensional reactive power space (DG space) into the n_{CN}-dimensional voltage space (CN space) by $\Delta U_{CN} = A_{CN,DG}^{Q} \cdot \Delta Q_{DG}$ (symbol explanations in table 5.2).

With this linear transformation it is possible to transform the grid voltage limitations from the n_{CN}-dimensional CN space into the n_{DG}-dimensional DG space. Assuming that voltage limits can be written as $\Delta U_{CN}^{min} < \Delta U_{CN} < \Delta U_{CN}^{max}$, voltage limitations in the DG space would look like $\Delta U_{CN}^{min} < A_{CN,DG}^{Q} \cdot \Delta Q_{DG} < \Delta U_{CN}^{max}$. This would transform the valid area in the CN space, which is a hypercube, into a parallelotope[12] in the DG space. The intersection of the set of valid generator states $Q_{DG}^{min} < Q_{DG} +$

[11] The last stated approach (chap. 5.2.2.6) does not use the whole EVB, because it tries to minimise the voltage range.

[12] also called hyper-parallelepiped

$\Delta Q_{DG} < Q_{DG}^{max}$ and the set of valid grid states $\Delta U_{CN}^{min} < A_{CN,DG}^{Q} \cdot \Delta Q_{DG} < \Delta U_{CN}^{max}$ form the solution set. Since both sets are convex, the solution set is convex too. Generally the solution set will have the form of a convex polytope. Any solution ΔQ_{DG} which is inside the convex solution set represents a valid grid- and DG-state. The aim of the objective function is to find the solution ΔQ_{DG}^{opt} inside the solution set, which represents the optimum according to the respective control strategy.

In principle it would be also possible to transform the reactive power limitations from the n_{DG}-dimensional DG space into the n_{CN}-dimensional CN space. Therefore it is necessary to calculate the inverse of the contribution matrix (see chap. 5.1.3.1), which does not lead to a unique result, since the column vectors of the contribution matrix can be linear dependent (especially when two DGs are connected to the same CN). Solving the problem this way leads to an optimal point ΔU_{CN}^{opt} in the grid voltage space, which would have to be transformed to an optimal point in the reactive power space similar to (5.8). In general the approach to solve the problem in the DG space is more straight-forward, therefore no further investigation will be made in solving the problem in the CN space.

Due to the assumption that the DGs control the voltage *range* and the TF controls the voltage *height* (stated in chap. 5.1.2.6), the *absolute* operational limits of the grid voltages given by the voltage lower- and upper-limit are not relevant and have to be replaced by *relative* limits that represent the requirement that the voltage range has to be smaller than the effective voltage band:

$$\max\left(U_{CN} + A_{CN,DG}^{Q} \cdot \Delta Q_{DG}\right) - \min\left(U_{CN} + A_{CN,DG}^{Q} \cdot \Delta Q_{DG}\right) < EVB$$

This would replace the $2n_{CN}$ constraints of voltage upper and lower limit by one single constraint, but this single constraint is non-linear. This means it will be hard to tell which form the set of the valid grid operations will have in the CN space and showing convexity is not trivial any more. Furthermore it is much more complex to solve optimisation problems under non-linear constraints than under linear constraints. Therefore it is reasonable to transform the single non-linear constraint into $n_{CN}(n_{CN}-1)$ linear constraints by replacing the max and the min function by all possible combinations of voltages: $\max(x_i) - \min(x_i) < c$ is equivalent to $x_i - x_j < c \; \forall i, j = 1...n$, but the combination $i = j$ does not have to be proven. This leads to $(U_{CNi} + A_{CNi,DG}^{Q} \cdot \Delta Q_{DG}) - (U_{CNj} + A_{CNj,DG}^{Q} \cdot \Delta Q_{DG}) < EVB \; \forall i, j \in 1...n_{CN} \; i \neq j$. Even though the number of voltage constraints increase quadratically with the number of CNs, the problem is nevertheless easier to solve than with one single non-linear constraint.

This set of linear inequalities defines a convex polytope in the DG space, because every inequality defines a valid half-space $(A_{CNi,DG}^{Q} - A_{CNj,DG}^{Q}) \cdot \Delta Q_{DG} < EVB - (U_{CNi} - U_{CNj})$, and the intersection of a finite number of half-spaces is a convex polytope. The voltage range constraints do not have a defined shape in the CN space, because it depends on the DGs' reactive power, and a change in reactive power will change the voltage constraints.

The change from absolute limits in the CN space to relative limits, which have a linear dependency on the DG space, does only change the form of the valid area in the CN space, but the form of the solution set in the DG space remains a convex polytope.

Based on these considerations, different voltage control strategies are defined in the following chapters and their objective functions are stated. The objective function is used to find in the solution set (that is shaped as a convex polytope) the optimal point that corresponds to the control strategies aim.

5.2.2.2 Minimise the Reactive Power Contribution of the controllable DGs

Simulation *mode G* (see tab. 6.2): This control strategy drives all DGs at $cos\varphi = 1$ when the grid situation allows it. In situations where the voltage range exceeds the EVB it uses as little reactive power as possible to bring the voltage range back to EVB. This control strategy has the smallest impact on the grid, because reactive power will be used only when it's needed for voltage control.

Mathematical formulation This control strategy can be formulated as a non-linear optimisation problem under linear constraints:

$$\begin{gathered}\min_{\Delta Q_{DG}} \sum_{DGs} |Q_{DG} + \Delta Q_{DG}| \\ Q_{DG}^{min} \leq Q_{DG} + \Delta Q_{DG} \leq Q_{DG}^{max} \\ \max\left(U_{CN} + A_{CN,DG}^{Q} \cdot \Delta Q_{DG}\right) - \min\left(U_{CN} + A_{CN,DG}^{Q} \cdot \Delta Q_{DG}\right) < EVB\end{gathered} \tag{5.15}$$

Q_{DG} are the actual DGs' reactive powers, and ΔQ_{DG} are the changes in reactive powers, which are the multidimensional constrained parameters of the optimisation problem. $Q_{DG}^{min} = Q_{DG}^{min}(P_{DG})$ and $Q_{DG}^{max} = Q_{DG}^{max}(P_{DG})$ are the reactive power limits the DGs can provide in their actual operation state (depending on their actual active power P_{DG} and their PQ operation diagram). U_{CN} are the actual grid voltages and $U_{CN} + A_{CN,DG}^{Q} \cdot \Delta Q_{DG}$ are the new voltages which will appear in the grid according to the reactive power contribution matrix $A_{CN,DG}^{Q}$ when all DGs have executed the new reactive powers $Q_{DG} + \Delta Q_{DG}$.

Since the constraints form a convex polytope and the abs-function is convex [31, chap. 3] too, this problem is classified as a non-linear optimisation problem under linear constraints, which always has an optimum that is unique and if an optimum is found, it is always the global optimum [31, chap. 4.2.2 and 3.2].

Comparison between the absolute and the quadratic minimisation function As it is the optimisation algorithm's goal to find the combination of DGs' reactive power where as little reactive power as possible will be needed, it is clear that the DGs with the highest reactive power contribution according to the contribution matrix cells will be used to prevent voltage range violation. This fact will be illustrated at the following example:

Consider a simple grid with only one feeder and two DGs connected to this feeder, leading to a CN at the TF busbar, one CN at the first DG and one CN at the second DG. An exemplary CM for this grid is shown beside.

A^Q	DG_1	DG_2
CN_{TF}	0	0
CN_1	0.01	0.01
CN_2	0.01	0.02

Assuming $EVB = 0.04$pu and $U^{example1} = \begin{pmatrix} 1.000 \\ 1.021 \\ 1.042 \end{pmatrix}$pu, voltage range is 0.042pu $> EVB$, so the absolute optimisation function will return a change in reactive power of $\Delta Q^{example1} = \begin{pmatrix} 0 \\ -0.1 \end{pmatrix}$MVAr, because $\begin{pmatrix} -0.2 \\ 0 \end{pmatrix}$MVAr will solve the voltage range violation too, but using DG_1 for voltage control it will need twice as much reactive power as if DG_2 is used. Assuming the actual $Q_{DG} = \begin{pmatrix} 0 \\ 0 \end{pmatrix}$MVAr and the negative reactive power limits by $Q^{min} = \begin{pmatrix} -0.5 \\ -0.1 \end{pmatrix}$MVAr, the second DG will be at its limit after reactive power changes were executed. Having a grid situation with an increased range, for example $U^{example2} = \begin{pmatrix} 1.000 \\ 1.021 \\ 1.043 \end{pmatrix}$pu would lead to a voltage range of 0.043pu, which can only be reduced to EVB by utilising both DGs - so only if the "most ideal" DG (in this case DG_2) is not able to handle overvoltage alone, reactive power from other DGs is used (in this case DG_1) leading to $\Delta Q^{example2} = \begin{pmatrix} -0.1 \\ -0.1 \end{pmatrix}$MVAr.

The replacement of the absolute minimisation function by a quadratic minimisation function in (5.15) leads to:

$$\begin{gathered}\min_{\Delta Q_{DG}} \sum_{DGs} (Q_{DG} + \Delta Q_{DG})^2 \\ Q_{DG}^{min} \leq Q_{DG} + \Delta Q_{DG} \leq Q_{DG}^{max} \\ \max\left(U_{CN} + A_{CN,DG}^{Q} \cdot \Delta Q_{DG}\right) - \min\left(U_{CN} + A_{CN,DG}^{Q} \cdot \Delta Q_{DG}\right) < EVB\end{gathered} \tag{5.16}$$

This will completely change the results of the example given above, which can be explained with the help of diagram 5.10: When assigning the reactive power of DG_1 to the x-axis and the reactive power of DG_2 to the y-axis, the equipotential lines from the absolute minimisation function are the 45° rotated

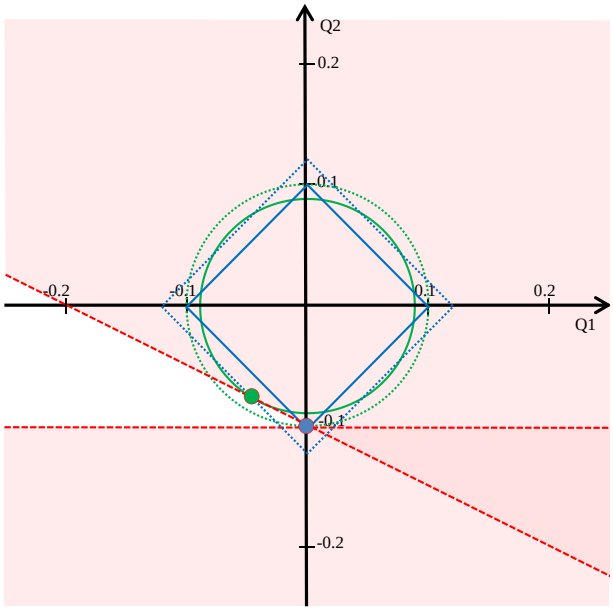

Figure 5.10: Two dimensional comparison of absolute objective function (5.15) (equipotential lines displayed in blue) and quadratic objective function (5.16) (equipotential lines displayed in green). Two constraints mark the invalid area (light-red) and curtail the valid area (white). The optimal solution of the absolute function (blue point) differ from the optimal solution of the quadratic function (green point).

squares (displayed in blue) and the equipotential lines from the quadratic function are circles (displayed in green lines). Both, squares and circles, represent higher function values when they are bigger (or - in other words - further away from the centre). The reactive power constraint of DG_2 is the horizontal dotted line and the voltage range constraint is the tilted dotted line (both displayed in red).Both constraints mark the invalid area in light-red. Therefore the solution of the absolute optimisation problem lies at the Q_2-axis (displayed as a blue point), because here the first square (the solid blue one) reaches the valid area (seen from the centre). The solution of the quadratic optimisation problem lies somewhere beside the absolute problem solution at the voltage range constraint (displayed as a green point), because here the first circle (the solid green one) reaches the valid area (seen from the centre).

The solution of the quadratic optimisation is $Q_{DG} = \begin{pmatrix} -0.04 \\ -0.08 \end{pmatrix} MVAr$, where in fact 20% more reactive power is used than in the absolute solution.

Generally spoken, the quadratic optimisation function utilises all available DGs that have an influence on the voltage range, even if their contribution is very small compared to the contribution of the DG with the highest influence, which will be used in the absolute optimisation algorithm. The higher the contribution of the DG, the more reactive power will be requested from it.

In practice this can be an advantage, because in real grid operation, where communication can be unreliable, it is more robust to distribute the necessary reactive power to many DGs, so there is no “single point of failure”. Furthermore, it might be better to avoid going on the limits of the DGs’ PQ operation diagram, which can be better achieved by the quadratic optimisation function. Finally it must be mentioned that from an implementational point of view the quadratic optimisation function is easier to handle than the absolute function, because optimisation algorithms can encounter difficulties in the convergence progress at the break of slope where the gradient of the function changes its sign. The only big drawback of the quadratic function is that it requests more reactive power than necessary.

The simulations were generally done with a quadratic optimisation function, because the quadratic function is easier to optimise (from an algorithmic point of view).

5.2.2.3 Minimise the Reactive Power arose from Controlling

Simulation *mode J* (see tab. 6.2): In general the reactive power requested from DGs participating in voltage control is negative in generator's perspective (capacitive), and positive in the grid's perspective (consuming reactive power), because the voltage rise of the feeding DG has to be compensated. This means that in the long run grids with voltage control based on reactive power control tend to consume reactive power, which can be a significant difference to uncontrolled grids and grids where no voltage control is necessary. It could lead to a higher loading of the transformer and of the superior grid, which could increase grid losses. Therefore it makes sense to formulate a voltage control strategy that tries to minimise the impact of the voltage control strategy on the overlying network level: The reactive power requested from DGs to perform voltage control has to be compensated by reactive power from DGs, which actually don't need to participate voltage control (probably DGs located near the transformer).

Fundamental mathematical formulation The first draft of the objective function of this control strategy is given by

$$\begin{gathered} \min_{\Delta Q_{DG}} \left(\sum_{DGs} Q_{DG} + \Delta Q_{DG}\right)^2 \\ Q_{DG}^{min} \leq Q_{DG} + \Delta Q_{DG} \leq Q_{DG}^{max} \\ \max\left(U_{CN} + A_{CN,DG}^{Q} \cdot \Delta Q_{DG}\right) - \min\left(U_{CN} + A_{CN,DG}^{Q} \cdot \Delta Q_{DG}\right) < EVB \end{gathered} \tag{5.17}$$

In contrast to the control strategy stated in chap. 5.2.2.2 there is no difference in the quadratic and the absolute optimisation function. The quadratic optimisation function (5.16) is a multi-dimensional paraboloid and the absolute optimisation function (5.15) also contains multiple abs-functions, leading to a multi-dimensional "muti-abs-surface". The control strategy stated here has only one square (because the sum is inside the square) and this square would correspond to a single abs-function with the same minimum. Since both functions are strictly monotonic increasing in both directions seen from the minimum, the optimisation results will be the same.

Penalising unnecessary reactive power The single quadratic function creates a minimum that is not a single point as it is the case in the optimisation functions in chap. 5.2.2.2, because multiple combinations of reactive power can lead to a zero sum. This makes the optimisation algorithm non-deterministic, because the optimisation function does not determine one single state as the optimum, but a whole $(n_{DG} - 1)$-dimensional space with n_{DG} as the dimension of the problem and the number of the optimisation parameters.

For instance, imagine a situation where all DGs are operated at zero reactive power and it comes to a situation where reactive power is needed to fulfil the voltage range constraint. At this time one DG starts to consume reactive power and a second DG compensates this reactive power. When the grid situation is gone where reactive power is needed, both DGs will continue generating reactive power, because for the optimisation function the situation is "optimal". To avoid this phenomenon, reactive power generation will be punished as in chap. 5.2.2.2, so the DGs' reactive power will come back to zero immediately when the grid situation allows it. To realise this, (5.17) changes to

$$\begin{gathered} \min_{\Delta Q_{DG}} \left(\sum_{DGs} Q_{DG} + \Delta Q_{DG}\right)^2 + c_1 \sum_{DGs} \left(Q_{DG} + \Delta Q_{DG}\right)^2 \\ Q_{DG}^{min} \leq Q_{DG} + \Delta Q_{DG} \leq Q_{DG}^{max} \\ \max\left(U_{CN} + A_{CN,DG}^{Q} \cdot \Delta Q_{DG}\right) - \min\left(U_{CN} + A_{CN,DG}^{Q} \cdot \Delta Q_{DG}\right) < EVB \end{gathered} \tag{5.18}$$

The factor c_1 has to be small enough so that the primary control strategy won't be influenced very much, because if $c_1 \approx 1$ the aim to drive all DGs with zero reactive power will weigh more than the aim to minimise the sum of the requested reactive power. It must be mentioned that with the second summand in the objective function the control objective which is represented by the first summand won't be executed exactly, because both summands interfere. The factor $c_1 = 0.001$ was estimated to get a good behaviour of the control strategy.

Weighting of the summands Even if the second part in (5.18) has a single optimum, the small weighting factor weakens this optimum. The optimum of the whole objective function (5.18) is still a multi-dimensional space as explained in the previous chapter.

For instance, imagine a grid with three DGs and two feeders: The first DG is connected to a feeder with a high voltage rise and therefore it has to generate reactive power to reduce voltage range. The second and the third DG located at the other feeder can compensate the reactive power produced by the first DG. The objective function is equal for the case the second DG compensates the reactive power, for the case the third DG compensates the reactive power, and for the case both DGs compensate the reactive power from the first DG.

To avoid his phenomenon each summand in the sum can be weighted to tell the optimisation algorithm that some solutions are better than others. In fact it does not make sense if a DG somewhere at the end of the grid compensates reactive power that was produced in another transformer branch to avoid voltage range violation. So it is preferred to let the DGs near the transformer compensate the reactive power that is requested from the DGs that have to reduce the voltage range. As discussed in chapter 4.3, the CM values contain the line impedance and therefore the values can be interpreted as rough information of how much losses will be produced when a DG generates reactive power. Since CM values are typically very small (< 0.02pu/MVAr) it was decided to make an exponential weighting, so for every DG a weighting factor $w_{DG} = \exp(c_2 \cdot A^Q_{CN_{DG},DG})$ was introduced with CN_{DG} representing the CN the DG is connected to. The factor $c_2 = 100$MVAr/pu was estimated to generate a good numerical behaviour of the objective function. This leads to

$$\begin{gathered}\min_{\Delta Q_{DG}} \left(\sum_{DGs} Q_{DG} + \Delta Q_{DG}\right)^2 + c_1 \sum_{DGs} \exp(c_2 \cdot A^Q_{CN_{DG},DG}) \left(Q_{DG} + \Delta Q_{DG}\right)^2 \\ Q^{min}_{DG} \leq Q_{DG} + \Delta Q_{DG} \leq Q^{max}_{DG} \\ \max\left(U_{CN} + A^Q_{CN,DG} \cdot \Delta Q_{DG}\right) - \min\left(U_{CN} + A^Q_{CN,DG} \cdot \Delta Q_{DG}\right) < EVB\end{gathered} \tag{5.19}$$

This does not completely solve the problem, because it can happen that two DGs have exactly the same reactive power contribution to their feeding point - especially when two DGs are connected to the same node.

Penalizing reactive power changes In such cases in practice it will be irrelevant which DG produces the reactive power. It is just necessary to assure a continuous controller output, because providing a deterministic solution is not possible without further information. Therefore the change in reactive power can be penalised as well, so that it will be disadvantageous if reactive power is unnecessarily shifted from one DG to another DG with exactly the same contribution. This will add a term $c_2 \sum_{DGs} \left(\Delta Q_{DG}\right)^2$ to the objective function, where $c_2 = 0.005$ was chosen to get a good behaviour of the control strategy.

$$\begin{gathered}\min_{\Delta Q_{DG}} \left(\sum_{DGs} Q_{DG} + \Delta Q_{DG}\right)^2 + c_1 \sum_{DGs} \exp(c_2 \cdot A^Q_{CN_{DG},DG}) \left(Q_{DG} + \Delta Q_{DG}\right)^2 + c_2 \sum_{DGs} \left(\Delta Q_{DG}\right)^2 \\ Q^{min}_{DG} \leq Q_{DG} + \Delta Q_{DG} \leq Q^{max}_{DG} \\ \max\left(U_{CN} + A^Q_{CN,DG} \cdot \Delta Q_{DG}\right) - \min\left(U_{CN} + A^Q_{CN,DG} \cdot \Delta Q_{DG}\right) < EVB\end{gathered} \tag{5.20}$$

5.2.2.4 Minimise the Current Flow at the Transformer

Simulation *mode K* (see tab. 6.2): The aim of this control strategy is to reduce the reactive power flow over the transformer as good as possible so that transformer losses and losses at the HV connection point are minimised. Therefore an additional information is required - the actual transformer's reactive power flow. Due to the fact that the TF already has to be equipped with measurements and a control unit, this can be seen as a negligible effort and expense. In the linearised view of the grid, the controllable DGs have to generate the negative value of the actual TF's reactive power flow to compensate it to zero. But in principle with this control strategy an arbitrary desired value can be defined, which can arise - for instance - from a reactive power demand of the HV grid or another adjacent MV grid.

Fundamental mathematical formulation The desired value $Q^{desired}$ is the reactive power which all DGs have to produce – in case of minimising transformer losses $Q^{desired} = -Q^{TF}$.

The first draft of the objective function of this control strategy is given by

$$\begin{gathered} \min_{\Delta Q_{DG}} \left(\sum_{DGs} \Delta Q_{DG} - Q^{desired}\right)^2 \\ Q_{DG}^{min} \leq Q_{DG} + \Delta Q_{DG} \leq Q_{DG}^{max} \\ \max\left(U_{CN} + A^{Q}_{CN,DG} \cdot \Delta Q_{DG}\right) - \min\left(U_{CN} + A^{Q}_{CN,DG} \cdot \Delta Q_{DG}\right) < EVB \end{gathered} \tag{5.21}$$

Objective function enhancements The objective function stated above suffers from the same problems described in 5.2.2.3, therefore two additional terms have to be added leading to an objective function that consists of three terms like in (5.20): The second term brings the reactive power demanded from the DGs back to zero when it is possible and the third term avoids controller discontinuities in cases where the function has – despite the weighting of the second term – a non-singular optimum. This leads to

$$\begin{gathered} \min_{\Delta Q_{DG}} \left(\sum_{DGs} \Delta Q_{DG} - Q^{desired}\right)^2 + c_1 \sum_{DGs} \exp(c_2 \cdot A^{Q}_{CN_{DG},DG}) \left(Q_{DG} + \Delta Q_{DG}\right)^2 + c_2 \sum_{DGs} \left(\Delta Q_{DG}\right)^2 \\ Q_{DG}^{min} \leq Q_{DG} + \Delta Q_{DG} \leq Q_{DG}^{max} \\ \max\left(U_{CN} + A^{Q}_{CN,DG} \cdot \Delta Q_{DG}\right) - \min\left(U_{CN} + A^{Q}_{CN,DG} \cdot \Delta Q_{DG}\right) < EVB \end{gathered} \tag{5.22}$$

In this case $c_1 = 10^{-6}$ and $c_2 = 0.005$ were chosen to produce a good behaviour of the objective function.

It has to be kept in mind that the squared first term gives equal results as the absolute function, but the square in the second and the third term were chosen because it is robust and easier to handle than absolute functions (the error is negligible).

5.2.2.5 Minimise the Current Flow at selected Grid Lines

Simulation *mode L* (see tab. 6.2): It is expected that grid losses can be significantly reduced if DGs minimise the reactive power flow over well chosen lines in the grid. Of course, the optimal grid operation could be achieved if the real time power flow would be known from every line and every node in the grid, but in practice this is not realistic. Therefore the control strategy stated here assumes that a few lines in the grid can be found, where it is strategically reasonable to install a reactive power measurement. In the linearised model of the grid it can be assumed that every change in DGs' reactive power that is done behind the far end of this line will be completely transmitted over this line and in the long run it will effect the transformer.

A straight-forward strategy for selecting this measurement points could be to measure reactive power directly at the TF station at every TF feeder. But it has to be considered that reactive power flow can change significantly over a long feeder and it is generally not sure that a DG placed at the end of the feeder will reduce line losses when the DGs' reactive power is transported through the grid to the transformer. Imagine a disadvantageous situation, where the reactive power flow at a TF feeder is fed into the grid near the transformer. The compensation of this reactive power from the DG placed at the end of the feeder will reduce losses at the lines near the TF, but losses can be increased in the rest of the grid. So it has to be assured that reactive power measurements are not too far away from the feeding DGs.

Of course, determining the ideal placement of such a reactive power measurement is an optimisation problem too. It depends on the individual grid and power flow situation, on how many reactive power measurements are meaningful and where they are placed. In the scope of this work, reactive power measurements were placed according to estimations. This means that savings in grid losses can only be a guiding value, because it was not analysed if these savings can be increased by a better positioning of the measurements.

The Adjacency Matrix For this control strategy it is necessary to know which DG is connected behind which reactive power measurement – in other words which DG can influence which line's reactive power. This information contains topology information just as the CM and it has to be provided externally just as the CM. This information is given in the adjacency matrix $B^{Q}_{line,DG}$, in which the columns represent the DGs and the lines the measurement-lines they are connected to. A matrix cell is 1 if a DG is connected behind a measurement line and 0 otherwise. A DG can be connected behind multiple measurement lines, because it is possible that measurements are cascaded. A column of $B^{Q}_{line,DG}$ does not necessarily contain only a single 1 and it can also be that there is no measurement upstream. The lines of the matrix have to contain at least one 1. Zero lines have to be excluded.

Mathematical formulation With the desired reactive power at the measured lines $Q^{desired}_{line} = -Q^{meas}_{line}$ the essential component of the objective function is[13]

$$\begin{gathered} \min_{\Delta Q_{DG}} \sum_{lines} \left(B^{Q}_{line,DG} \cdot \Delta Q_{DG} - Q^{desired}_{line} \right)^2 \\ Q^{min}_{DG} \leq Q_{DG} + \Delta Q_{DG} \leq Q^{max}_{DG} \\ \max\left(U_{CN} + A^{Q}_{CN,DG} \cdot \Delta Q_{DG} \right) - \min\left(U_{CN} + A^{Q}_{CN,DG} \cdot \Delta Q_{DG} \right) < EVB \end{gathered} \tag{5.23}$$

Objective function enhancements As it was done in the last two chapters and explained in chap. 5.2.2.3, it has to be avoided that the DGs' reactive power only increases losses and possible remaining equipotential-hyperplanes at the functions optimum have to be prevented, leading to

$$\begin{gathered} \min_{\Delta Q_{DG}} \sum_{lines} \left(B^{Q}_{line,DG} \cdot \Delta Q_{DG} - Q^{desired}_{line} \right)^2 + c_1 \sum_{DGs} \exp(c_2 \cdot A^{Q}_{CN_{DG},DG}) \left(Q_{DG} + \Delta Q_{DG} \right)^2 + c_2 \sum_{DGs} \left(\Delta Q_{DG} \right)^2 \\ Q^{min}_{DG} \leq Q_{DG} + \Delta Q_{DG} \leq Q^{max}_{DG} \\ \max\left(U_{CN} + A^{Q}_{CN,DG} \cdot \Delta Q_{DG} \right) - \min\left(U_{CN} + A^{Q}_{CN,DG} \cdot \Delta Q_{DG} \right) < EVB \end{gathered} \tag{5.24}$$

The constants $c_1 = 10^{-6}$ and $c_2 = 0.005$ were chosen as in the previous chapter.

5.2.2.6 Minimise the Voltage Range

Simulation *mode I* (see tab. 6.2): This control objective differs significantly from the control objectives stated above, because it does not use the whole available EVB. It minimises the voltage range - the range between the highest and the lowest node in the grid. This means that the last line of the previously stated problem formulations turns into the minimisation function:

$$\begin{gathered} \min_{\Delta Q_{DG}} \left(\max(U_{CN} + A^{Q}_{CN,DG} \cdot \Delta Q_{DG}) - \min(U_{CN} + A^{Q}_{CN,DG} \cdot \Delta Q_{DG}) \right) \\ Q^{min}_{DG} \leq Q_{DG} + \Delta Q_{DG} \leq Q^{max}_{DG} \end{gathered} \tag{5.25}$$

It has an affinity with the control objective that minimises the voltage deviation from nominal voltage in eq. (5.6). The difference is that this control strategy is only interested in reducing the distance between the highest and the lowest voltage and the voltages in between the boundary values are not important.

Special attention must be paid on the type of the optimisation function, which is not polynomial any more. The max- and the min-function are static functions, but they can't be replaced by a polynomial of low order, so the derivative can't be expressed analytically and the gradient is not continuously. Therefore the optimisation algorithm used must not depend on analytical gradients and if the gradient is calculated numerically, the algorithm has to cope with non-continuous gradients. The minimising functions stated in the previous chapters are of good nature compared with the minimising function stated here.

[13] Again, the squared function should be an absolute one, but for a better solvability the quadratic function is preferred.

5.2.3 Coordinated Voltage Control Concepts with Active Power Curtailment

Active power curtailment was initially stated in chap. 5.1.2 and omitted, because the control objective discussed was not suitable for active power curtailment. In this chapter the technically optimal form of active power curtailment is discussed for appropriate control objectives.

5.2.3.1 Conflicting Areas

When controlling active power some additional things have to be considered, which are unimportant when controlling reactive power:

- Active power has financial value and curtailing reactive power can mean financial losses for the DG owner.
  This is definitely the case by wind-, PV- and river power plants, but it must not be the case in reservoir power stations and biomass power plants.
  Therefore active power curtailment of DGs has to be used as little as possible - only if there is no other possibility to operate the grid in a stable state.
- The DG that will solve voltage problems best by reducing active power is often not the DG that would suffer the least financial losses by reducing active power.
  Therefore it is necessary to distinguish between technical solutions (which would solve grid problems best) and economical solutions (which minimise financial losses of the DG operators).
- If the curtailed DGs are not owned by the same holder, a fair solution might be preferred instead of a technically or a financially optimal solution.
  Here several aspects might be important to the DG owner: Whose DG was first installed into the grid and the installation of which DG made active power curtailment necessary?

For including DGs in coordinated voltage control concepts, existing contracts have to be adapted or extended, but due to the aspects mentioned above, including active power curtailment into contracts is far more complex than controlling only reactive power.

5.2.3.2 Objective Function Enhancement for appropriate Control Strategies

Active power curtailment only makes sense when operating voltage control concepts that keep grid voltages within a range of the whole available EVB (from chap. 5.2.2.2 to 5.2.2.5). Control concepts that try to optimise grid voltages in general (chap. 5.1.2.7 and chap. 5.2.2.6) are not suitable for active power curtailment since they will reduce active power even if it's not necessary (because they don't consider the EVB). Before the objective functions (5.16), (5.20), (5.22) and (5.24) will be enhanced by the active power control objective, the enhancement will be analysed first:

Basic Formulation of the Technical Optimisation Approach The control objective of maximising the active power output can be stated as

$$\begin{gathered} \min_{\Delta P_{DG}} -\sum_{DGs}(P_{DG}+\Delta P_{DG}) \\ P_{DG}^{min} \leq P_{DG}+\Delta P_{DG} \leq P_{DG}^{primary} \\ \max\left(U_{CN}+A_{CN,DG}^{P}\cdot\Delta P_{DG}\right)-\min\left(U_{CN}+A_{CN,DG}^{P}\cdot\Delta P_{DG}\right) < EVB \end{gathered} \tag{5.26}$$

The change in DGs' active power ΔP_{DG} causes – according to the active power CM $A_{CN,DG}^{P}$ – a change in grid voltages. The minimal DGs' feeding power P_{DG}^{min} and the actual available DGs' primary energy $P_{DG}^{primary}$ are the constraints for the resulting active power $P_{DG}+\Delta P_{DG}$. The summand P_{DG} in the objective function is constant and could be left out because it does not change the behaviour of the function.

When omitting reactive power, the resulting optimisation problem is classified as a linear optimisation problem under linear constraints.

Special attention must be paid on the upper limit $P_{DG}^{primary}$of $P_{DG} + \Delta P_{DG}$ in cases where the actual supply of active power is not exactly known (for example in PV and wind power plants), because sending a DG an active power set value $P_{DG} + \Delta P_{DG}$ that can't be achieved will perturb the control objective in the currently stated form.

Enhancement of Reactive Power Objective Functions The active power enhancement of the reactive power objective functions (5.16), (5.20), (5.22) and (5.24) are done in the same way. Active power enhancement will only be stated for the control objective (5.16) that uses as little reactive power as possible for voltage range control:

$$\begin{gathered}
\min_{\Delta Q_{DG}} \sum_{DGs} \left(Q_{DG} + \Delta Q_{DG}\right)^2 - c \cdot \sum_{DGs} \Delta P_{DG} \\
Q_{DG}^{min} \leq Q_{DG} + \Delta Q_{DG} \leq Q_{DG}^{max} \\
P_{DG}^{min} \leq P_{DG} + \Delta P_{DG} \leq P_{DG}^{primary} \\
\max\left(U_{CN} + A_{CN,DG}^{Q} \cdot \Delta Q_{DG} + A_{CN,DG}^{P} \cdot \Delta P_{DG}\right) - \min\left(U_{CN} + A_{CN,DG}^{Q} \cdot \Delta Q_{DG} + A_{CN,DG}^{P} \cdot \Delta P_{DG}\right) < EVB
\end{gathered} \tag{5.27}$$

The constant factor c is the penalty factor for active power curtailment and tells the objective function rather to use reactive power than curtailing active power.

5.2.3.3 Conclusion and Outlook

The proposed control objective for active and reactive power offers the best solution from the grids perspective. This means that with this control objective active power is curtailed as little as possible and active power curtailment is done at the position in the grid, where the voltage situation can be influenced best. This also means that different types of primary energy supply and different financial losings or "fairness / neighbourhood" approaches are not considered.

When implementing centralised voltage control concepts with active power curtailment, economical approaches can be considered as important or even more important as technical approaches. A very comprehensive study of this topic was done in [34]. Since it is hard to tell which economical and technical models that satisfy all stakeholders will be established in future, no further investigation is done in active power curtailment concepts within this work and the simulations are executed only for reactive power control strategies. But it must be mentioned that an active power curtailment based on coordinated voltage control concepts (which will be used only as a last instance to avoid voltage violations - e.g. $1-5\%$ time of the year) will definitely be an alternative to the current practice, where the integration of a DG into the grid is prohibited when voltage problems can't be ruled out with certainty.

Chapter 6

Simulation of the Proposed Control Algorithms

For the two distribution grids 'Lungau' and 'Nenzing', detailed grid models and one-year active- and reactive-power measurements were used to simulate the power flow in the grids over one year, while in parallel applying the control strategies discussed in the last chapter.

6.1 Simulation Environment

PowerFactory DIgSILENT PowerFactory Version 14.1.6

Matlab MathWorks Matlab Version R2010a

Hardware no special requirements, Simulations were performed on four virtual machines (4x3Ghz CPU, 4GB RAM) in parallel

PowerFactory is a power systems analysis and engineering tool, which offers grid simulation capabilities. In the so-called RMS-Simulation (Root Mean Square) the dynamic and transient behaviour of power systems can be analysed, as well as the long-term behaviour of power systems. To model the power system behaviour in time, PowerFactory offers a simulation language, the so called DSL (DIgSILENT Simulation Language). Within this DSL, active and reactive power time series ("profiles") can be assigned to loads and generators in the grid. When running a DSL simulation, a power flow is continuously calculated to represent the actual grid situation, which depends on these profiles. Within user-defined DSL control elements, any information that is available by the power flow calculation can be used for controlling user-defined grid elements. Within a DSL control block it is possible to establish an interface to a Matlab engine, transfer all necessary information to Matlab, perform calculations and use the calculation results from Matlab in the RMS-Simulation.

With this simulation environment, a one-year simulation can be done in two to three hours.Depending on the time Matlab needs for its calculations (which depends on the complexity of the objective function and the optimisation algorithm), a simulation for one-year can last up to four days.

To automatise the simulation procedure PowerFactory offers a so called remote communication interface (RCOM). With this interface it is possible to send simulation control commands from a windows batch script to PowerFactory. This made it possible to sequentially start and run simulations which lasted more than two weeks without further interaction or supervison.

6.1.1 Optimisation Algorithm

All optimisation problems introduced in chap. 5 are convex optimisation problems of a non-linear objective function under linear constraints (nonlinear were transformed into linear constraints). To solve this kind of problem Matlab offers the built-in function `fmincon`, which in principle supports this type of

problem. Unfortunately the performance of the Matlab `fmincon` is poor (this function can solve various problems and is not designed explicitly for this kind). For problems with a high number of dimensions, `fmincon` does not find a solution (this means it does not find a way out of the constrained area into the valid area), even if a valid area exists. The SS 'Nenzing' was simulated with 61 controllable DGs leading to a 61-dimensional problem, which was not solvable by Matlab's `fmincon` utilising the built in "interior-point method". A straightforward Matlab implementation of an interior point optimisation method was available, which did not suffer from the problem not finding a solution if it existed, but suffered from the problem of a very weak performance. Due to the fact that the objective functions stated in chap. 5 are generally of good nature and in principle easy to solve, an optimisation algorithm was developed in Matlab which was optimised to solve these types of problems. With this control algorithm it was possible to solve the 61 dimensional problems - depending on the boundary conditions and the objective function - within a time varying from most times below one second up to around 30 seconds in very adverse boundary conditions. This fast convergence behaviour has two reasons: Firstly, the grid situation only changes slightly from one simulation time to the next, so boundary conditions are similar and the optimum of the new time step will be near the last optimum. Secondly, gradient information has to be provided and a "distance-to-direction-dependent-optimum"-function, which tells the algorithm based on a given direction, how far the local optimum of the objective function is away when following the given direction. This "distance-to-direction-dependent-optimum" is specified analytically and has to be calculated from a partial derivative of the objective function.

6.2 Grid Models

6.2.1 Grids

Figure 6.1 and 6.2 show the grid models of the grids in normal switching state that were used for the one-year simulations. Grey lines and nodes are deactivated or not connected to the active grid. Both distribution stations have two transformers in parallel (n-1 criterion for power systems), but their kind of operation is different:

In SS 'Lungau', TF1 supplies the western region of 'Lungau' (region with grey lines (deactivated) on the left hand side), and TF2 supplies the eastern region of 'Lungau' (region with black lines on the right hand side). Coordinated voltage control in 'Lungau' was only performed in the eastern region, so the western region is inactive in the grid model.

In SS 'Nenzing', TF1 and TF2 alternating supply the grid, the TFs are alternated monthly. The grey (deactivated) lines belong to the neighbour distribution stations.

Grid characteristics of both SS are summarised in table 6.1.

6.2.2 Scenarios

For both grids growth scenarios exist. In these scenarios DGs are modelled, which actually do not exist in the grid, but which are likely to be built in future. All control strategies are simulated in both grids for the basic scenario and the growth scenario. Details about the basic and the growth scenario are summarised in table 6.1.

It is expected that coordinated voltage control will be necessary when DGs are connected according to the growth scenario, while in the basic scenario local control strategies will be sufficient to operate the grid within stable voltage limits.

6.2.3 Legend to Symbols

In both grid models the existing controllable DGs are highlighted with blue circles and loads (predominantly LV-grids) are not shown. The DGs which are part of the growth scenario are highlighted with green circles. The reactive power measurements are marked with yellow circles.

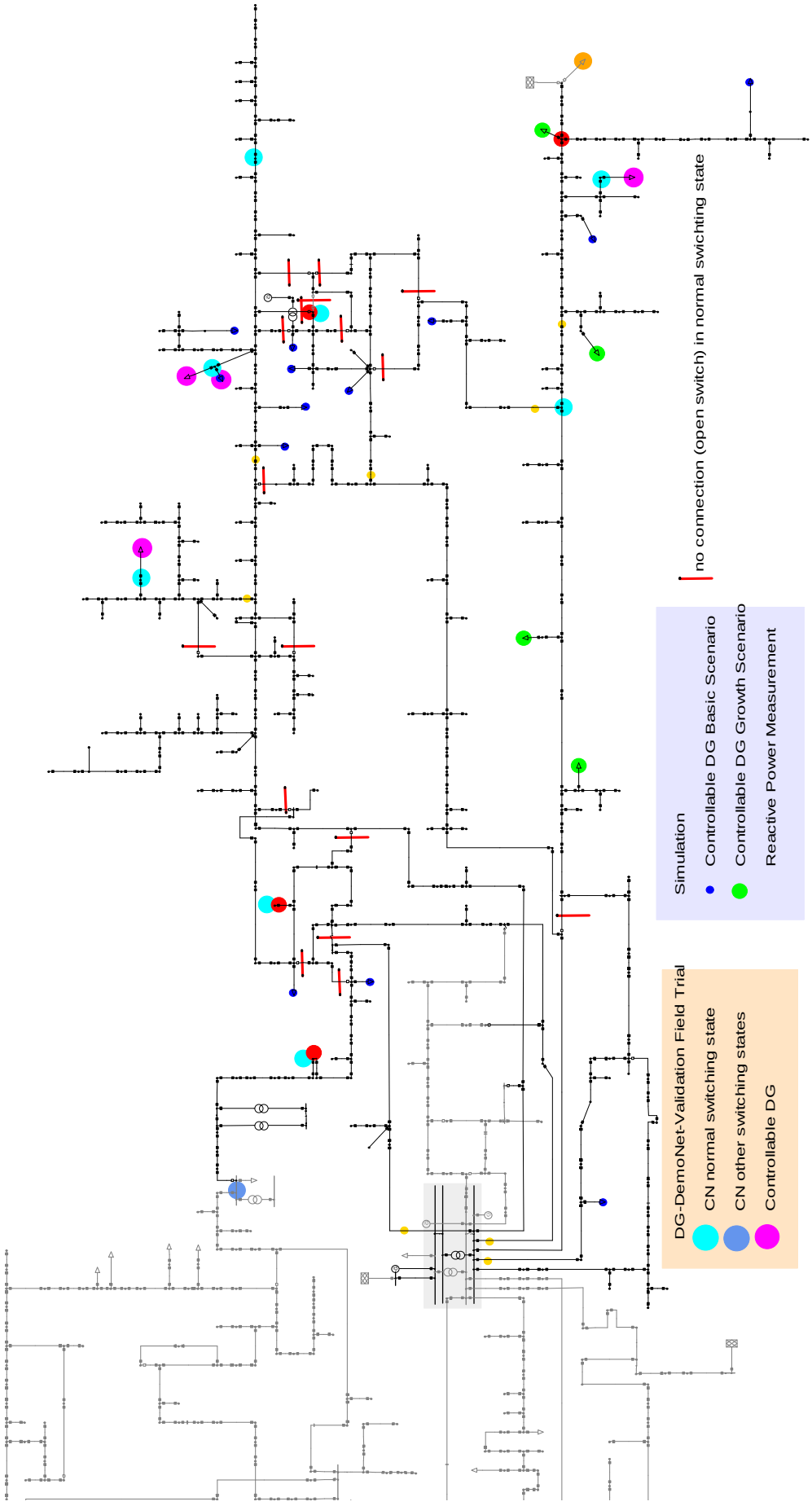

Figure 6.1: PowerFactory grid model of SS 'Lungau'

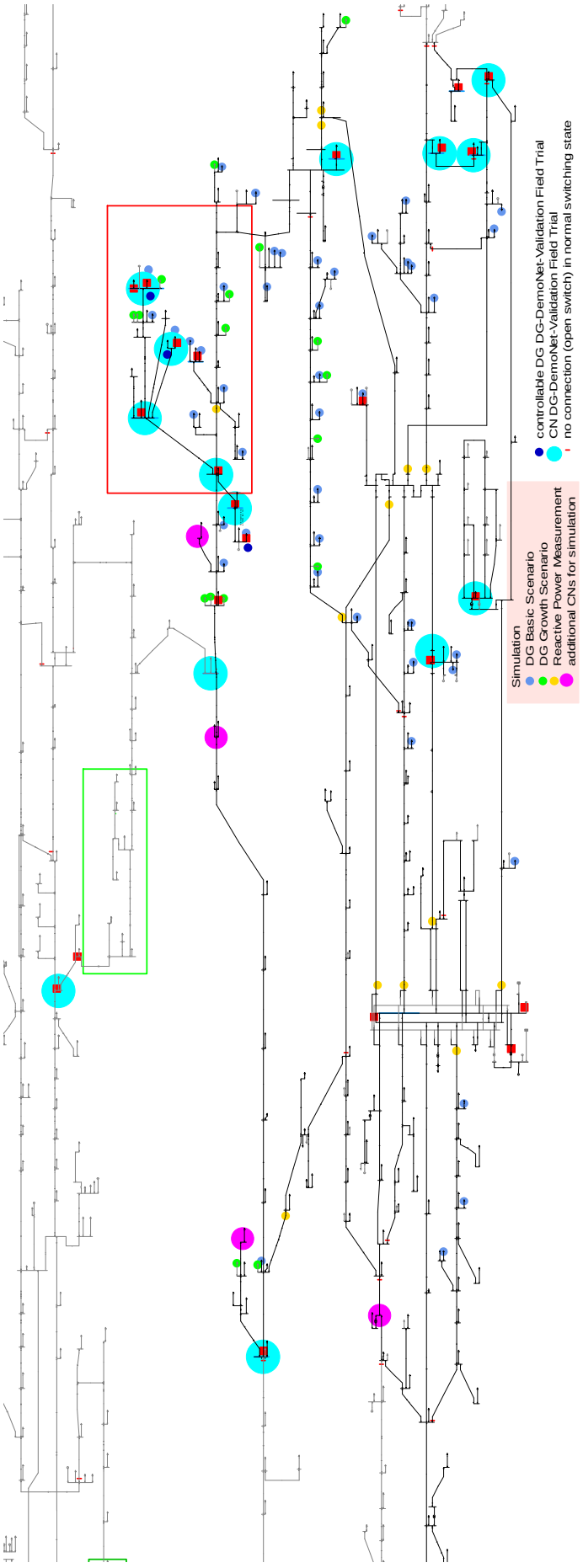

Figure 6.2: PowerFactory grid model of SS 'Nenzing'

			SS 'Lungau'	SS 'Nenzing'
Grid Charact-eristics		transformer nominal apparent power [MVA]	32	40
		maximal active power consumption [MW] *	23.5	31.8
		minimal active power consumption [MW] *	3.2	2.4
		number of loads	266	146
Scenario	Basic	maximal active power generation [MW] *	7.9	32.8
		minimal active power generation [MW] *	1.4	0.4
		number of DGs	16	44
	Growth	nominal feeding power increase [MW]	6.5	16.6
		maximal active power generation [MW] *	13.7	45.3
		minimal active power generation [MW] *	2.2	1.7
		number of DGs	20	61

Table 6.1: Grid characteristics: Values marked with * are based on aggregated data according one-year profiles (the 1-percentile was taken for minimal values and the 99-percentile for maximal values)

Power systems are built meshed (n-1 criterion for system stability), but operated tree-shaped to reduce losses. The open switches that turn the meshed grid into a tree are marked with red cross-lines.

The CNs that were chosen to be implemented in the DG-DemoNet Validation field trails are marked in light blue.

6.3 Simulation Settings

The one-year measurement data for the active- and reactive power load and generation profiles were available as 15min average values in an interval of 15min. Performing the simulations with a 15min time-step has the disadvantage that the chronological interaction of level controller and range controller can't be simulated. Especially from 6:00 to 7:00 in the morning changes in the 15min average values can be very high, so the voltage situation in the grid can significantly change. In such cases it is not possible to gain a representative behaviour of the control strategies when simulating with a 15min time step. Therefore the simulation time step was set to 3min, which means that within two 15min average values the control strategy will be operated 5 times based on a linear interpolation of the load profiles. This assures smooth control behaviour and a representative statement about the utilisation of the DGs and the TF's tap-changer.

Summing up, the 15min average values are linear interpolated to simulate one year in 3min time-steps, which leads to 175200 controller cycles during a simulated year.

The following parameters were set:

Parameter	Value	Unit	Description
level control mode	minimum-tapping		see chap. 5.2.1.2
voltage upper limit U^{UL}	1.05	pu	[2)]
voltage lower limit U^{LL}	0.99 [1)]	pu	[2)]
tap hysteresis h	0.002	pu	see chap. 5.2.1.3 [2)]
AVC deadband U^{DB}	0.02 [3)]	pu	see chap. 2.2.1.1 [2)]
DGs minimal cosφ	0.9	1	see chap. 6.3.1

[1)] In SS 'Nenzing' in basic scenario 1.005pu was chosen, because otherwise coordinated control would not be needed during the whole year.

[2)] same value as it is operated in the DG-DemoNet Validation field trial in both grids

[3)] AVC deadband is the same in both grids, but the TF's nominal tap-change-height ΔU^{tap} is different (-0.015275pu in SS 'Lungau' and -0.0112755pu in SS 'Nenzing')

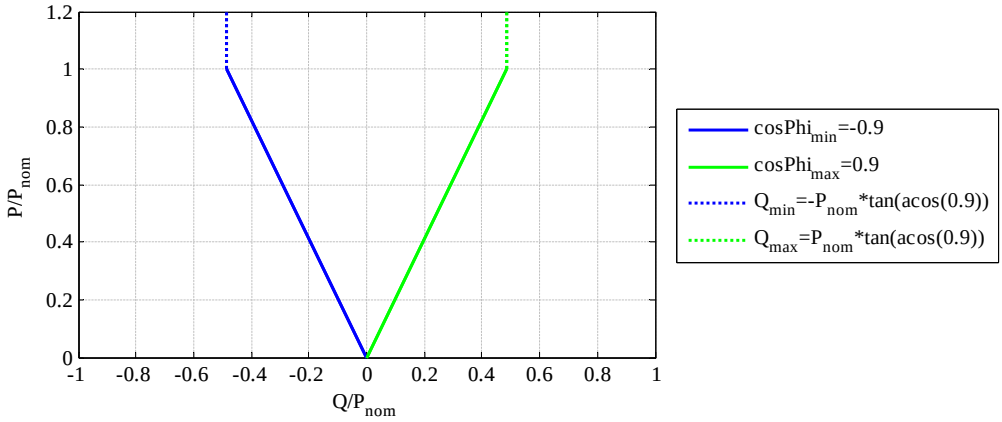

Figure 6.3: PQ diagram of every controllable DG in simulation

6.3.1 DGs PQ Diagram

The parameter with probably the highest influence on simulation results is the amount of reactive power the DGs can provide. Although old DGs are not able to provide reactive power and only newly installed DGs are capable of providing a $cos\varphi = 0.9$, it was assumed that all DGs in the grid - independently of their age and whether they are hydro, wind or PV plans - are able to operate at $cos\varphi = 0.9$. To operate $cos\varphi = 0.9$ at nominal active power the generator has to be 11% overdimensioned, which increases the generator costs.

Reasons for performing the simulations at $cos\varphi = 0.9$ are:

- According to [13] it is actually required that newly installed DGs are able to operate at $cos\varphi = 0.95$ or $|Q_{max}(P)|/P = 0.329$ (which corresponds to a generator oversizing of 5-6%), but it is likely that in future $cos\varphi = 0.9$ or $|Q_{max}(P)|/P = 0.484$ will be required.
- The simulations were made to compare the impact of different coordinated control strategies on grid losses and transformer tap-changes. The differences between the control strategies are more significant if more controllable reactive power is available.

The PQ diagram (which marks the limits of the valid operational area of the DGs) used in the simulations for all DGs is shown in fig. 6.3.

6.4 Simulation Suite

To gain an extensive overview over different voltage control concepts two simulations were performed without controlling DGs (to have a reference scenario) and four simulations were performed with all DGs in local voltage control in addition to the six simulations with coordinated voltage control applied. The simulated distributed control strategies are explained in the following chapters, and the coordinated control strategies were already explained in chap. 5. All simulated control strategies are summarised in table 6.2.

6.4.1 Conventional Minimum-Tapping without DG Control

Simulation *mode A*: In chap. 5.2.1.2 different kinds of level control modes are explained, which can safely be operated when the actual spreading (range) of the grid voltages is smaller than the effective voltage band, $S < EVB$. If $S > EVB$, the level control mode must be switched to upper limit because this control mode avoids overvoltage, which is considered as more critical than undervoltage. This simulation mode does not use the level control mode extensions for times when $S > EVB$ which are described in

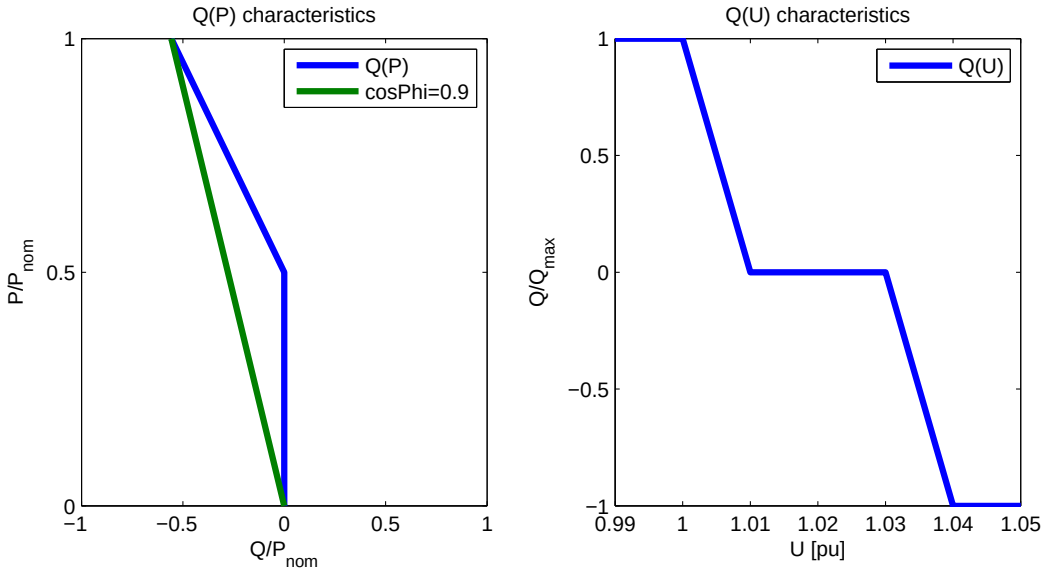

Figure 6.4: Local control characteristics: left: constant $cos\varphi$ and $Q(P)$, right: $Q(U)$

Sim. *mode*	TF control mode	DG control mode	DG control strategy	Description
A	conventional min. tap.	off	none	$cos\varphi = 1$, see chap. 6.4.1
B	extended minimum tapping		none	$cos\varphi = 1$, see chap. 6.4.2
C		local	constant $cos\varphi$	$cos\varphi = -0.9$, see chap. 6.4.3
D			Q(P)	Characteristic see fig. 6.4, chap. 6.4.4
E			Q(U)	Characteristic see fig. 6.4, chap. 6.4.5
F	extended centered		Q(U)	Characteristic see fig. 6.4, chap. 6.4.5
G	extended minimum tapping	coordinated	$\min\sum_{DGs}(Q_{DG})^2$	see chap. 5.2.2.2
H			$\min\sum_{CNs}(\bar{\Delta}U_{CN})^2$	see eq. (5.6)
I			min range	see chap. 5.2.2.6
J			$\min(\sum_{DGs} Q_{DG})^2$	see chap. 5.2.2.3
K			min Q^{TF}	see chap. 5.2.2.4
L			min Q^{lines}	see chap. 5.2.2.5

Table 6.2: Overview of the simulated control strategies (simulation *modes A ... L*), which are executed for each grid in each scenario

5.2.1.3. It is performed to compare the amount of time where undervoltage occurs with and without the level control extensions. DGs always run with zero reactive power.

6.4.2 Extended Minimum-Tapping without DG Control

Simulation *mode B*: This simulation mode defines the reference scenario for all other simulation modes. The level control mode minimum-tapping switches into upper-limit-extended in times where $S > EVB$ as described in 5.2.1.3. DGs are not controlled and run with $cos\varphi = 1$.

6.4.3 Extended Minimum-Tapping with DGs running constant $cos\varphi$

Simulation *mode C*: Due to the fact the voltage at the feeding point of the DG increases the higher the feeding power becomes, it can make sense to let all DGs consume more reactive power the more active power is generated. $Q \propto P$ is equivalent to $cos\varphi = const$. Since it is a local control strategy, this reactive power control works independently at every DG and is independent from all other DGs.

6.4.4 Extended Minimum-Tapping with DGs running $Q(P)$

Simulation *mode D*: Running DGs at a constant $cos\varphi$ as described in 6.4.3 might solve voltage rise problems, but it might be a waste of reactive power and lead to an increase in grid losses. When the DG operates at a fraction of its nominal power, reactive power consumption might not be needed, because the voltage rise at the reduced feeding is too small to exceed limits. Therefore it can make sense to run $cos\varphi = 1$ up to a certain active power offset and starting to consume reactive power at this active power offset. The P(U) characteristic of this control behaviour is shown in the left figure in 6.4, where it is compared with the constant $cos\varphi$ characteristic.

6.4.5 Extended Minimum-Tapping with DGs running $Q(U)$

Simulation *mode E*: Another improvement in avoiding unnecessary reactive power is to consume reactive power when the voltage at the feeding point is very high and produce reactive power when voltage is very low. In between high and low voltage there is a voltage deadband where no reactive power has to be generated or consumed. This control strategy is very robust since it automatically calms voltage changes in the grid. This leads to a reduction of necessary transformer taps, because the DGs running $Q(U)$ perform absolute voltage control and not voltage range control as stated in chap. 5. The Q(U) characteristic of this control mode is shown in the right figure 6.4.

6.4.6 Extended Centered with DGs running $Q(U)$

Simulation *mode F*: As described above, the reactive power produced depends on the absolute grid voltages and therefore on the TF controller strategy. Running the TF controller in upper-limit will cause DGs to consume reactive power, running in lower-limit will cause DGs to generate reactive power. To avoid unnecessary reactive power, which will be generated when running in minimum-tapping mode (chap. 6.4.5), the DGs' $Q(U)$ control mode was simulated with TF in control mode centered. This keeps all grid voltages as good as possible in the centre of the voltage band and reactive power production caused by the $Q(U)$ characteristic will be minimised.

6.5 Simulation Results

As described above, simulations were calculated for both investigated grids for the basic scenario (DG penetration from the year 2012) and the growth scenario (realistically estimated DG penetration in future). The analysed aspects are summarised in the following paragraph and detailed descriptions of the individual results are given directly below the figures.

The main interest of this work is the impact of the proposed control strategies on the grid losses and the number of necessary tap-changes. The grid losses are calculated as active power losses in all MV grid lines and in the MV TF, so losses in the HV grid or in the LV grids are not considered (fig. 6.5, 6.15, 6.24, 6.34). As the HV side of the TF is held constant (slack), the number of necessary tap-changes will be smaller than in real where the HV grid's voltage can significantly vary. This has the advantage that the MV grid's behaviour can be studied uncoupled from the HV grid, leading to more comprehensible results that are more universally valid than if the HV voltage would vary (fig. 6.6, 6.16, 6.25, 6.35).

Another focus in the results is the impact of the control strategies on the voltage range, especially the voltage range arising with the distributed control modes (meaning DGs operated in local control mode). While in the control *mode A* (reference) and *B* where DGs are not controlled, the range will be largest. All other scenarios will have a significantly reduced range, and the range of the coordinated control *modes G* to *L* should not exceed EVB, because satisfying range constraints has higher priority than following other optimisation objectives (see fig. 6.8, 6.17, 6.26, 6.36).

It is also instructive to analyse the maximum and minimum grid voltages to determine the correct functionality of the control strategies (fig. 6.9, 6.19, 6.28, 6.38).

Furthermore the grids loading (active power over the TF) and the total DGs' injected power will be shown in combination with the minimal reactive power that is necessary to keep voltages within the given limits. Here the different seasonal demands on the grid and the order of magnitude of reactive power necessary for controlling is visualised (fig. 6.10, 6.20, 6.29, 6.39).

To get an idea of the amount of reactive power that is requested from the DGs the sum of all DGs' reactive power is shown, which gives information of how much reactive power is transferred additionally into the HV grid (fig. 6.11, 6.21, 6.30, 6.40). Furthermore the absolute sum of all DGs' reactive power is shown to visualise the behaviour of the different control strategies (fig. 6.12, 6.22, 6.31, 6.41).

Finally it might be interesting in how far the different control strategies alter the power flow over the TF (fig. 6.13, 6.23, 6.32, 6.42) and over selected lines (fig. 6.14, 6.33). This visualises the behaviour of the different control strategies concerning TF and line and losses.

Notes for the diagrams Most diagrams are plotted as duration curves, which means that each time series of simulation results were sorted ascending individually. Each point in such a line tells how much time (of the year in these cases) the plotted value was smaller than the ordinate value (shown directly by the abscissa value) and how much time the plotted value was bigger than the ordinate value (shown by the time interval given by the abscissa value to the end of the diagram). This leads to clearly and definitely readable diagrams, but dynamic information is lost. Insights in the grid dynamics are given in the diagrams where the time series of the simulation results were directly plotted. It can be seen that the main period ("first harmonic" of steady-state power flow) of the grid is one day and due to the fact that load behaviour is significantly different on weekends, also a weekly period ("seventh harmonic" of steady-state) exists.

All boxplots show the 0-, 1-, 50-, 99- and 100-percentiles, so they are not standard boxplots (which show the 25% quartiles).

Since the simulation modes often have very similar results, many curves in the figures are congruent. Therefore line colours, line style and line thickness were chosen to offer a good readability in many diagrams, but it was not possible to consider all overlappings.

Since the set of presented results is equal for each grid in each scenario, diagram descriptions are made in detail for the first grid SS 'Lungau' in the first basic scenario. Repeating the explanations of the figure's content is omitted for the other scenarios and grids, instead the differences to the basic scenario are stressed.

6.5.1 SS 'Lungau'

6.5.1.1 Basic Scenario

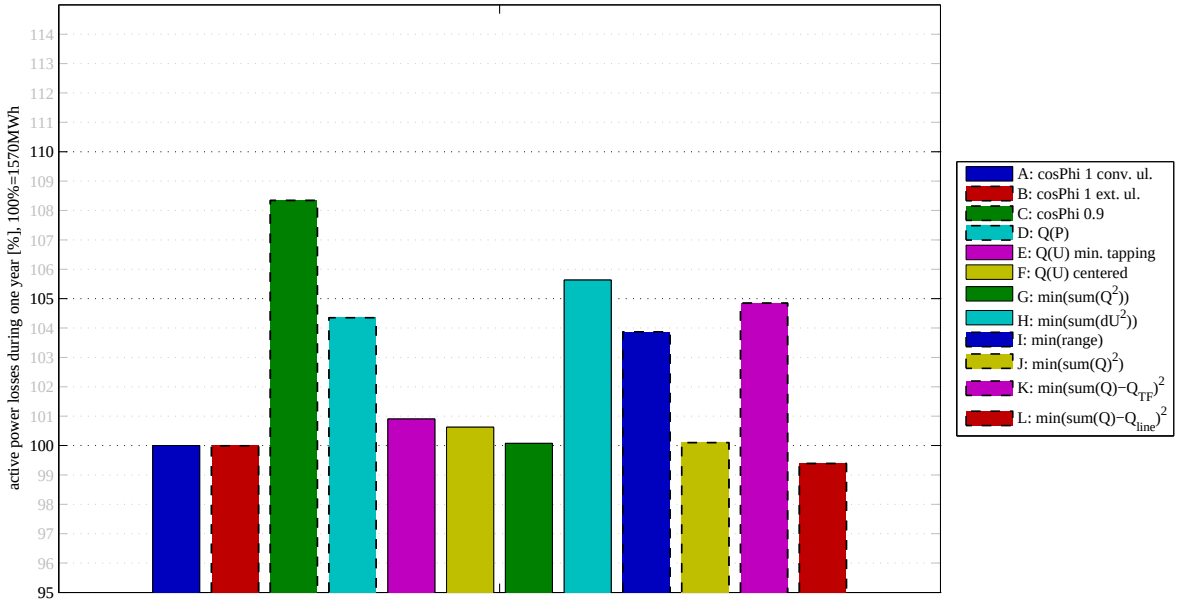

Figure 6.5: SS 'Lungau' basic scenario - grid losses (line and transformer) in %, base is simulation *mode A* with 1570MWh (which is 1.5% of the total load's consumption): In the distributed voltage control *modes A* and *B* no reactive power is fed by the DGs, so line losses are low compared to the *mode C* where all DGs are operated at $cos\varphi = 0.9$. *Mode C* can be considered as the worst case scenario, because DGs are all operated at their maximum reactive power output.

It is clear that operating DGs in a Q(P) control mode according to fig. 6.4 (*mode D*), losses will still be high but significantly smaller than in *mode C*.

Even if the result of *mode E* and *F* (where all DGs are operated in a Q(U) control mode) look promising, it must be mentioned that voltage limits are violated for around 2% of the year when operation these scenarios (see fig. 6.9).

Mode G (first coordinated voltage control mode) minimises the usage of the DGs' reactive power, therefore losses did not increase significantly (because reactive power is only needed several hours during a year. All voltages are kept within its limits, like in all other coordinated voltage control modes - see fig. 6.9).

Trying to bring all voltages as close as possible to nominal voltage (as it is done in *mode H*) needs very much reactive power, leading to a high increase in grid losses. But in fig. 6.8 it can be seen that the voltage range can be reduced significantly.

A similar reduction in range followed by similar increases in grid losses is the result of *mode I*, where the voltage range is minimised. Here only the highest and the lowest grid nodes are considered. Only DGs that can influence this nodes are utilised, therefore grid losses are smaller than in *mode H*.

Mode J is similar to *mode G*, because the minimal reactive power that is necessary to solve voltage problems is compensated by free DGs as good as possible, leading to a loss increase that is slightly higher than the one in *mode G*, but still insignificant.

The increase in losses in *mode K* can be considered controversially, because minimising the reactive power flow over the TF will probably reduce HV grid losses, but if only the MV grid is considered, losses increase significantly. This is because no information is given from which feeder the reactive power comes from. In the SS 'Lungau', not every feeder has a DG connected, and two feeders have many DGs connected, so simply minimising TF's reactive power is not optimal (see fig. 6.1).

When additional reactive power measurements on selected grid lines are available, losses can be decreased in *mode L* compared to *mode A* and grid voltages can be kept within the given limits. It must be noted that the selection of grid voltage measurements (see yellow points in fig. 6.1) are based on estimations, so the presented result cannot give any prediction how far grid losses can be reduced by this (or a similar) kind of coordinated voltage control.

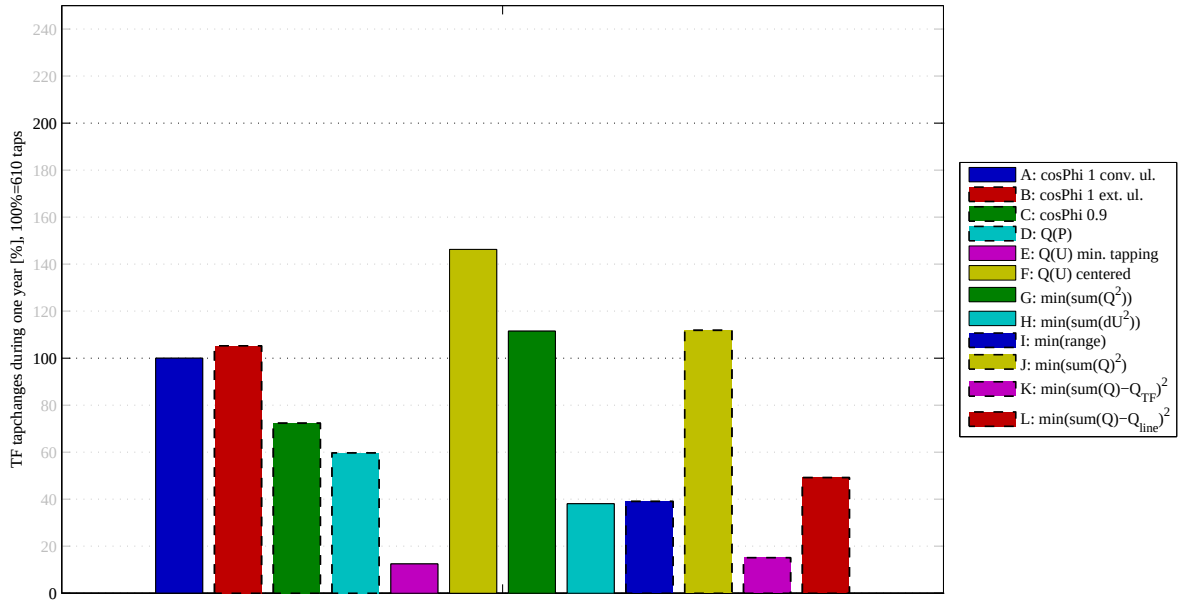

Figure 6.6: SS 'Lungau' basic scenario - tap-changes in %, base is *mode A* with 610 tap-changes during a year: Because the HV voltage that supplies the MV TF was set constant, the results above (showing less than two taps per day) are unrealistically low (in reality, in SS 'Lungau' in average 15 to 20 taps per day are common). This ideal environment makes an independent comparison of the different control modes possible:
Of course *mode B* uses a little bit more tap-changes than *mode A*, because up-tapping in upper-limit-extended is performed a little bit earlier than in upper-limit (see chap. 5.2.1.3).
Since the permanent consumption of reactive power in *mode C* reduces the DGs' impact on grid voltage, tap-changes can be reduced when running $cos\varphi = 0.9$.
No explanation can be given why the number of tap-changes in *mode D* is smaller than in *mode C*.
Mode E uses the fewest number of tap-changes, because running the DGs in Q(U) control mode naturally balances voltage fluctuations absolutely, while all other control modes work with relative deviations.
The high increase in tap-changes in *mode F* is caused in the change of the level control mode to centered, where grid losses are reduced compared to *mode E*. This mode is the only one that uses a control strategy different to minimum tapping with the intention to solve non-ideal situations where the all grid voltages are very near a voltage limit and many DGs produce reactive power unnecessarily. Reactive power can be saved in these situations when the level controller brings grid voltages to the centre of the voltage band, so that the DGs' feed-point voltages will be in a region where no reactive power is necessary.
Mode G and *mode J* differ only around 15% of the year from *mode B*, therefore results are similar.
The surprisingly low number of tap-changes in *mode H* and *I* can be reasoned by the significant reduction of the voltage range, leading to more space in the voltage band and a bigger scope for the minimum-tapping strategy.
Even more surprising is the low number of tap-changes in *mode K*, where reactive power flow over the TF is minimised. Since the TF's series impedance is mainly responsible for the TF's voltage drop, the reduction of the TF's reactive power flow can significantly reduce TF MV busbar voltage variation (when TF HV voltage is constant), which explains this good result.
Minimising reactive power flow at selected grid lines also leads to a lower reactive power variation at the TF, because reactive power variations are balanced in a local scope, so tap-changes in *mode L* also decreased compared to *mode A*.

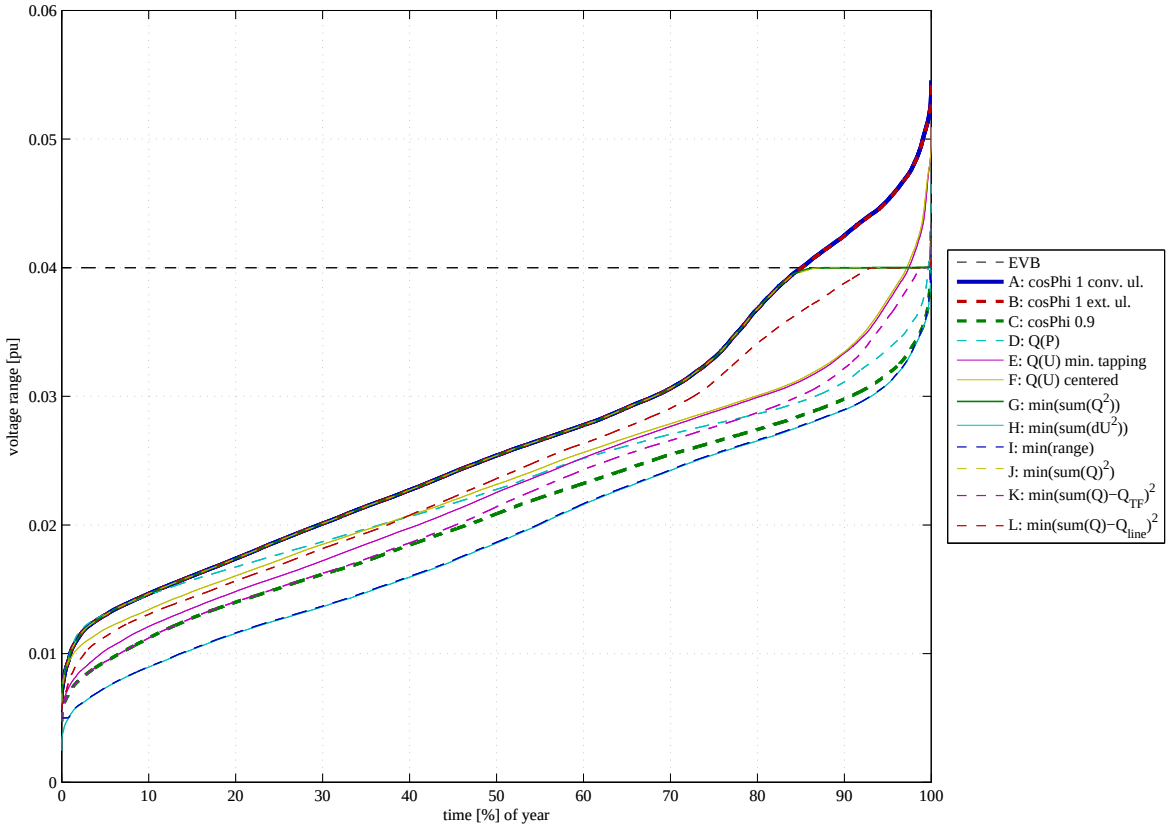

Figure 6.7: SS 'Lungau' basic scenario - duration curve of voltage range [pu]:
Of course, *mode A* and *B* show the highest ranges which significantly exceed the effective voltage band EVB (the range's limit under which grid voltage can be kept within the limits guaranteed).
It is readily identifiable that *mode C* and *D* solve voltage range problems - at the expenses of heavily increased grid losses as shown in fig. 6.5.
Mode E and *F* are not able to keep voltage within secure ranges for 3 to 4% of the year. Main reasons for this are situations where grid voltages are low (voltage range is near the lower limit) and DGs connected to the nodes with higher grid voltages don't contribute reactive power. If grid voltages get below the lower limit, up-tapping would be possible, because then these DGs would start consuming reactive power. But in these control modes the centralised operated level controller does not know that up-tapping could solve undervoltage without leading to overvoltage.
Mode G behaves like *mode A* and *B* in 85% of the year, because in this time voltage range is below the EVB and therefore no reactive power is needed. In the remaining 15% of the year the optimisation algorithm calculates the minimal reactive power that is necessary to bring the exceeding voltage range back to EVB. Therefore the duration curve of *mode G* uncouples from the curves of *mode A* and *B* and follows the EVB indicator line.
Similar to *mode G*, *mode J* tries to use as little reactive power as necessary and furthermore tries to minimise the amount of requested reactive power so that reactive power impact is balanced. Therefore this curve is congruent with the duration curve of *mode G*.
Even if the control objective of *mode H* and *J* differ (*H* minimises all voltage violations from mean voltage, and *J* minimises only the range), their impact on the voltage range is similar, resulting in congruent curves. It is interesting that voltage ranges could be hold below 0.035pu for even 97% of the year (this can be seen as a sign that a high DG penetration in MV grids will be possible in future, where active power curtailment as a last control instant will be necessary very seldom).
Mode K and *L* behave as all coordinated control modes, so they follow their control objective, but in times of high ranges the reduction of voltage range is predominant, leading to a "cut" of these control modes at EVB.

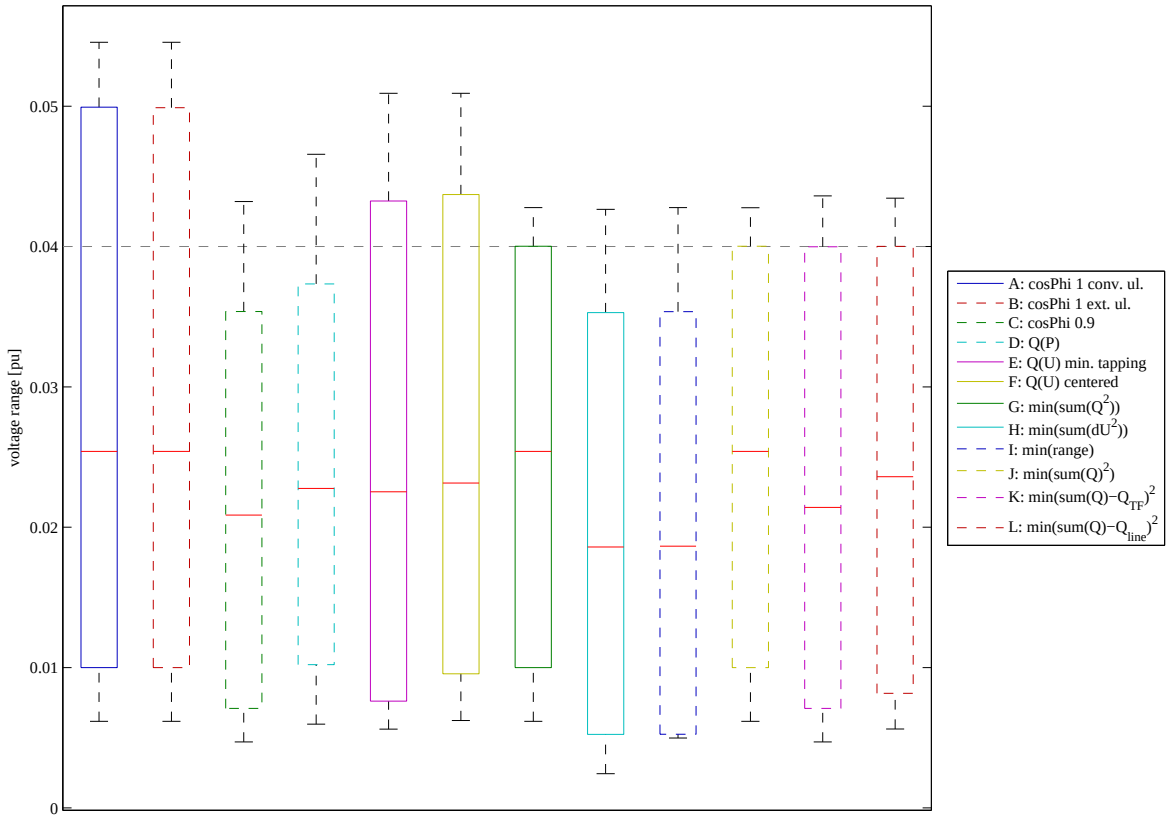

Figure 6.8: SS 'Lungau' basic scenario - boxplot of voltage range [pu] (boxplots show the 1% and 99% percentiles):

To illustrate the important results of the voltage range duration curves shown in fig. 6.7, a boxplot diagram was generated for the voltage ranges. It is readily identifiable that all coordinated voltage control modes (*mode G* to *L*) are able to keep 99% of the voltage ranges below the EVB, but some outliers are in every control strategy leading to a maximal voltage range of around 0.043pu. These violations are reasoned on extraordinary grid situations and non-ideal convergence due to contribution matrix variations and significant changes in grid from one control step to the next (in some very seldom cases the 3min control interval is too coarse).

Furthermore the excess of voltage range in *mode A*, *B*, *E* and *F* are clearly identifiable.

It is interesting to see that there are a few grid situations with very small ranges, where *mode H* performs significantly better than *mode I* (even if the 1% percentiles are equal, the minima differ around 0.0025pu - no reason can be given for this phenomenon).

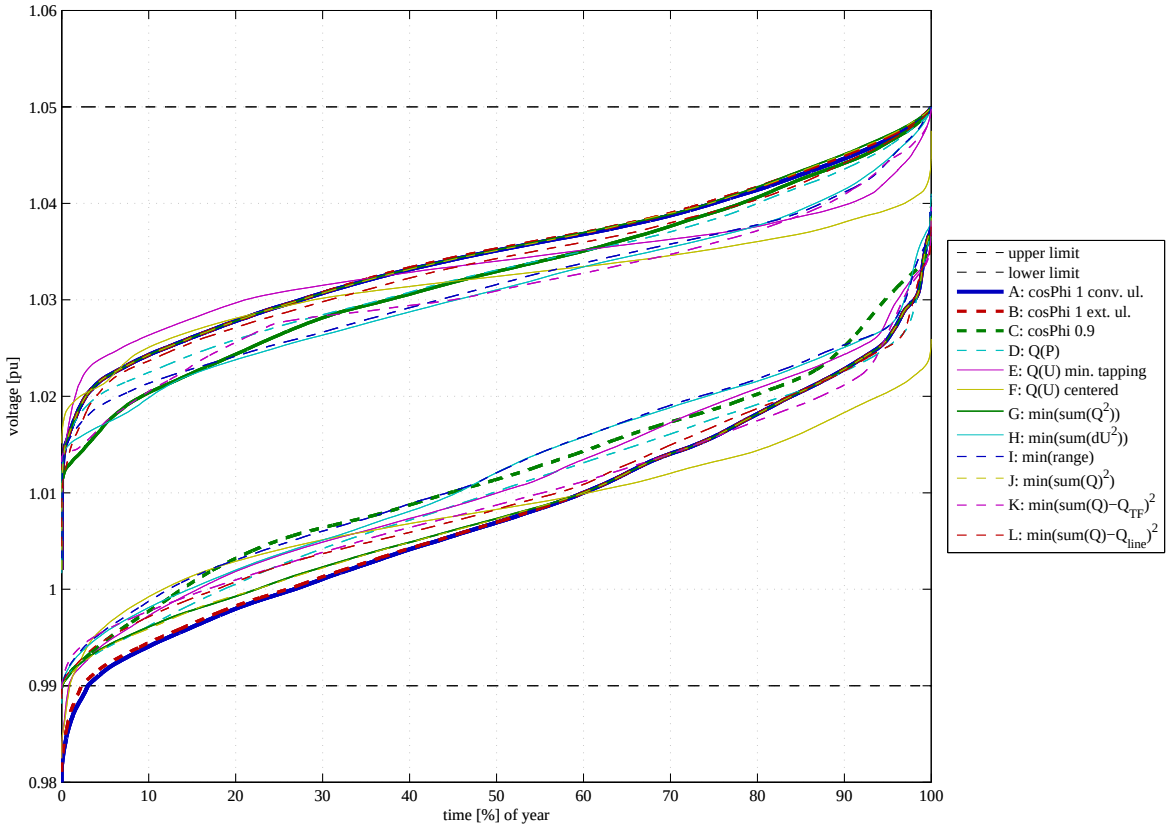

Figure 6.9: SS 'Lungau' basic scenario - duration curve of maximal and minimal grid voltages [pu]: In this plot the upper curve of each mode shows the duration curve of the maximal grid voltage and the lower one the duration curve of the minimal grid voltage. The duration curves are not synchronised, so each curve is sorted ascending individually.

All control modes were able to operate the grid below the upper limit, but lower limit is violated in *mode A* (~3% of the year), *B* (~2.5%), *E* and *F* (both around 1%). In this grid the extension of the level control mode to upper-limit-extended in times of high ranges brings an improvement in voltage violation in only 0.5% of the year. A higher improvement was predicted, because the conventional upper-limit is able to avoid voltage violations up to a range of $EVB = VB - U_{DB} = 0.04pu$, while the extension of the level control mode upper-limit is able to avoid voltage violations up to $VB - \Delta U_{tap} - h = 0.0427pu$ in this grid. The reason for this is the good result of *mode A*, which is hard to improve: While voltage range exceeds is 15% of the time EVB (fig. 6.7), voltage violation occurs only 3% of the time (a variation of slack voltage would lead to a higher violation of *mode A*).

The centered level control mode of *mode F* is responsible for the significantly different duration curves, which are lower (centered) in times when the other control modes have higher grid voltages.

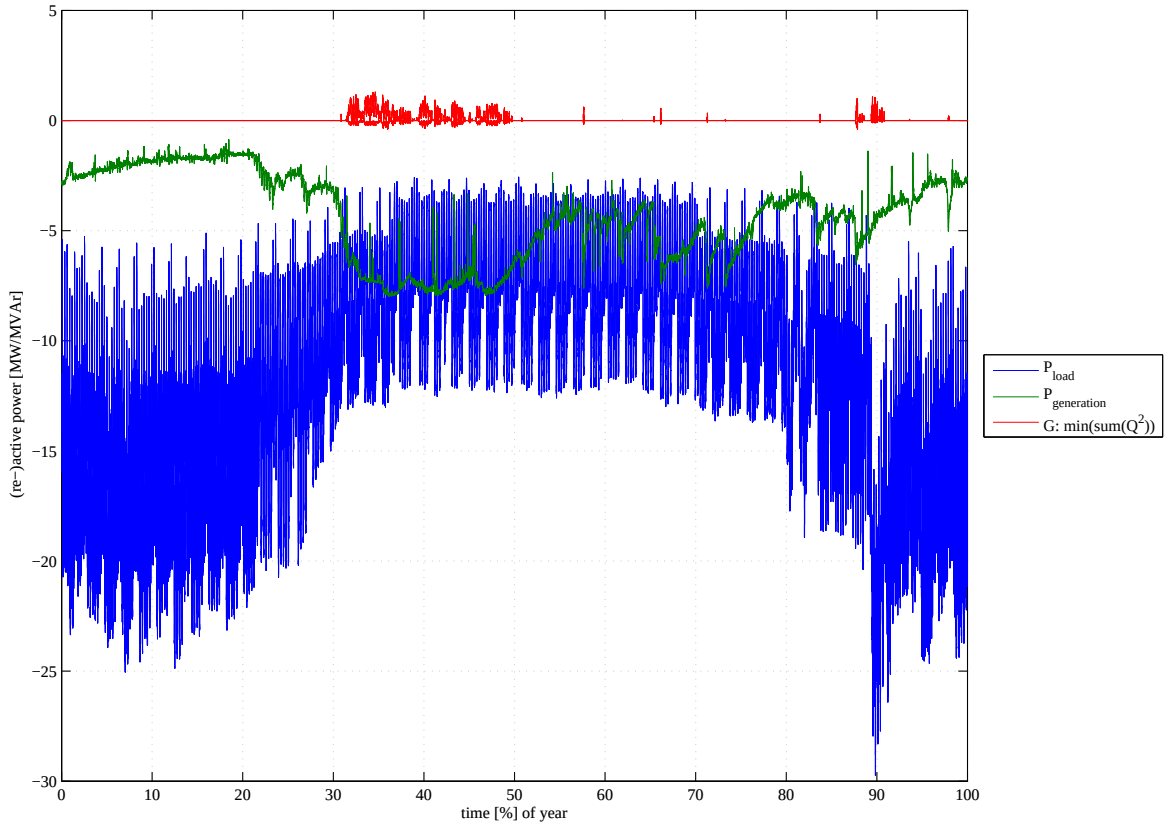

Figure 6.10: SS 'Lungau' basic scenario - time series of load's active power demand ($-P_{load}$) and DGs' active power feed-in ($P_{generaion}$) in [MW] and minimal reactive power demand on DGs to keep voltages within voltage limits (calculated in *mode G*) in [MVAr]:
The sign of load's active power demand was changed to offer a better comparability to the generation.
In this plot the time axis corresponds to the real time, e.g. 0% is Jan. 1st and 100% is Dec. 31st. Therefore the grid dynamics that are lost in the duration curves are visible: Especially in summer the continuous repetition of five weekdays with higher load peaks followed by two days of reduced load peaks can be identified.
In winter consumption is higher than in summer (not only due to increased lightning and electric heaters but also due to ski lifts) and generation is lower. In spring snow melting leads to high generation and afterwards generation increases after rainfall.
Voltage ranges get too high in times of high generation, so reactive power control is primary necessary in spring and all other seasons the grid can be mainly operated without DG control.

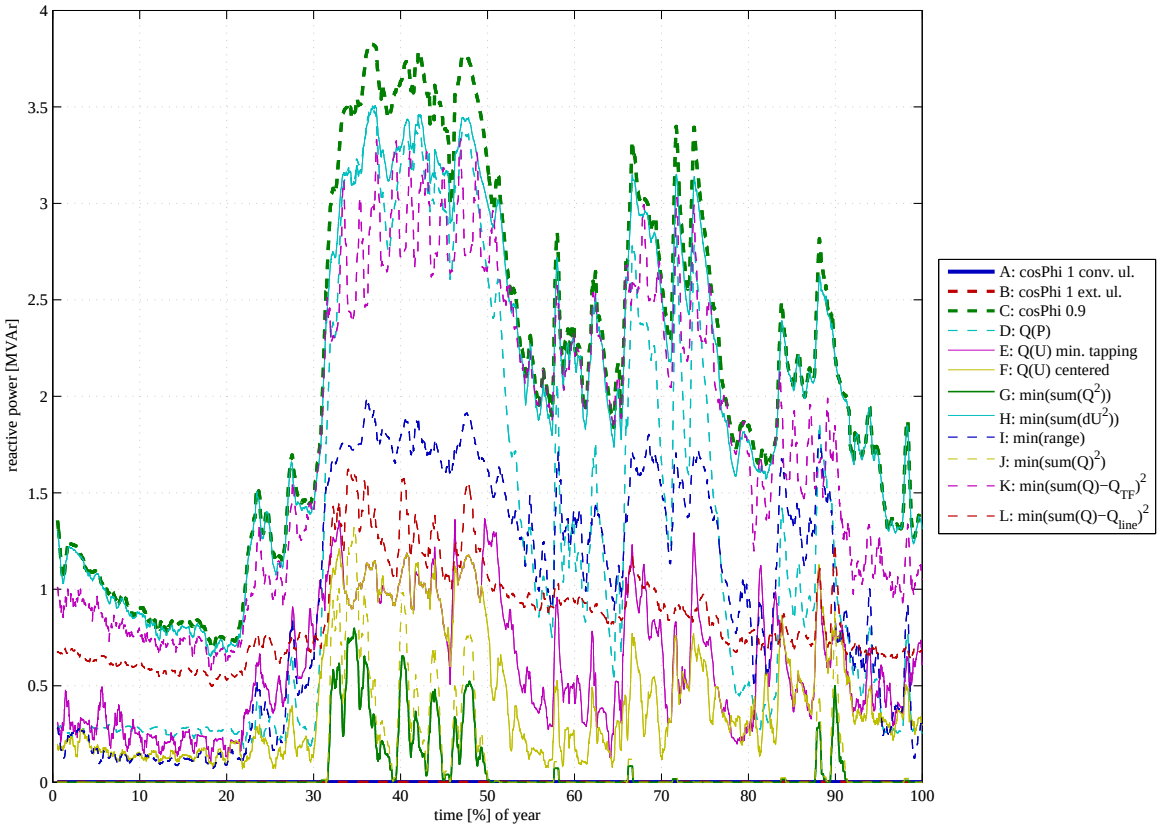

Figure 6.11: SS 'Lungau' basic scenario time series of absolute sum of DGs' reactive power [MVAr] that is requested by the control mode (the *absolute* sum has the advantage that the complete requested reactive power can be visualised, avoiding abolishing of reactive power due to different signs): The curve is filtered with a 2days gliding average, because otherwise the "daily noise" would make the plot unreadable.

While the reactive power of *mode A* and *B* is zero, reactive power of *mode C* is always the maximum according the actual active power generation, so all other modes will be between this borders. The control mode that comes closest to the maximal reactive power of *mode C* is *mode H* (which minimises the voltage deviation from mean voltage). Here reactive power is permanently nearly at maximum, meaning that every DG is utilised. *Mode I* does not utilise every DG because it only minimises the voltage range, leading to moderate reactive power demands. In spring *mode D* (running Q(P) control) is also near the maximum, while it does not use that much reactive power in autumn and winter. *Mode K* also uses much reactive power and successfully reduces TF's reactive power - but grid losses are increased. Both Q(U) *modes E* and *F* use moderate reactive power, while of course the centered *mode F* uses less than *mode E*. It is readily identifiable that *mode G* and *J* use fewest reactive power - mainly during spring.

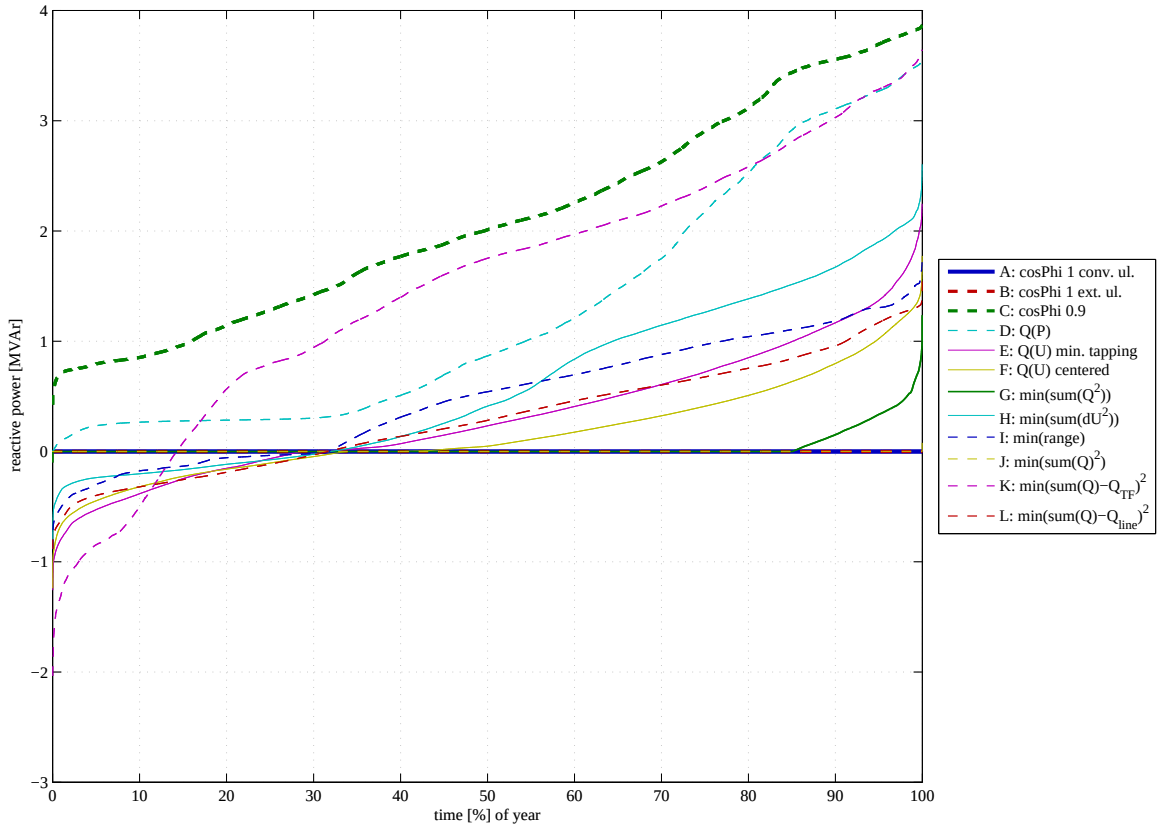

Figure 6.12: SS 'Lungau' basic scenario - duration curve of sum of DGs' reactive power [MVAr]: This figure shows similar information as the last figure, but reactive power is summed with sign and duration curve is used instead time series.
Mode A and *B* don't use any reactive power and the sum of reactive power of *mode J* is also zero (which means that the optimum of the objective function was always within the valid hyper-parallelotope and no constraint prohibited the optimum). Very similar to this is *mode G* which only uses reactive power 15% of the year. Minimising TF's reactive power in *mode K* leads to the most negative reactive powers and of course *mode C* uses the most positive reactive power.

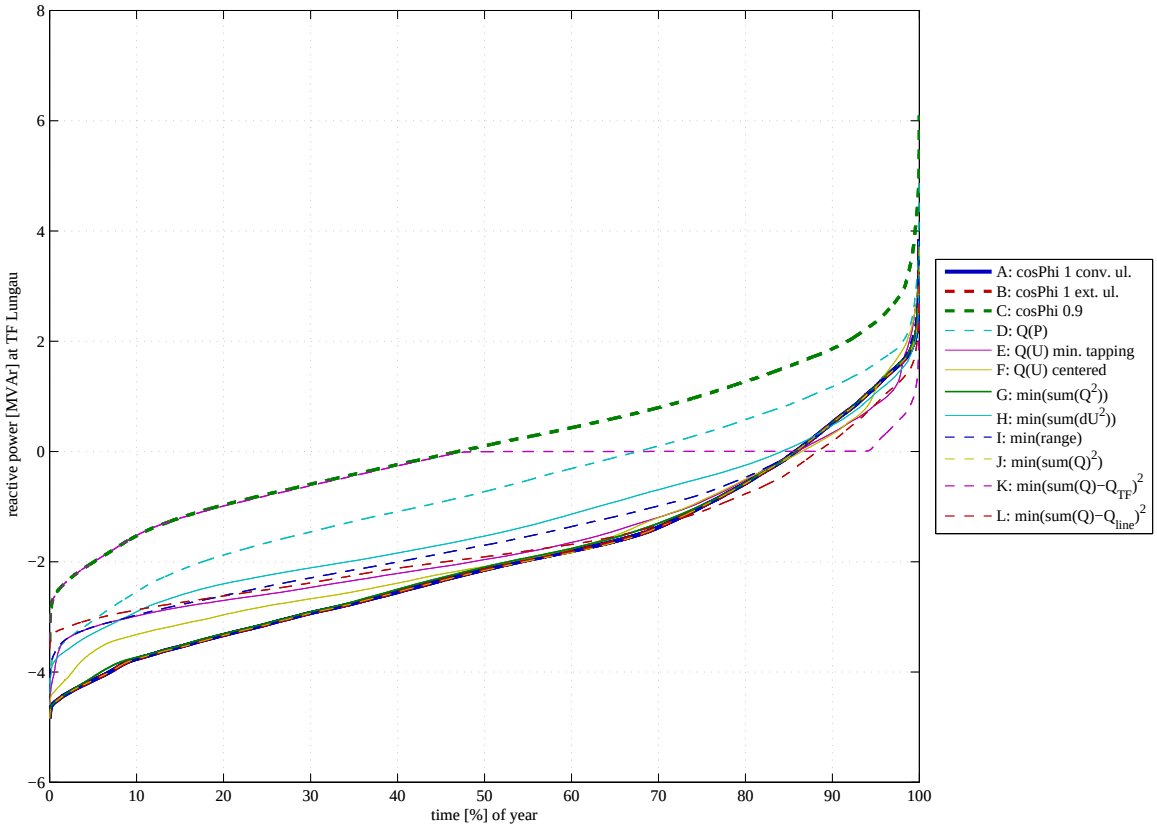

Figure 6.13: SS 'Lungau' basic scenario - duration curve of reactive power flow over the transformer [MVAr]:
Operating *mode C* minimises the TF's reactive power flow during around half of the year, therefore *mode K* is congruent with *mode C* within this timespan, but *mode K* keeps at zero reactive power when the *mode C* duration curve crosses the zero line. Nearly 50% of the year *mode K* is able to keep TF's reactive power at zero and only about 6% of the year TF's reactive power flow is positive.

Fig. 6.14 on the next page shows the duration curves of all reactive power measurements of the grid lines selected for reactive power optimisation which are highlighted by yellow dots in fig. 6.1. At all lines except feeder 'Mauterndorf' reactive power duration curves cross the zero-line, which is the optimisation goal for *mode L*. The higher the spreading of the different modes (different duration curves) is, the more controllable reactive power is located behind this line and the more possibilities are given to balance the lines reactive power flow. Most lines reactive power is reduced to zero in *mode K* for the bulk of the year - the higher the available reactive power, the better the zero-reduction.
With the objective function of *mode L* it is also possible to locate multiple measurements cascaded, so situations where reactive power on one line is optimised to zero while reactive power on other lines increase can be avoided. This is the reason why duration curve of *mode L* at feeder 'Madling' does not exactly fit the zero-line but lies slightly below it: The optimisation procedure realises that bringing the reactive power on this line to zero would increase reactive power on 'line 0436->0408' (plot directly below the plot of 'Madling'), therefore the least square approach finds a compromise where reactive power is slightly below zero at 'Madling', while it is slightly above zero at 'line 0436->0408'.

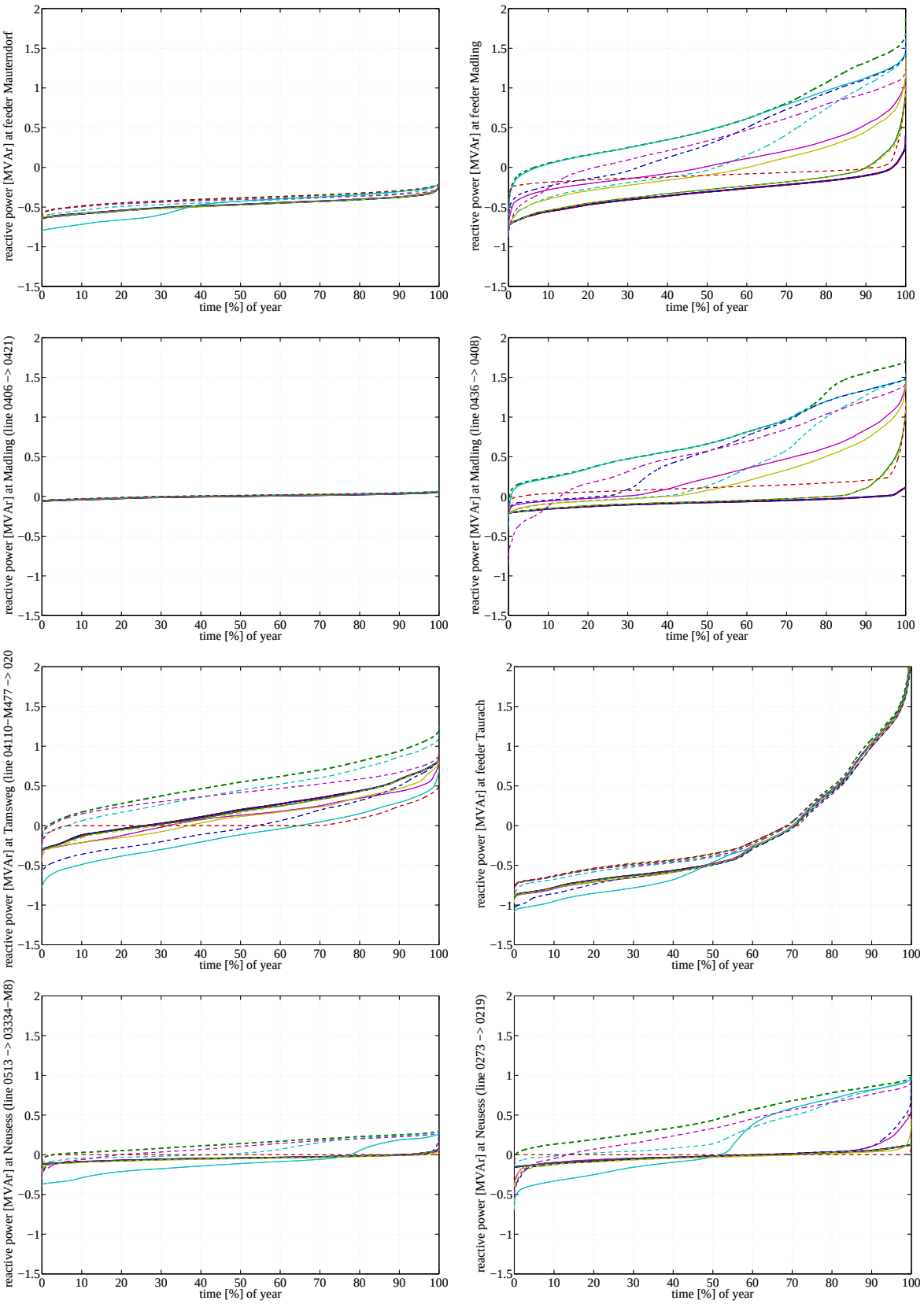

Figure 6.14: SS 'Lungau' basic scenario - duration curve of reactive power flow over distribution station feeder and grid lines [MVAr] (explanation and line legend on the previous page).

6.5.1.2 Growth Scenario

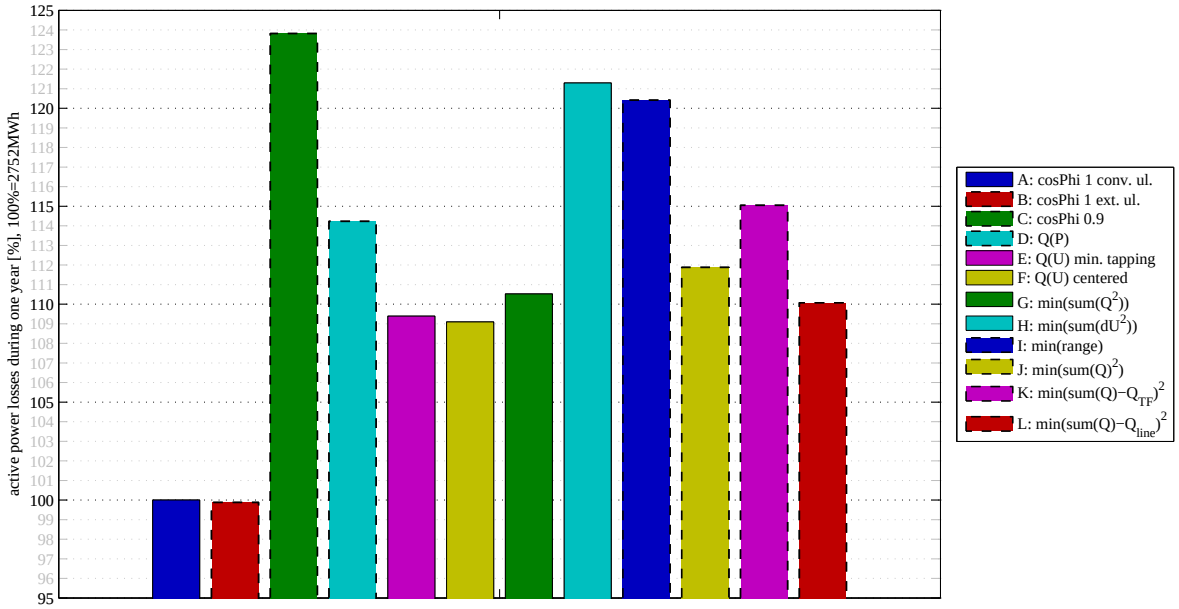

Figure 6.15: SS 'Lungau' growth scenario - grid losses (line and transformer) in %, base is simulation *mode A* with 2752MWh (which is 2.7% of the total load's consumption): These results look similar to the grid losses of the basic scenario shown in fig. 6.5 and reasons for the proportion of the results are identical to the reasons given in the description of fig. 6.5. Some aspects are remarkable when comparing these results:
In the growth scenario more generation is hosted than in the basic scenario, so more active power that is demanded by the loads can be provided locally, which can decrease grid losses. Therefore the difference between grid losses of *mode A/B* and *mode C* is significantly higher in the growth scenario (24%) than in the basic scenario (8%). This shows that even if *mode C* (running DGs in $cos\varphi = 0.9$) solves voltage range problems in both scenarios, it can be considered as a suboptimal solution due to the high increase in grid losses.
Both Q(U) control strategies (*mode E* and *F*) produce less losses than *mode G* (which uses as little reactive power as possible to solve range violations), but similar to the basic scenario, these control modes in the simulated form did not solve voltage range problems for about 32% of the time.
Mode L produces slightly less grid losses than *mode G*, but in contrast to the basic scenario it was not possible any more to reduce grid losses below the values of *mode A* and *B*.
The careful reader might see that losses of *mode B* are slightly below the losses of *mode A*, which is reasoned in the p/q-constant model of loads and generation. The extended upper-limit in *mode B* is able to tap up earlier in times of low grid voltages, so having p/q-constant elements in the grid leads to a decrease in grid current (leading to a decrease in grid losses) at higher grid voltages.

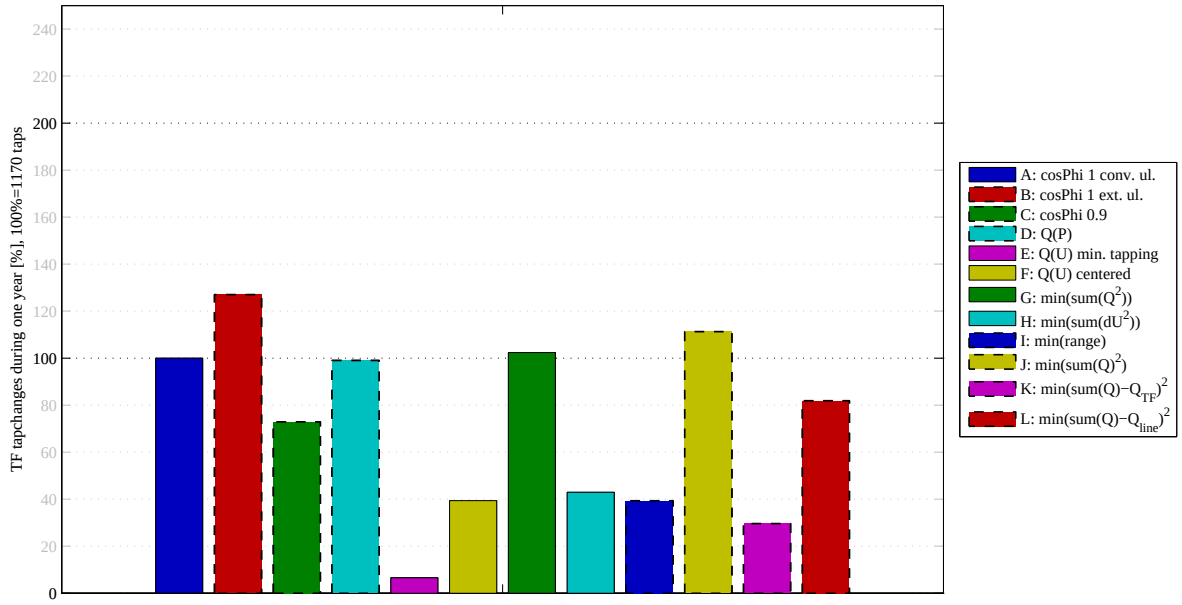

Figure 6.16: SS 'Lungau' growth scenario - tap-changes in %, base is scenario A with 1170 tap-changes during one year. Results are similar to the tap-changes of the basic scenario shown in fig. 6.6, therefore only the differences to the basic scenario will be described here:
The most outstanding difference is the decrease of necessary tap-changes in centered Q(U) control (*mode F*), which is reasoned in the high voltage range: The higher the voltage range, the less tap positions are available that hold all grid voltage within the voltage band. When there is only one tap position, there is no difference between the level control modes (upper-limit, lower-limit, centered, minimum-tapping) any more.
While in the basic scenario *mode B* used around 5% more taps than *mode A*, in the growth scenario *mode B* used around 30% more taps (the time of voltage violation was reduced by around 2,5% as it is shown in fig. 6.19). This is reasoned in the high increase in extended upper-limit operating time: While in the basic scenario, the extended level control mode was operated 15% of the year, it is operated 67% of the year in the growth scenario (fig. 6.17).

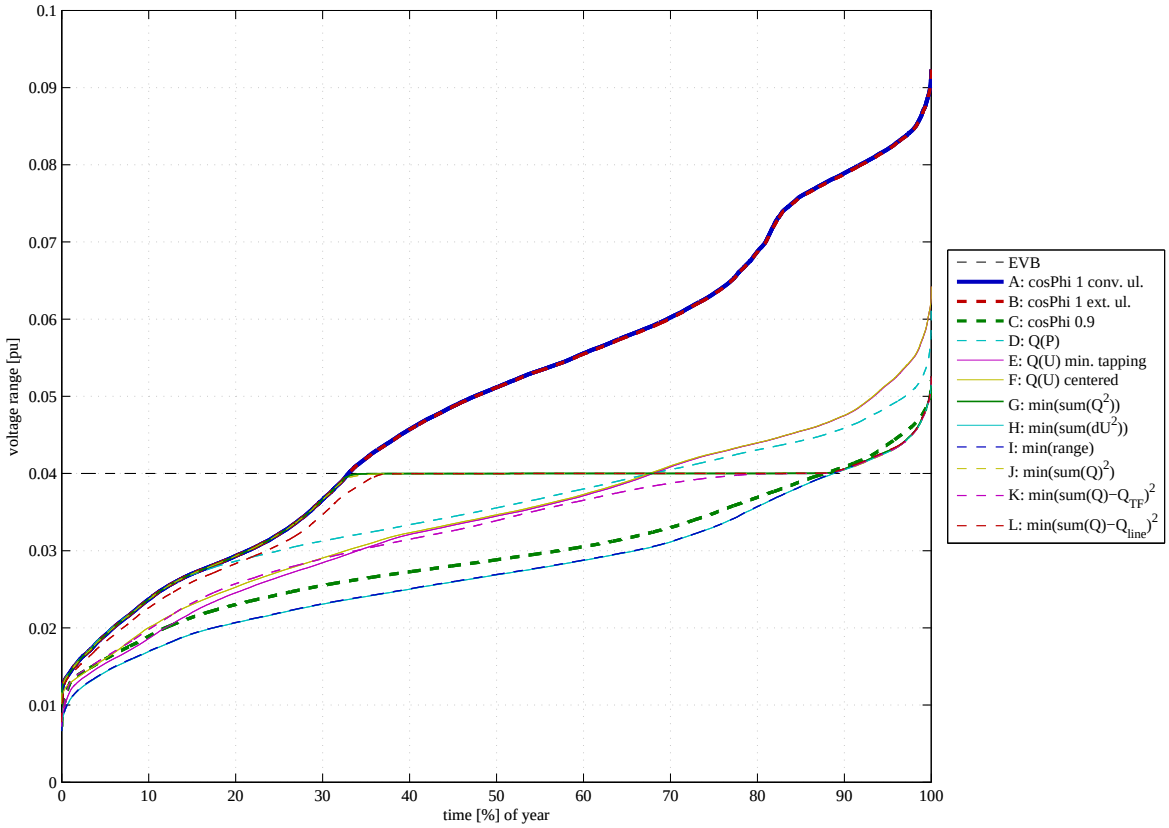

Figure 6.17: SS 'Lungau' growth scenario - duration curve of voltage range [pu]:
Even if this diagram looks very different to fig. 6.7 of the basic scenario, because the time of ranges higher or equal the EVB increased from 15% in basic scenario to 67% in the growth scenario, the explanations given in the description of fig. 6.7 are still valid, so only the differences will be stressed here: In both basic and growth scenario, *mode A*, *B*, *D*, *E* and *F* are not able to keep voltage ranges below the EVB. In the basic scenario all other *modes* are able to do so, which is not possible any more in the growth scenario: All coordinated control modes and *mode C* exceed EVB for 12% of the year, leading to a maximal voltage range of around 0.05pu. Nevertheless the level controller was able to keep grid voltages within its limits for around 99% as it can be seen in fig. 6.19.
It is very interesting that the simple $cos\varphi = 0.9$ mode leads in times when the range exceeds the EVB to similar ranges like the coordinated control strategies.
Overall, this figure shows that operating the grid in the growth scenario is completely impossible without reactive power control and also local control modes Q(U) and Q(P) are insufficient. If grid losses have to be kept low, this grid cannot be operated without coordinated voltage control concepts.
Based on the assumption that grid voltages have to be kept within a voltage band of 0.06pu, this grid is very near at its limit concerning DG hosting capacity.

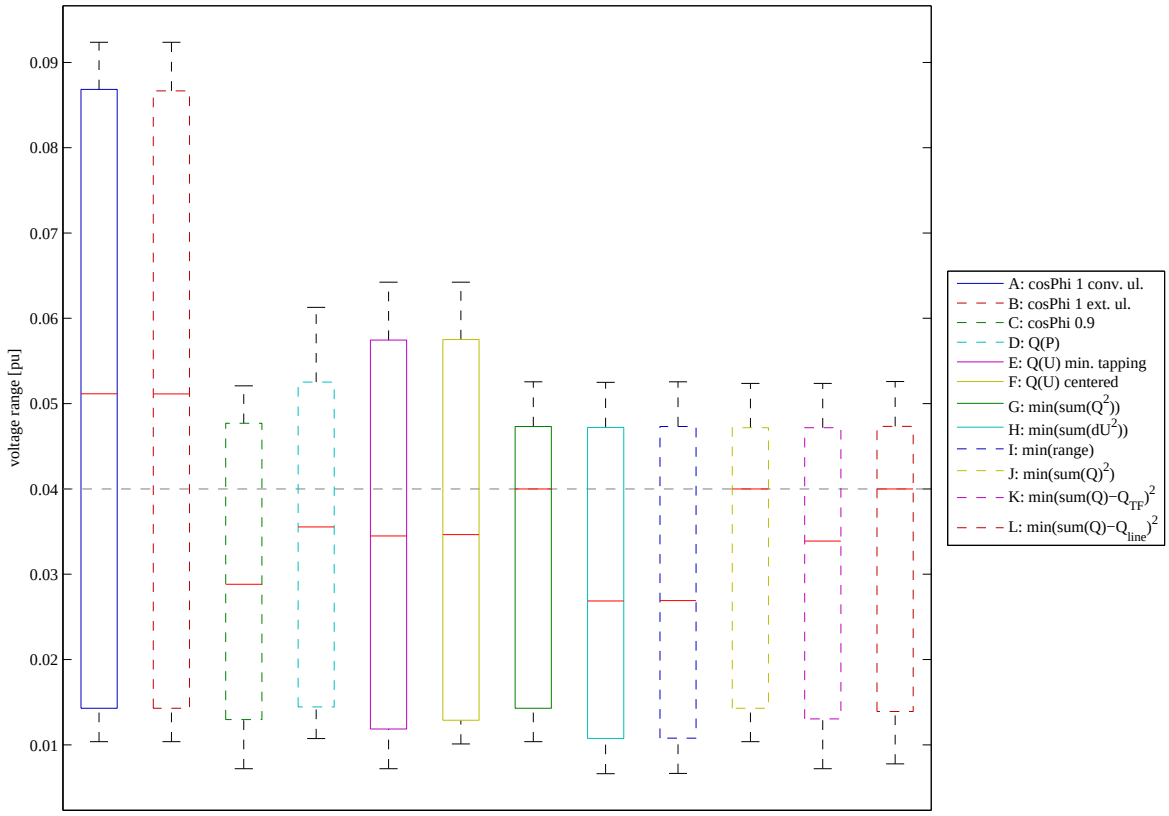

Figure 6.18: SS 'Lungau' growth scenario - boxplot of voltage range [pu] (boxplots show the 1% and 99% percentiles). The results of this figure are also similar to interpret as the results of the basic scenario shown in fig. 6.8.

As shown in the comparison of voltage range duration curves (fig. 6.17), in the growth scenario even the coordinated voltage control strategies are not able to keep 99% of the time the voltage range below the EVB. In fact, 99% of the time all grid voltages can be held below 0.047pu. Since the extended upper-limit is capable of handling voltage ranges up to $VB - \Delta U_{tap} - h = 0.0427 pu$, only an insignificant violation of voltage limits is expected and confirmed in fig. 6.19.

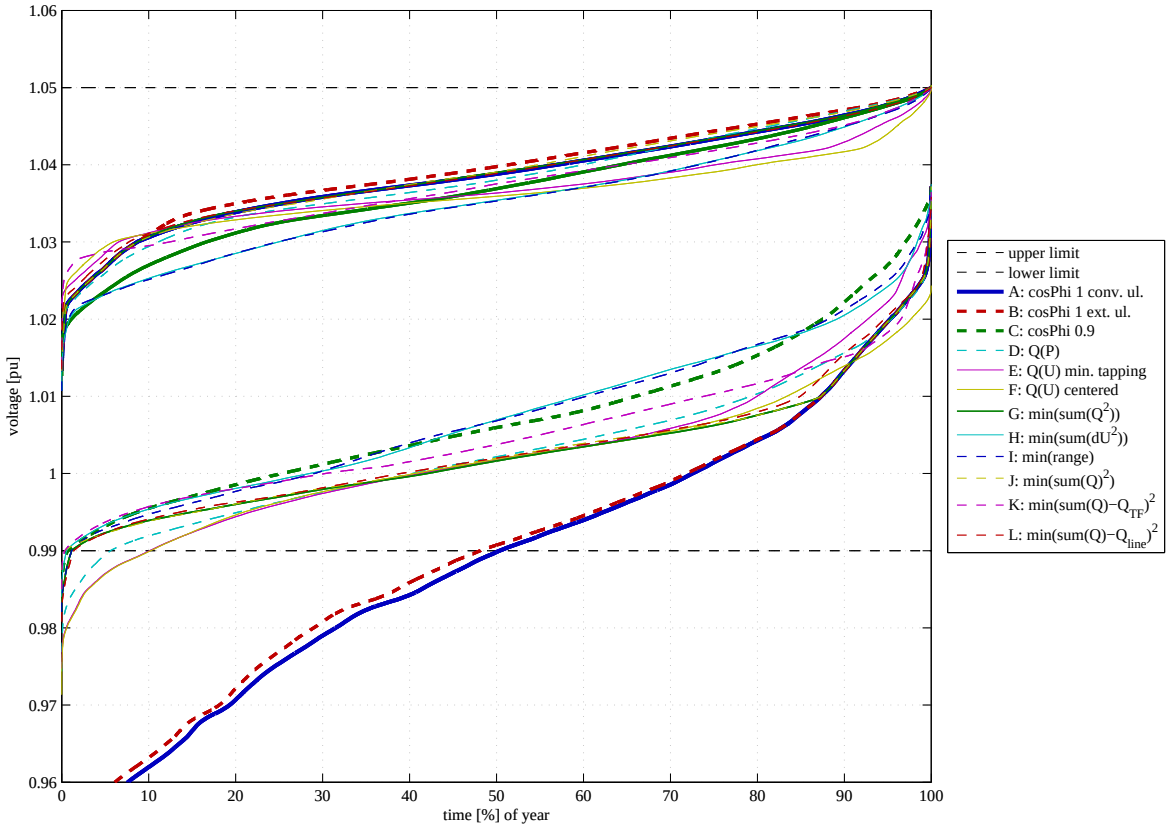

Figure 6.19: SS 'Lungau' growth scenario - duration curve of maximal and minimal grid voltages [pu]: The figure is explained in detail in the correspondent diagram of the basic scenario in fig. 6.9 and only relevant differences between the basic and the growth scenario are discussed here:
Of course, the high voltage ranges of *mode A* and *B* shown in fig. 6.7 lead to very low minimal grid voltages that fall below 0.96pu (because the strategy of the level controller is to avoid overvoltage to save life-time of the electrical equipment). *Mode A* and *B* lead to violated grid voltages in around 50% of the year and *mode E* and *F* violate voltage limits around 10% of the year. *Mode D* running a Q(P) control is more successful with only 5% violations. All other control modes lead to voltage violates for below 1.3% of the year (As mentioned in the description of fig. 6.8, these violations are partly due to the simulation time step of 3minutes which can cause a non-ideal convergence due to CM non-linearities when grid situation change significantly from one time-step to the next).

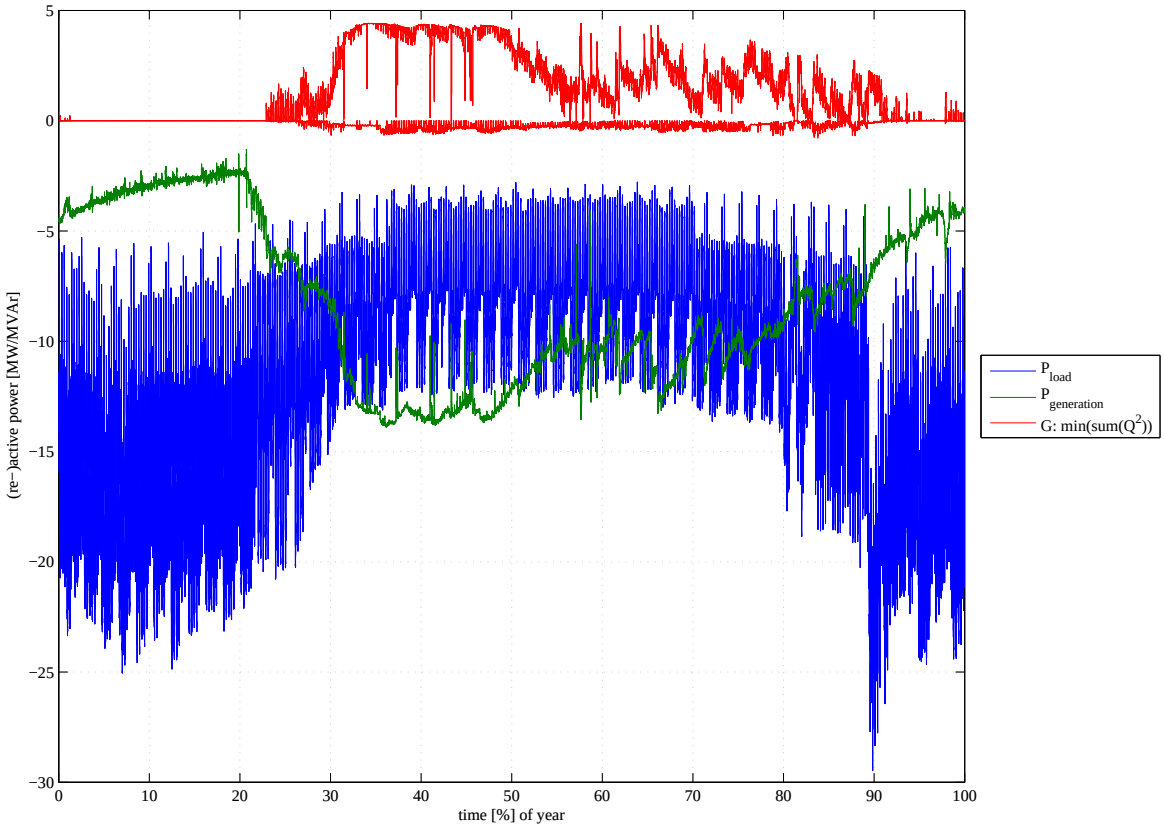

Figure 6.20: SS 'Lungau' growth scenario - time series of loads active power demand ($-P_{load}$) and DGs' active power feed-in ($P_{generaion}$) in [MW] and minimal reactive power demand on DGs to keep voltages within voltage limits (calculated in *mode G*) in [MVAr]: The detailed explanation to this figure is given in fig. 6.10, where the load curve is exactly the same in the basic and the growth scenario. The generation curve differs due to the increase in DG penetration in the growth scenario, leading to a higher mount of necessary reactive power to compensate high voltage ranges. It can be seen that in the growth scenario reactive power is necessary in spring, summer and autumn and not only in spring as it was the case in the basic scenario.

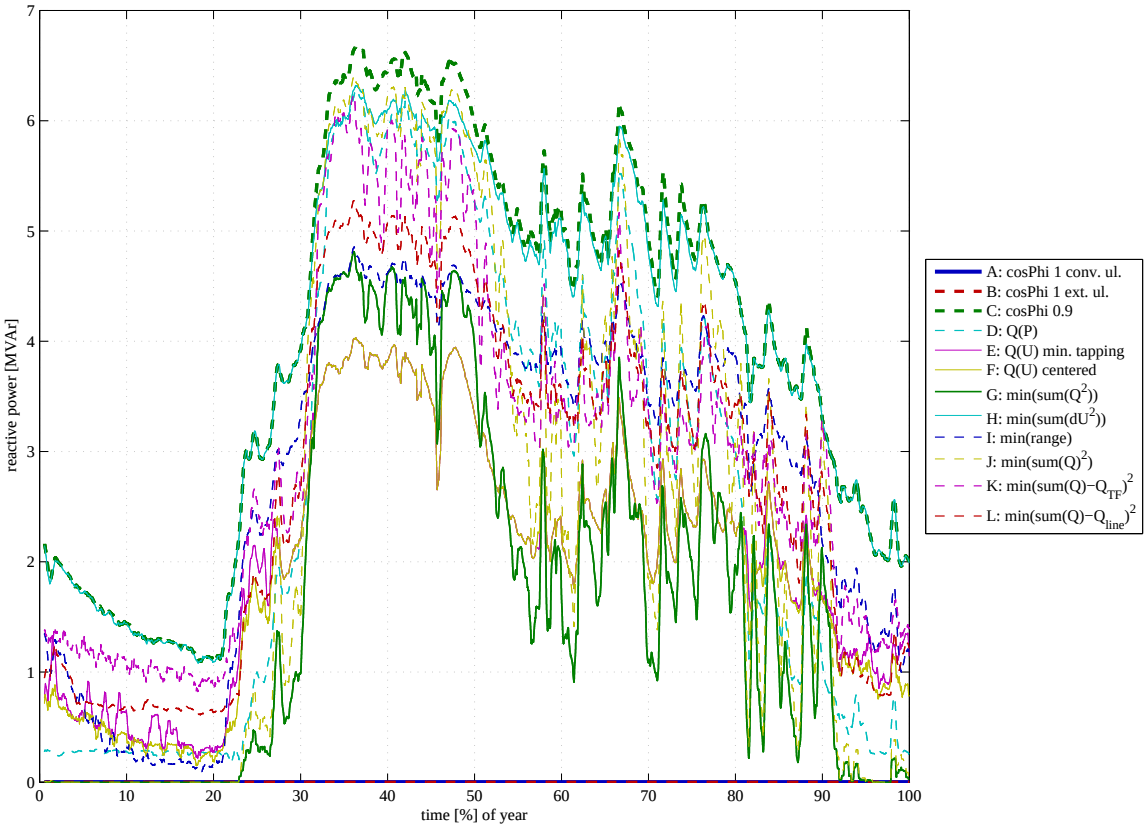

Figure 6.21: SS 'Lungau' growth scenario - time series of absolute sum of DGs' reactive power [MVAr] that is requested by the control mode (the curve is filtered with a 2days gliding average):
A detailed description of what is seen here is given in fig. 6.11 of the basic scenario.
While in the basic scenario the maximal absolute sum of reactive power provided by the DGs was below 4MVAr, it significantly increased to nearly 7MVAr in the growth scenario (see *mode C*).
The most significant difference is given in the results of *mode G*. While in the basic scenario not more than 1MVAr of reactive power was necessary to solve range violations most of the time, in the growth scenario up to nearly 5MVAr reactive power is necessary during snow melting.
In the basic scenario *mode E* and *F* used more reactive power than *mode G* without successfully keeping voltage ranges small, but interestingly in the growth scenario these modes use less reactive power than *mode G*.

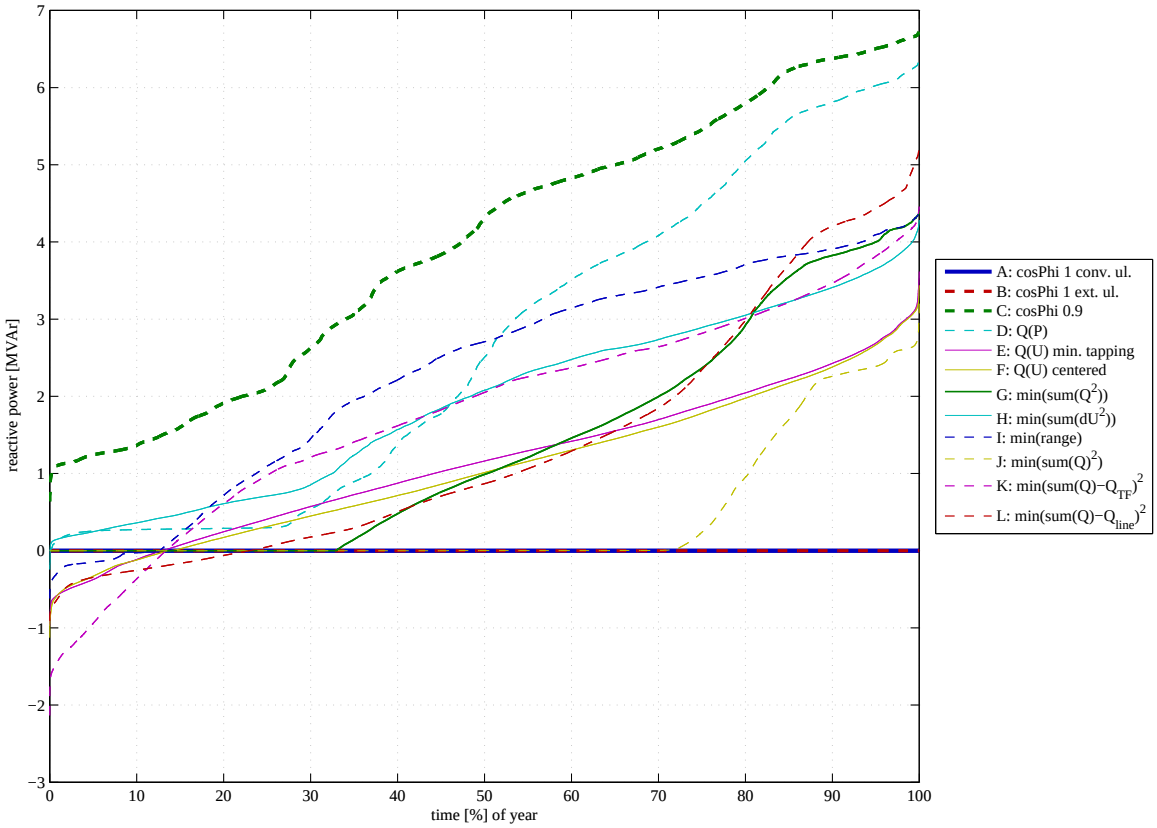

Figure 6.22: SS 'Lungau' growth scenario - duration curve of sum of DGs' reactive power [MVAr] (see fig. 6.12 of basic scenario for description):
It is readily identifiable that *mode J* is not able to reach its objective function goal to minimise the sum of requested reactive power for around 36% of the year, because in this time the range control objective overrules the optimisation objective. Nevertheless the time where the sum of the DGs' reactive power is held at zero doubled compared to *mode G*.

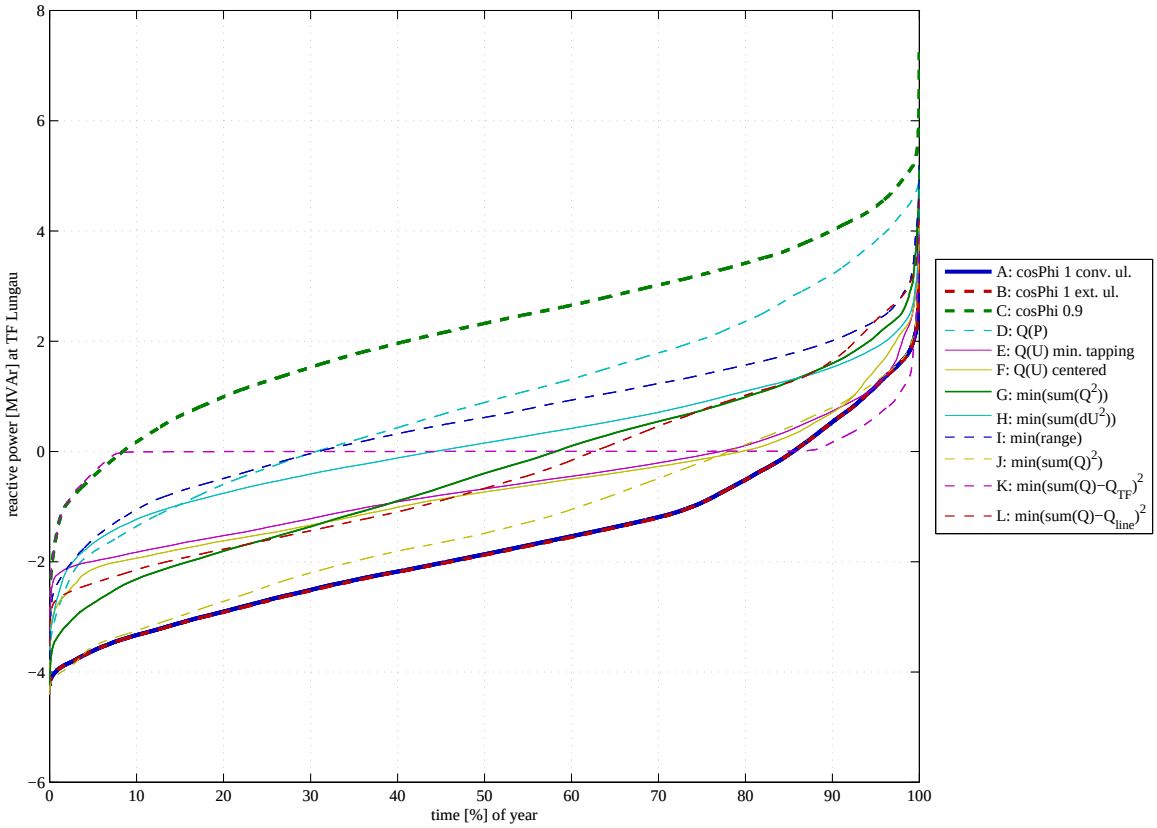

Figure 6.23: SS 'Lungau' growth scenario - duration curve of reactive power flow over the transformer [MVAr] (see fig. 6.13 of basic scenario for description):
The increase in hosted DGs brings more controllable reactive power, so the times the reactive power flow over the transformer is zero (objective from *mode K*) increased from nearly 50% in basic scenario to 90% in the growth scenario.

The results of the reactive power flow over selected grid lines are not shown here, because these results are quite similar to the results shown in fig. 6.14 (this is because all DGs that were added to the grid in growth scenario are connected to the same feeder 'Madling') and no relevant new insights can be obtained with these results.

6.5.2 SS 'Nenzing'

6.5.2.1 Basic Scenario

Note that in basic scenario the voltage lower limit for simulation was set from 0.99 to 1.005pu (so the valid voltage band was reduced from 0.06pu to 0.045pu), because otherwise due to the small voltage ranges in the grid no voltage control would be necessary during the whole year (so *mode G* and *J* would never request reactive power). By increasing the voltage band lower limit, it can be tested how the control modes behave when the grid's operating voltage range is reduced to an artificially low value.

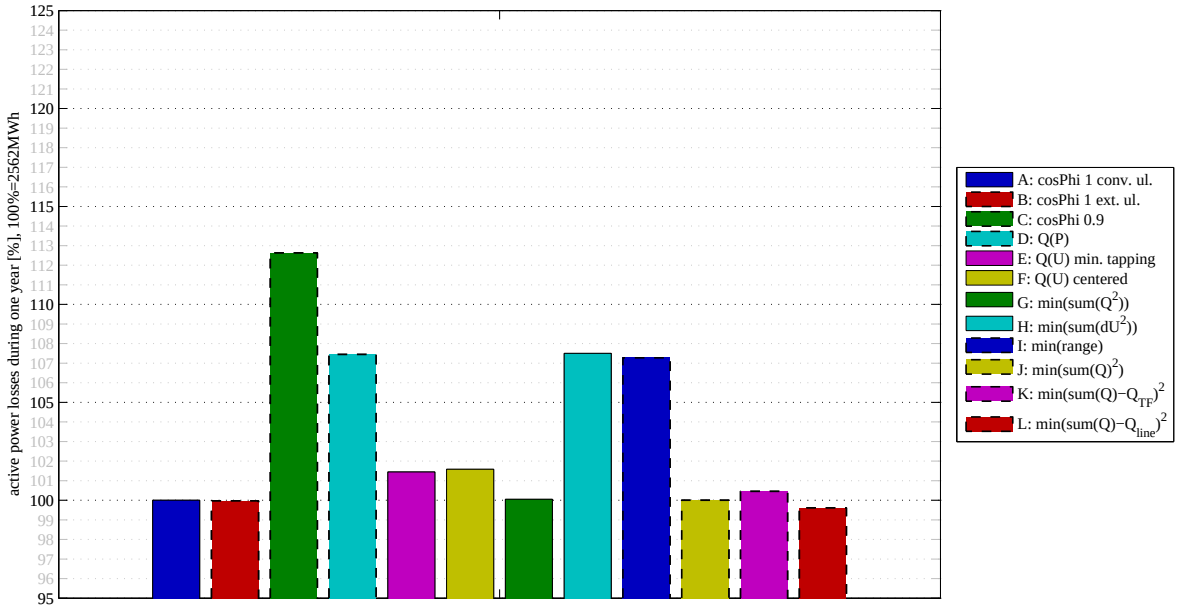

Figure 6.24: SS 'Nenzing' basic scenario - grid losses (line and transformer) in %, base is simulation *mode A* with 2562MWh (which is 1.8% of the total load's consumption): Even if the grid SS 'Nenzing' is completely different from SS 'Lungau', the results here look very similar to the results of SS 'Lungau' basic scenario in fig. 6.5, therefore only the differences of both figures are stressed here.
In principal losses are higher in SS 'Nenzing', but referred to the supplied load they are approximately equal. Loss variation is higher in SS 'Nenzing' (+12,5% in *mode C*) than in SS 'Lungau' (+8,4% in *mode C*), because in SS 'Nenzing' nearly 33MW generation is installed while in SS 'Lungau' nearly 8MW is installed. Therefore the impact of the different control modes is higher in SS 'Nenzing' than in SS 'Lungau'.
The only significant difference in the relation of the results is *mode K*, because here the minimisation of the TF's reactive power increases losses about 0.5% while in SS 'Lungau' they are increased by nearly 5%. This is reasoned in the more uniform spreading of the DGs over the whole grid in SS 'Nenzing', so the likelihood is higher that the DGs reduce the reactive power where it is generated. But in fact also in this grid *mode K* doesn't bring the expected reduction in grid losses (HV grid loss reduction not considered), therefore more information has to be considered for the reduction of grid losses like in *mode L*, which was able to reduce losses for around 0.3%. Also in SS 'Nenzing' the selection of reactive power measurement lines was done without optimisation, so no prediction can be made with this result, how far the losses can be reduced by optimising the placement of reactive power measurements.

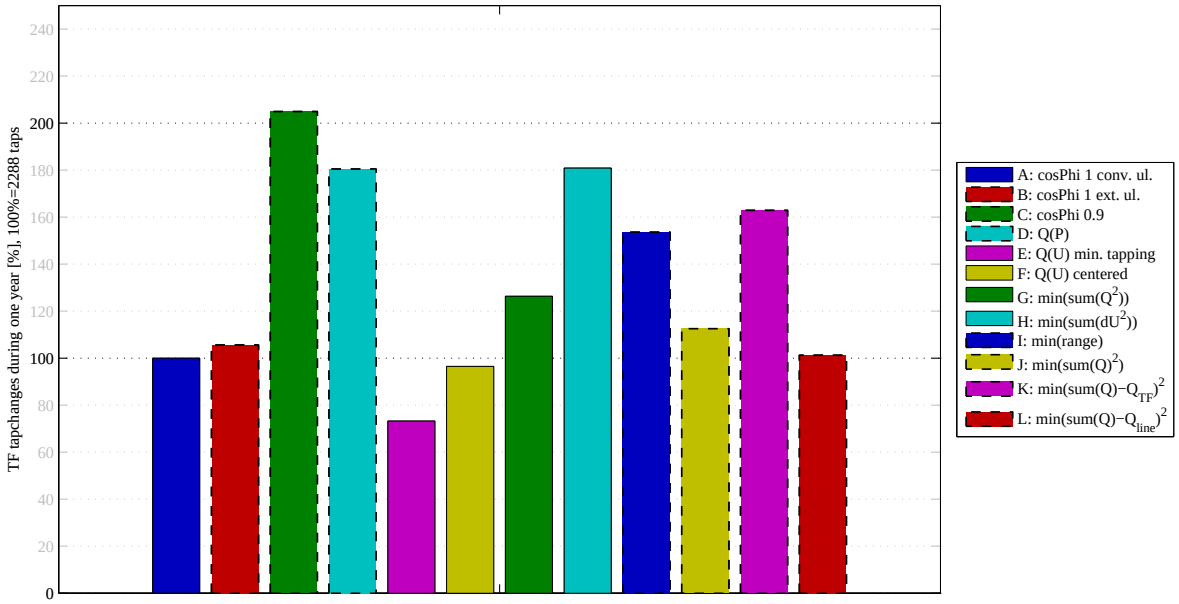

Figure 6.25: SS 'Nenzing' basic scenario - tap-changes in %, base is mode A with 2288 tap-changes during a year (see fig. 6.6 for description): Three significant differences between SS 'Lungau' (fig. 6.6) and SS 'Nenzing' lead to completely different results in the number of tap-changes:
Firstly, the nominal tap-change height in SS 'Nenzing' is with -0.0112755pu significantly smaller than -0.015275pu in SS 'Lungau', so the "Nenzing" OLTC needs much more tap-changes to balance load and generation variations.
Secondly, the valid voltage band was decreased, so the level control mode minimum-tapping had only little scope to avoid tap-changes.
Thirdly, three DGs in SS 'Nenzing' with a total nominal feeding power of 28MW are operated scheduled according to marked prices. This means these DGs idle around one half of the year and the other half they operate at their nominal feeding power with a changeover between idle and nominal power feeding that is fast compared to other grid dynamics (load and generation variation). This leads to many significant changes in grids loading and during this changeover and the TF has to perform up to three tap-changes during these situations.
So in SS 'Lungau' *mode C* was able to reduce necessary tap-changes because voltage rise at DG feeding points was reduced, but in SS 'Nenzing' the combination of significant changing of active power loading and significant changing of reactive power loading lead to a high increase in necessary tap-changes (and similar for *mode D*).
It is readily identifiable that *mode J* is able to reduce the number of tap-changes compared to *mode G*, because the minimal necessary amount of reactive power that is requested in *mode G* is balanced in *mode J*. This means that reactive power flow over the transformer does not change significantly in *mode J* compared to *mode A* and *B*, so changes of TF busbar voltage due to changes in voltage drop at the TF series impedance are minimised.

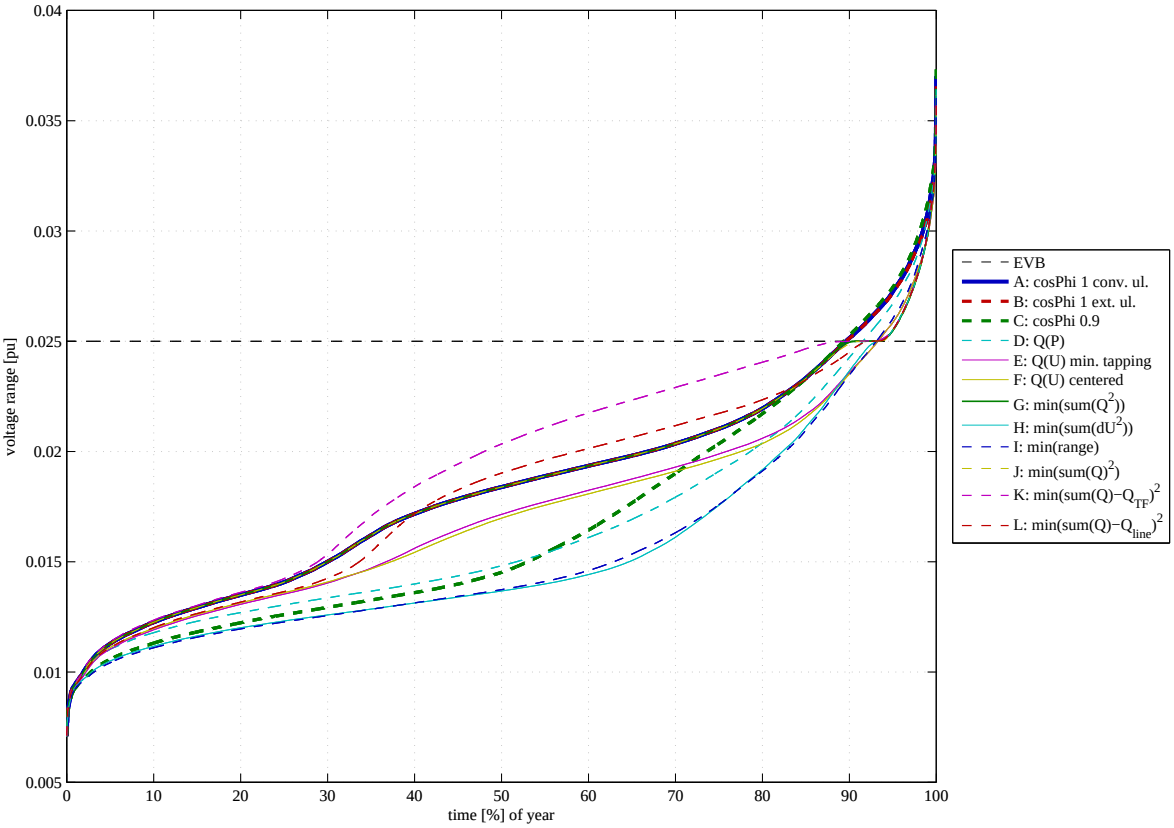

Figure 6.26: SS 'Nenzing' basic scenario - duration curve of voltage range [pu] (see fig. 6.7 for description):

A very surprising insight is that running *mode C* reduces voltage range in times of low ranges, but in times of high ranges, ranges resulting from *mode C* do not significantly differ from ranges of *mode A* and *B*. This is reasoned in the fact that the high voltage ranges do not occur during snow melting in spring where *mode C* could reduce voltage rise caused by DG feeding, but the high voltage ranges occur during winter caused by high load (ski lifts among other things) and in these times where the TF busbar voltage is the highest voltage in the grid consuming reactive power will not decrease voltage range and in fact it slightly increases voltage range.

It is readily identifiable that all coordinated control *modes G* to *L* are able to keep voltage ranges below EVB for 94% of the year, while all other (local) control modes perform inferior. In this scenario the EVB is reduced (resulting from the shift of the lower-limit to 1.005pu), therefore the 6% of the year where the voltage range is above the EVB are not critical - and in fact no voltage violations occurred as shown in fig. 6.28.

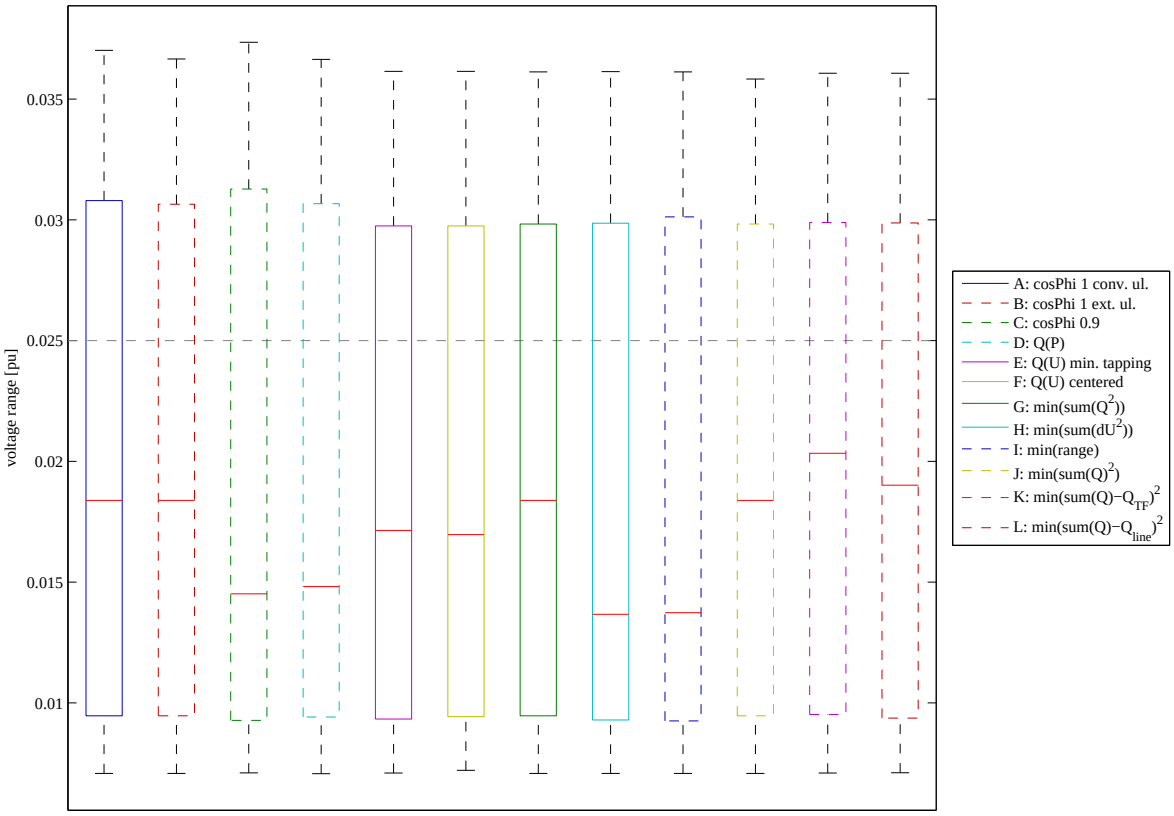

Figure 6.27: SS 'Nenzing' basic scenario - boxplot of voltage range [pu] (boxplots show the 1% and 99% percentiles):
Compared to the voltage range boxplots of SS 'Lungau' (fig. 6.8 and 6.18), the boxplots of the different control modes shown here are all very similar, which means that reactive power control is very limited at these boundary conditions: Of course, the voltage band can't be reduced arbitrary, and voltage ranges in SS 'Nenzing' basic scenario are already very low, so in this case it is not possible to achieve a significant improvement of the 99% percentiles and the maximum values, but influencing the median voltage range values is still possible.
The voltage ranges that exceed the EVB lead to voltage violations only in *mode A*, because the extended level control mode is able to keep grid voltages within the given voltage limits if voltage range is smaller than $VB - \Delta U_{tap} - h = 0.032pu$, therefore voltage range violations do not lead to voltage violations as shown in 6.19.

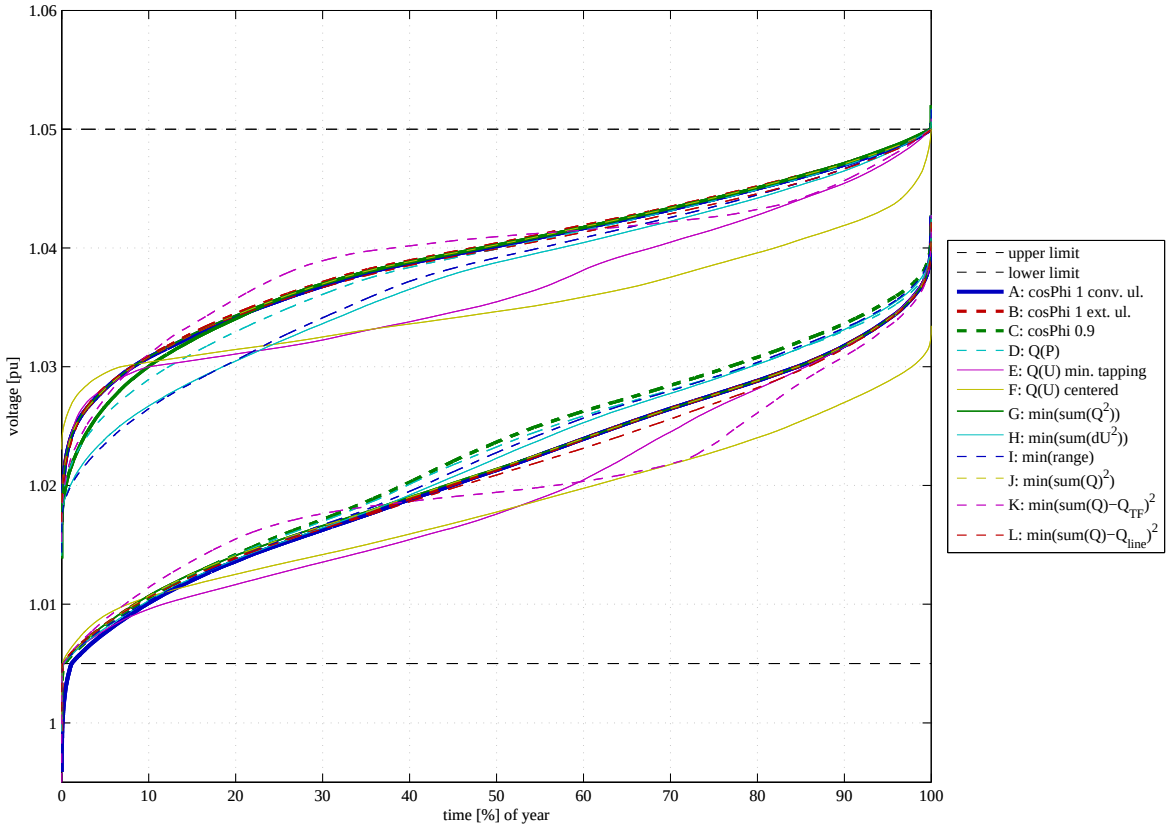

Figure 6.28: SS 'Nenzing' basic scenario - duration curve of maximal and minimal grid voltages [pu] (see fig. 6.9 for description):
This figure shows the advantage of the level control mode extension that is operated in *mode B* to *L*, which holds all grid voltages within the given voltage limits. The only violation is done in *mode A*, where around 1% of the year undervoltage occurs.

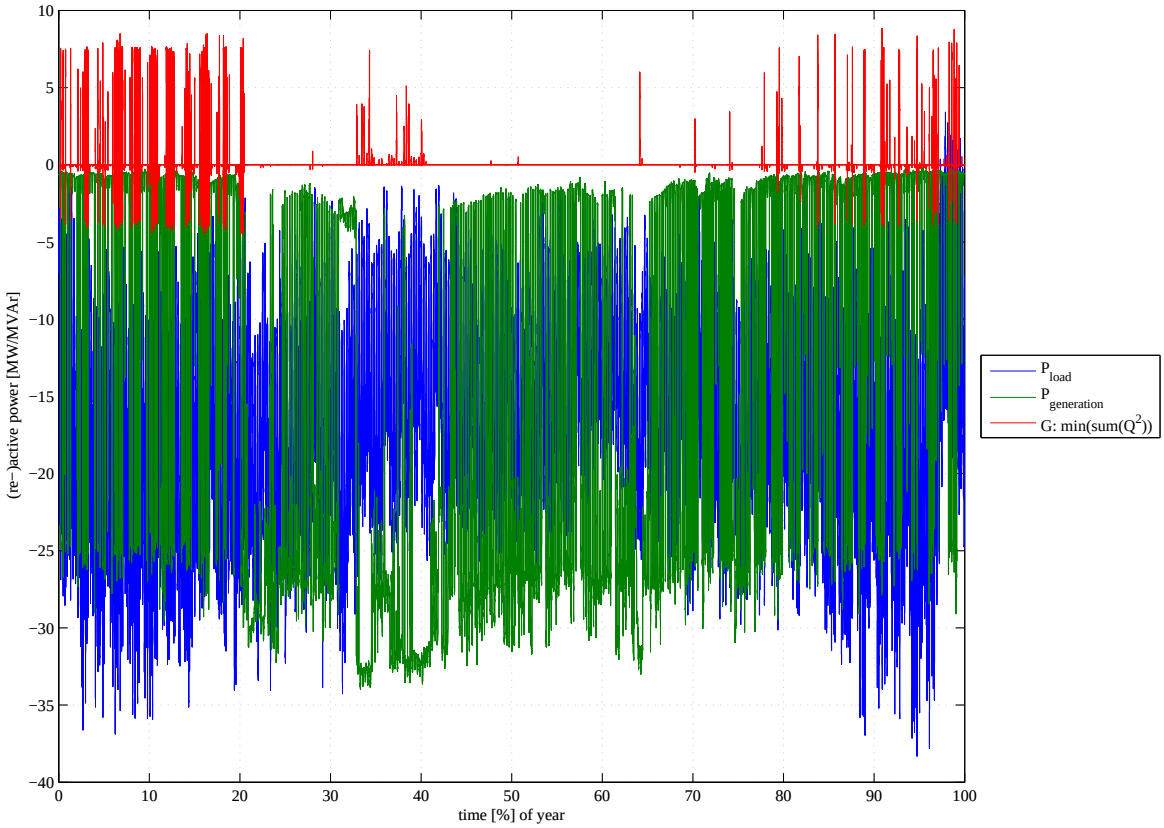

Figure 6.29: SS 'Nenzing' basic scenario - time series of loads active power demand ($-P_{load}$) and DGs' active power feed-in ($P_{generaion}$) in [MW] and minimal reactive power demand on DGs to keep voltages within voltage limits (calculated in *mode G*) in [MVAr] (see fig. 6.10 for detailed description):
The daily load variation is similar to the daily load variation of SS 'Lungau', but the seasonal load variation is smaller than in SS 'Nenzing'. The surprisingly high variation of generation in SS 'Nenzing' which does not exist in SS 'Lungau' is caused by the three DGs with total feeding power of 28MW that are scheduled operated (as mentioned in the description of fig. 6.25). Here it can be seen that these three DGs are started and stopped roughly spoken in a daily rhythm except in spring where these DGs are active permanently. Therefore reactive power that is minimal necessary to control voltage range also vary roughly spoken in a daily rhythm, and it can be seen that here in times of high generation no reactive power is needed, while it is needed predominantly in winter. This "inverse" situation is caused in the fact that the grid is well developed and in the basic scenario no reactive power control would be needed to safely operate the grid.

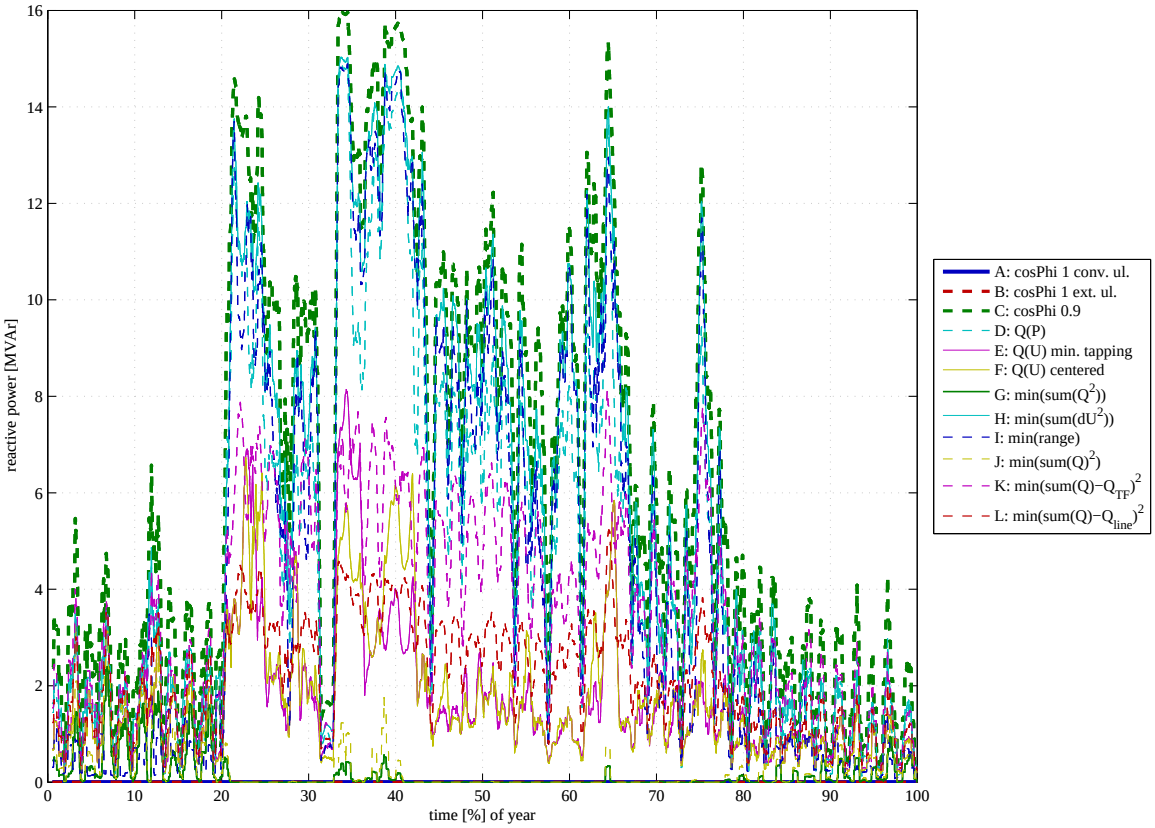

Figure 6.30: SS 'Nenzing' basic scenario - time series of absolute sum of DGs' reactive power [MVAr] that is requested by the control mode (see fig. 6.11 for detailed description):
The filtering with a 2-days gliding average balances the high scheduled generation variation, so that the seasonal generation variation can be seen in this figure, which is hardly identifiable in fig. 6.29. In fact many scheduled generation variations are still visible, because this diagram shows a significant higher dynamic than fig. 6.11 of SS 'Lungau' in basic scenario.
Mode G uses hardly any reactive power during spring and summer because it is not necessary, but during this time all local control modes use much reactive power that could be saved.

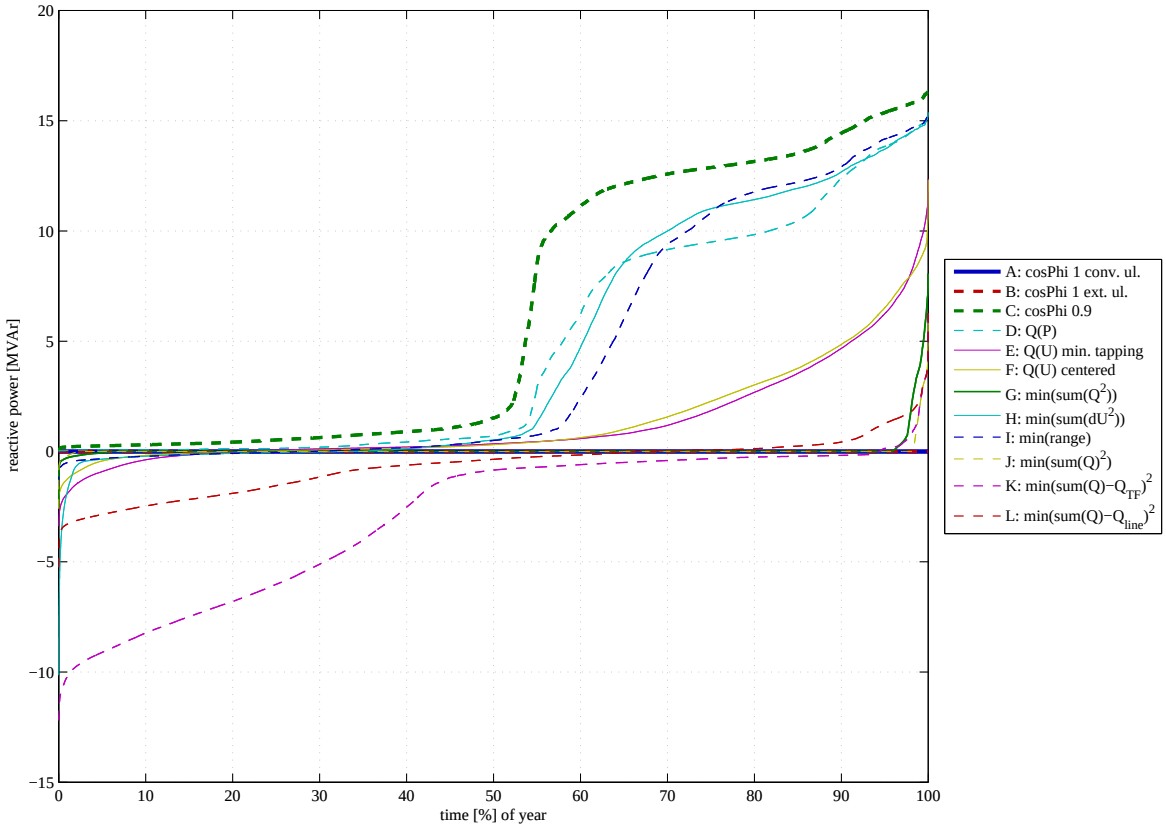

Figure 6.31: SS 'Nenzing' basic scenario - duration curve of sum of DGs' reactive power [MVAr] (see fig. 6.12 for detailed description):
The specific curve progression of *mode C* is reasoned in the scheduled operation of three scheduled DGs mentioned in the description of fig. 6.25: Since these DGs with 28MW feeding power in total dominate the rest of the DGs, the duration curves make it possible to see whether this DGs are active or not.
This figure shows that *mode J* is able to minimise the sum of the controlled reactive power for around 96% of the year, so only 4% of the year voltage range constraints are predominant.

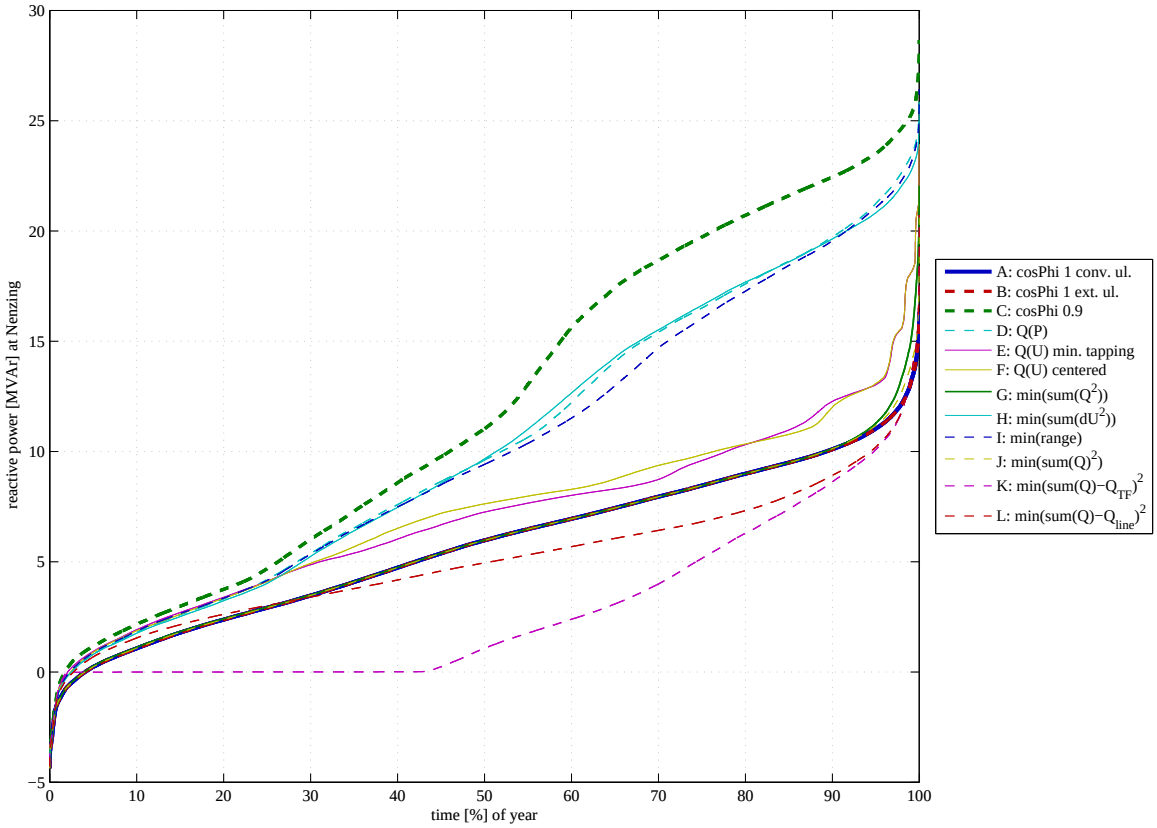

Figure 6.32: SS 'Nenzing' basic scenario - duration curve of reactive power flow over the transformer [MVAr] (see fig. 6.13 for detailed description):
It is readily identifiable that *mode K* is able to bring the TF's reactive power flow to zero for around 40% of the year. Therefore the production of reactive power (positive in generator's perspective) is necessary in contrast to SS 'Lungau', where mostly the consumption of reactive power (negative in generator's perspective) is necessary.

Fig. 6.33 on the next page show the duration curves of eight selected reactive power measurements of grid lines as input for reactive power optimisation. All reactive power measurement lines (14 altogether) are shown in fig. 6.2 highlighted by yellow dots, but only the eight figures with the highest controllable reactive power behind the measured line (having the highest variation in curve progression) are shown in this figure.
In contrast to the reactive power measurements in SS 'Lungau' (see fig. 6.14) where the duration lines of *mode L* fit the zero line where it was possible, in SS 'Nenzing' only a little duration curves of *mode L* fit the zero line. This is reasoned in the fact that in SS 'Nenzing' more reactive power measurements were used for simulation, therefore most DGs are placed behind more than one reactive power measurement and all reactive power measurements on the direct way between every DG and the TF were considered in the reactive power optimisation process.

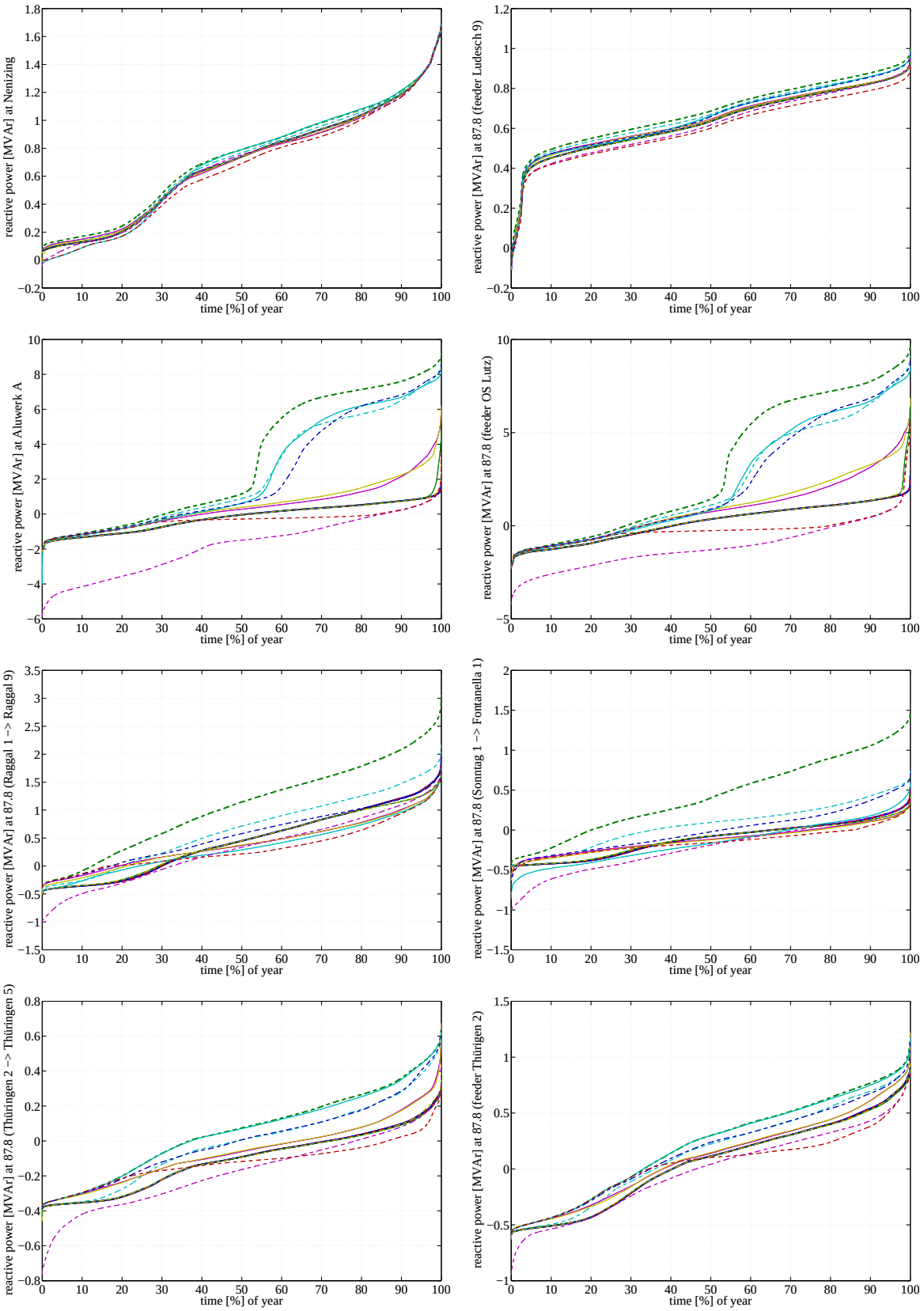

Figure 6.33: SS 'Nenzing' basic scenario - duration curve of reactive power flow over distribution station feeder and grid lines [MVAr] (explanation and line legend on the previous page).

6.5.2.2 Growth Scenario

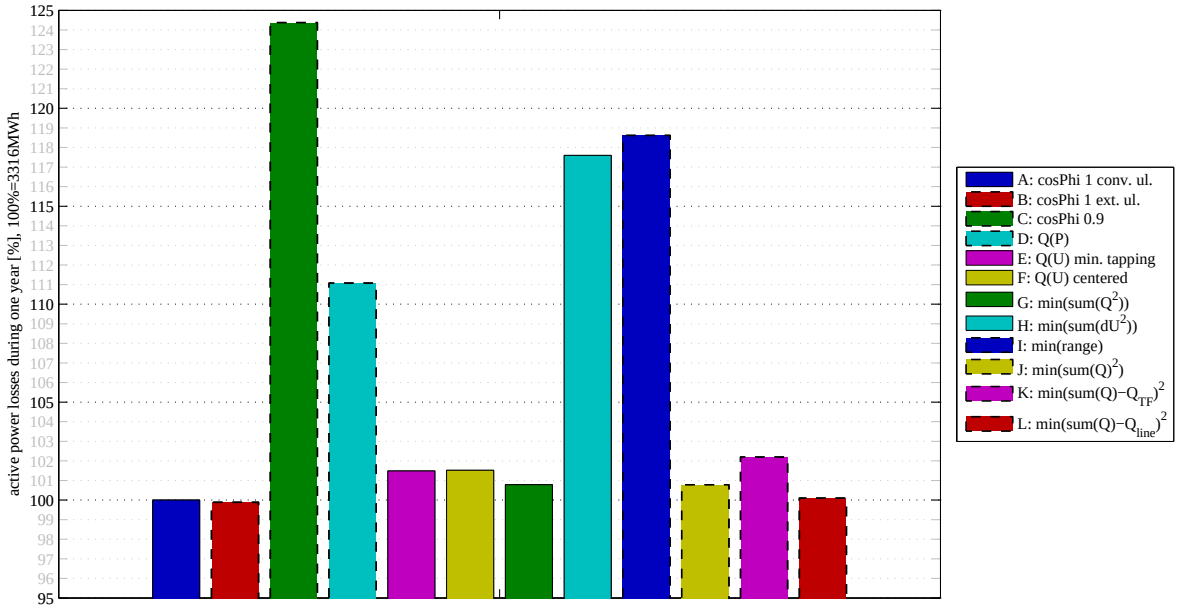

Figure 6.34: SS 'Nenzing' growth scenario - grid losses (line and transformer) in %, base is simulation *mode A* with 3316MWh (which is 2.3% of the total load's consumption):

Compared to the basic scenario (see fig. 6.24), losses in the growth scenario look very similar, because the major differences are only in *mode C*, *H* and *I* (it must be considered that basic scenario was simulated with reduced voltage limits, so the scenarios can't be compared directly). It is clear that *mode C*, *H* and *I* request very much reactive power from all DGs, so the increase in hosted DGs' feeding power from nearly 33MW to nearly 46MW leads to a significant increase in grid losses in these control modes.

Mode I produces higher grid losses than *mode H*, although *mode H* optimises all grid voltages and *mode I* only minimises the voltage range. This is because *mode I* requests more reactive power (absolutely) from the DGs than *mode H* (so the absolute sum is higher, see fig. 6.40), but the sum of reactive power requested in *mode I* is higher than in *mode H* (see fig. 6.41), so *mode H* produces less additional reactive power flow over the transformer (see fig. 6.42) and over grid lines.

It was possible to compensate the additional losses produced in *mode G* (below 1%) by minimising grid lines reactive power flow (*mode L*).

Like described in fig. 6.15, *mode B* produces slightly less losses than *mode A*, because the extension of the level control modes for times of high ranges enables earlier up-tapping in times of low grid voltages, so line current flow is reduced due to PQ-constant loads and DGs.

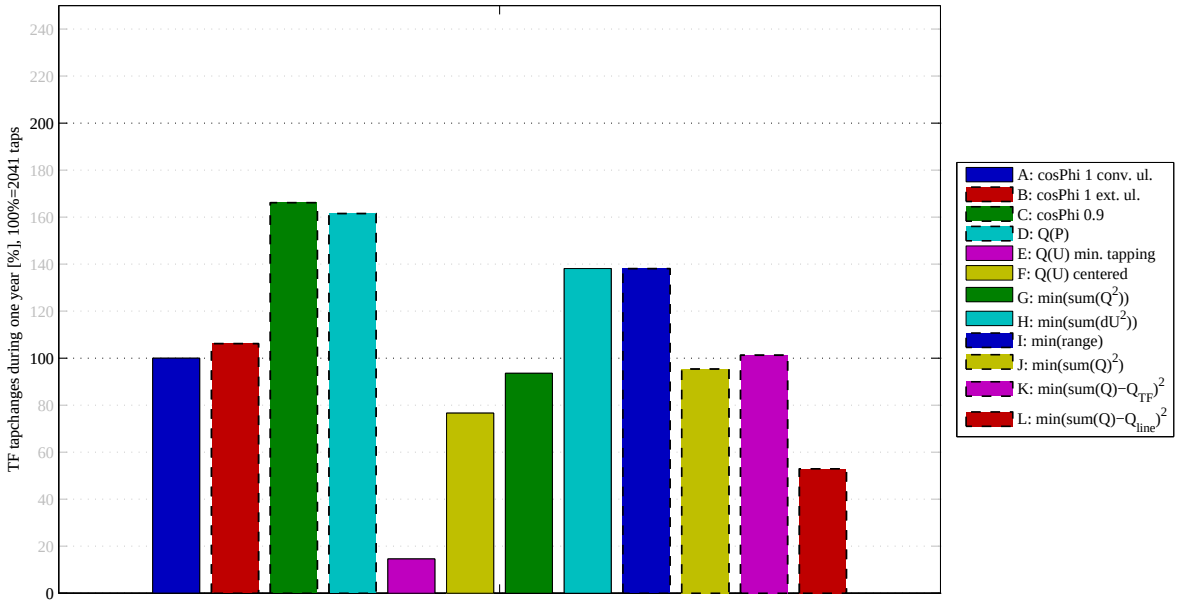

Figure 6.35: SS 'Nenzing' growth scenario - tap-changes in %, base is mode A with 2041 tap-changes (see fig. 6.6 for description):
The number of performed tap-changes in the growth scenario is smaller than the number of necessary tap-changes in the basic scenario, because voltage band was decreased in basic scenario (so minimum-tapping had only little scope to avoid tap-changes). Obviously the reset to the original voltage band has a higher impact on the number of tap-changes than the integration of nearly 17MW additional generation. 46MW controllable DGs contribute enough reactive power, so that tap-changes can be reduced to a sixth when operating *mode E*, where all DGs utilise their reactive power to absolutely control feed-point voltage.

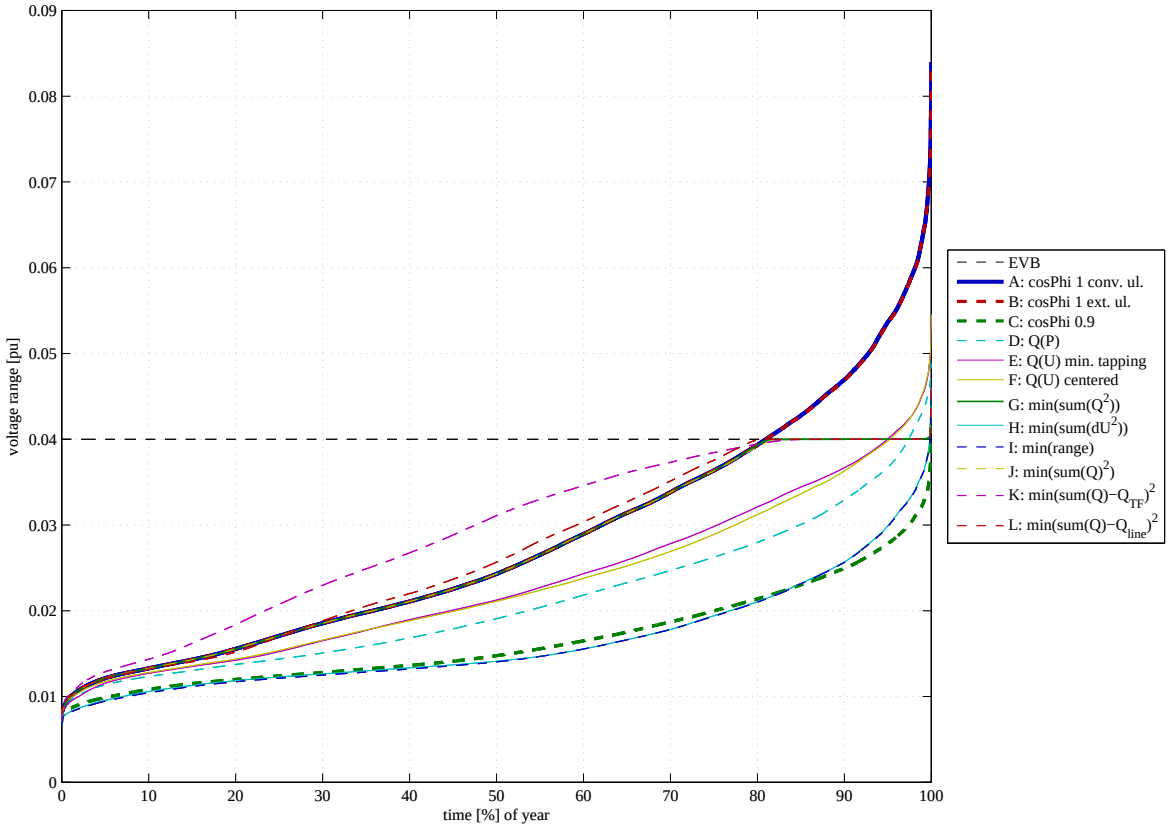

Figure 6.36: SS 'Nenzing' growth scenario - duration curve of voltage range [pu] (see fig. 6.7 for description):
All uncoordinated control modes lead to voltage range violation except *mode C* (*mode A* and *B* about 19%, *mode E* and *F* about 5% and *mode D* about 2.5% of the year).
It is readily identifiable that in times of high ranges *mode C* produces lower ranges than *mode H* and *I*, which can be reasoned in the linearisation of the contribution matrix: It was derived in chap. 4.3 that linear CM values are valid when the state of the grid is not far away from the point where the CM was linearised. 46MW controllable DGs offer controllable reactive power in the order of 23MW, which is definitely enough to "bring the grid far away" from the point the CM was calculated.

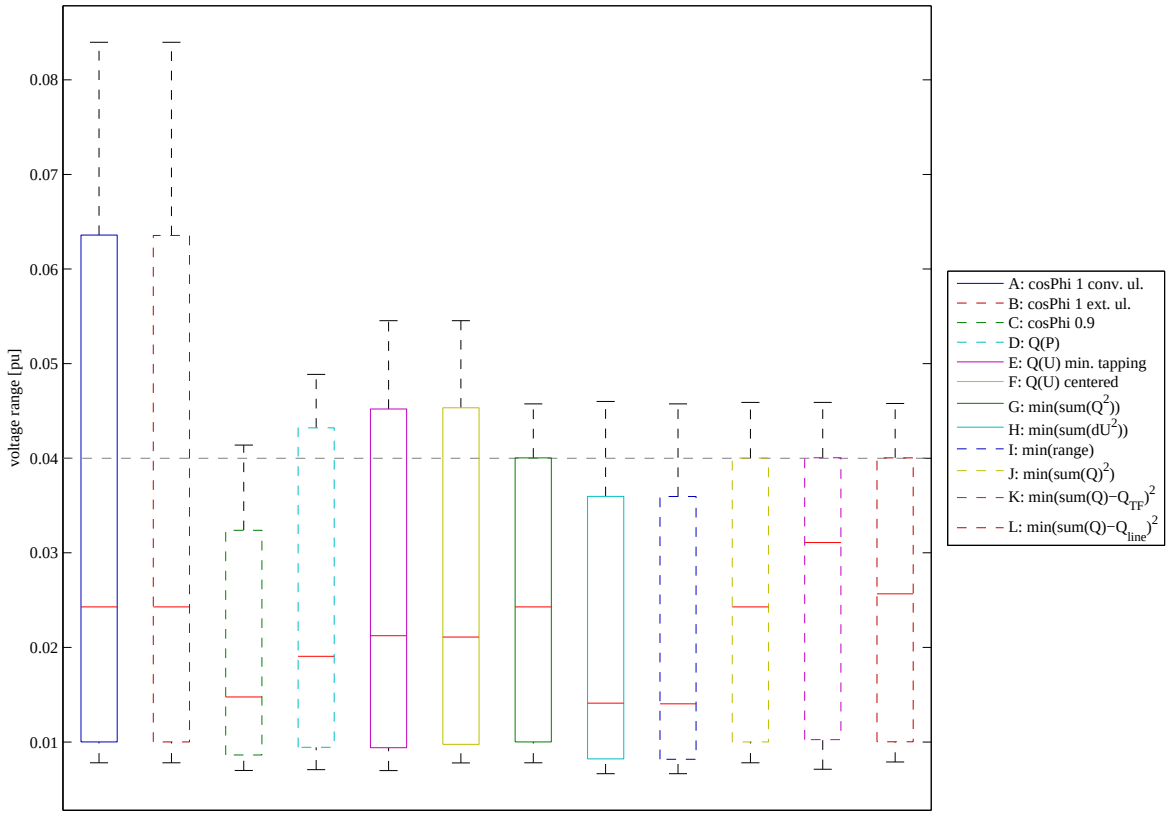

Figure 6.37: SS 'Nenzing' growth scenario - boxplot of voltage range [pu] (boxplots show the 1% and 99% percentiles):
In contrast to the basic scenario (fig. 6.27), where due to the well developed grid differences between the used voltage ranges of the simulated modes were insignificant, voltage ranges here have a high affinity to the ranges of SS 'Lungau' basic scenario shown in fig. 6.8, therefore only differences to this figure are stressed here:
Mode C uses less voltage range than *mode H* and *I*, which is explained in the description of fig. 6.36.
The 99% percentile of *mode D*'s voltage range is above the EVB while it is below the EVB in fig. 6.8.

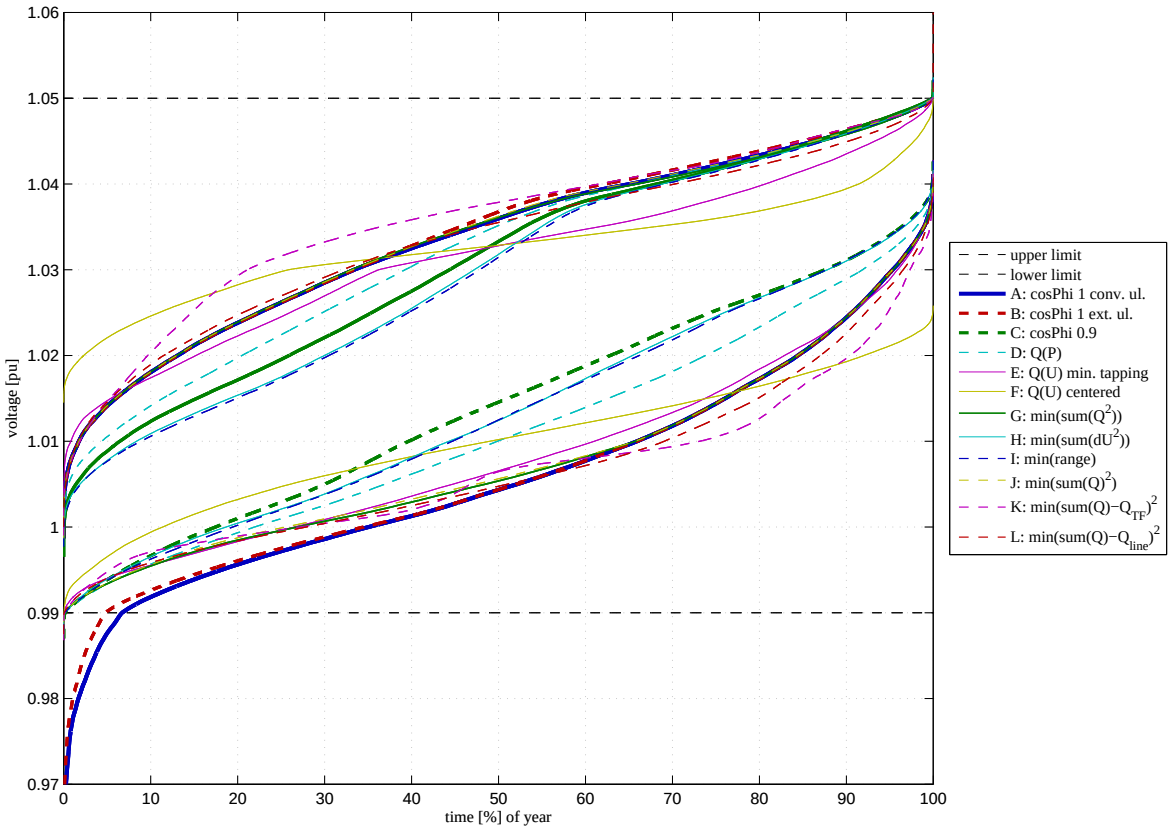

Figure 6.38: SS 'Nenzing' basic scenario - duration curve of maximal and minimal grid voltages [pu] (see fig. 6.9 for description):
Mode A and *B* are the only modes that lead to voltage limit violations (7% of the year in *mode A*, and 5% in *mode B*).

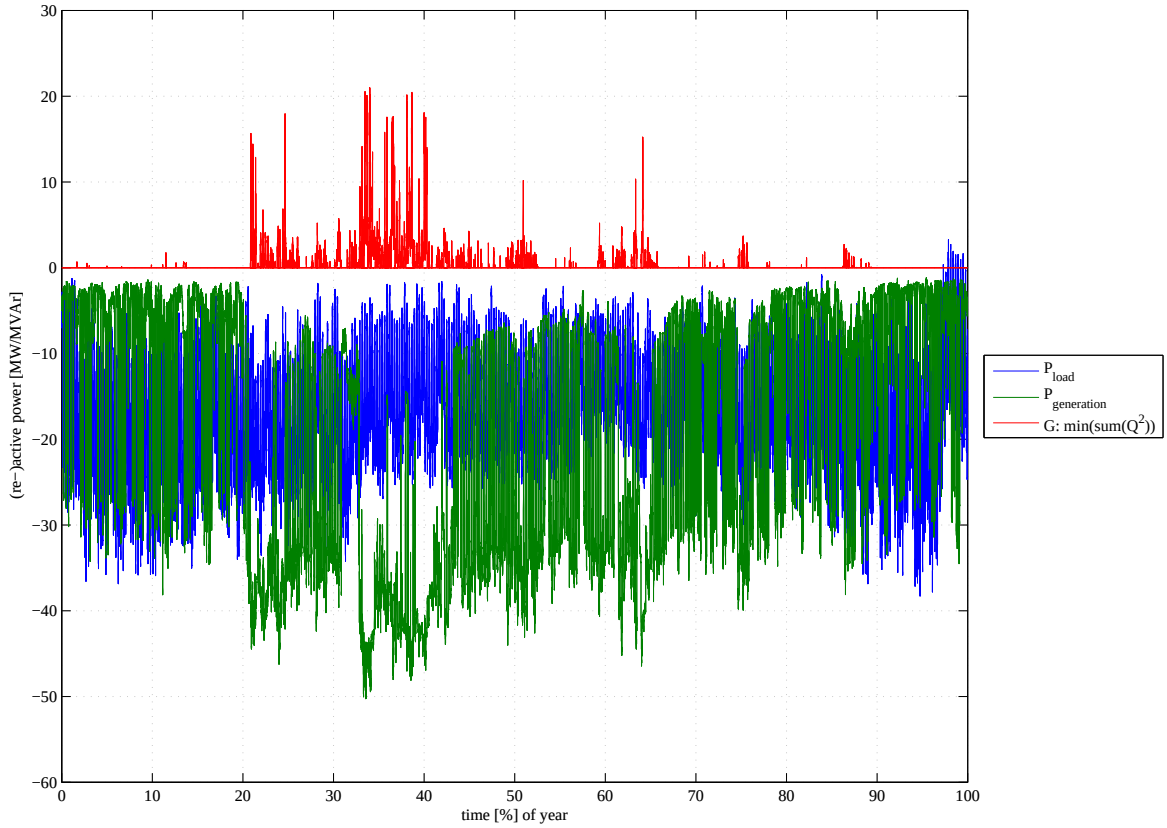

Figure 6.39: SS 'Nenzing' growth scenario - time series of loads active power demand ($-P_{load}$) and DGs' active power feed-in ($P_{generaion}$) in [MW] and minimal reactive power demand on DGs to keep voltages within voltage limits (calculated in *mode G*) in [MVAr] (see fig. 6.10 and fig. 6.29 for detailed description):
Load's active power demand is identical to the basic scenario (fig. 6.29), but generation increased for about 16MW nominal power. The high penetration of DGs in the growth scenarios causes a high active power excess during snow melting because generated power far exceeds the load's demand.
Reactive power contribution is mainly necessary in spring, but it is necessary consistently during in summer and autumn.

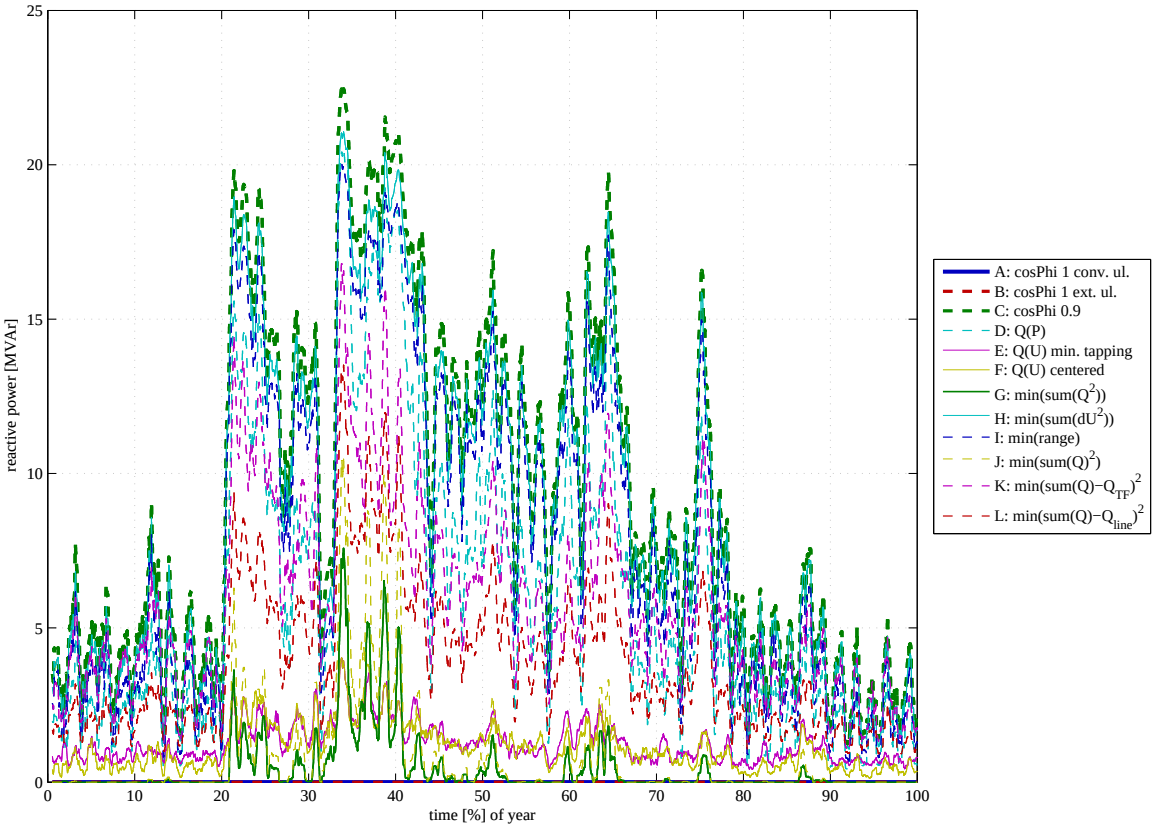

Figure 6.40: SS 'Nenzing' growth scenario - time series of absolute sum of DGs' reactive power [MVAr] that is requested by the control mode (see fig. 6.11 for detailed description):
Compared to the basic scenario (fig. 6.30), the maximum of requested reactive power increased from nearly 16MVAr to nearly 23MVAr (*mode C*).
The Q(U) control *modes E* and *F* use comparably little amount of reactive power during the whole year.

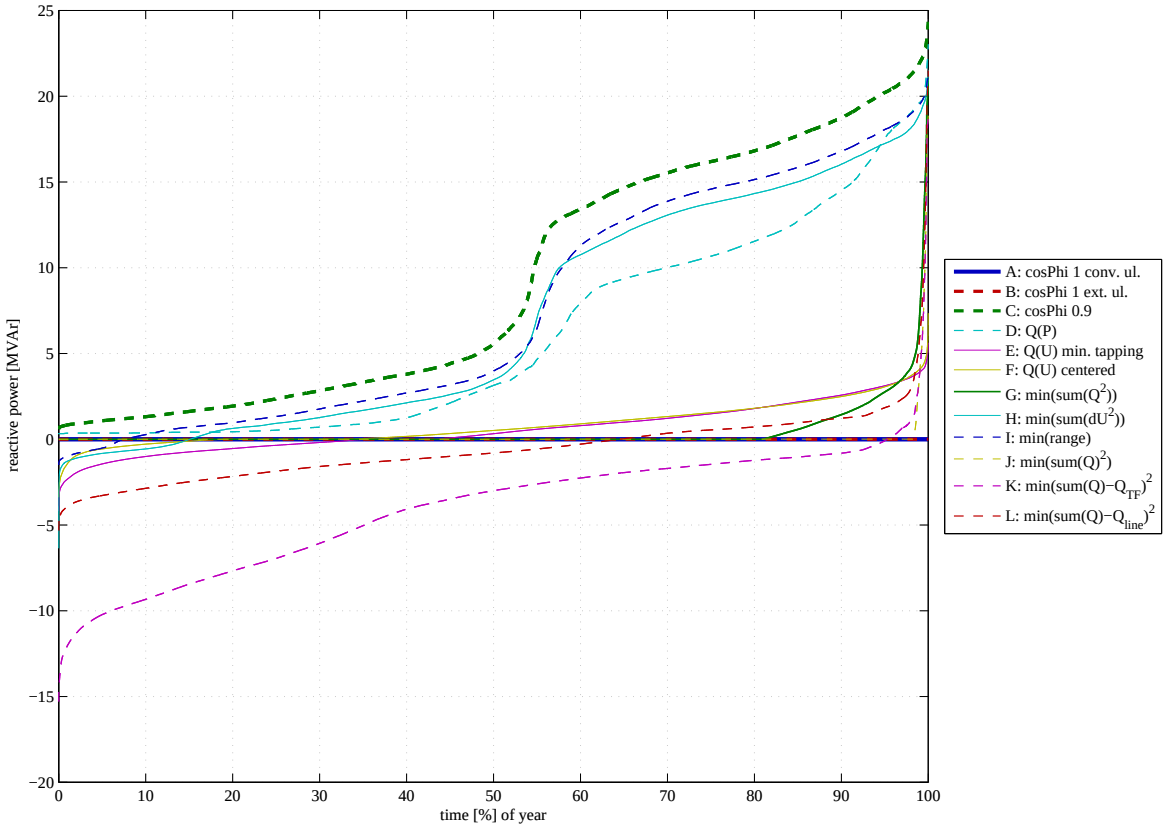

Figure 6.41: SS 'Nenzing' growth scenario - duration curve of sum of DGs' reactive power [MVAr] (see fig. 6.12 for detailed description):
Mode J was able to minimise requested reactive power to zero during 99% of the year.
In the basic scenario (fig. 6.31) the Q(U) control modes use more reactive power (up to 10MVAr) than in the growth scenario, which is reasoned in the reduced valid voltage band in basic scenario.
The sum of requested reactive power is higher in *mode I* than in *mode H*, which leads to higher grid losses as described in fig. 6.34.

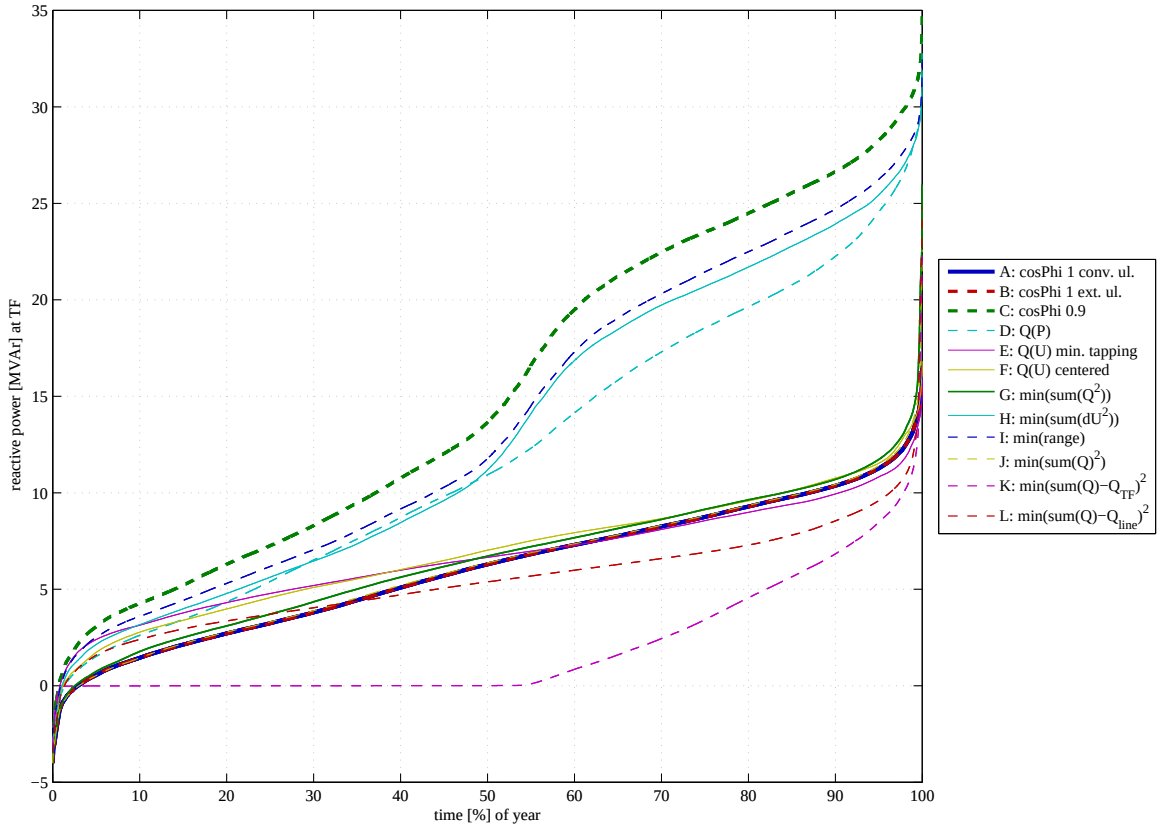

Figure 6.42: SS 'Nenzing' growth scenario - duration curve of reactive power flow over the transformer [MVAr] (see fig. 6.13 for detailed description):
The duration curves of this figure look very similar to the duration curves of the basic scenario in fig. 6.32. The only significant difference is that *mode K* was able to reduce the transformers reactive power flow to zero for about 54% of the year. Nevertheless losses increased by slightly more than 2% when operating *mode K*.

Chapter 7

Conclusion and Outlook

7.1 Summary

Integrating a high share of distributed generation (DG) into existing MV grids can cause unacceptable voltage rise at the DGs' feed-in-point. Grid reinforcement is considered as a very expensive solution that makes integration of renewables uneconomic. Utilising the existing medium voltage (MV) transformer's automatic voltage controller (AVC) and the capability of DGs to contribute reactive power offers an economical solution to integrate a high share of renewables. AVCs utilised with line drop compensation and DGs capable of running local reactive power control modes (constant $cos\varphi$, Q(U), Q(P)) are state of the art. These technologies have the advantage that they are independent from communication infrastructure, but with the disadvantage that existing infrastructure is not optimal utilised. Coordinated voltage control concepts are able to handle a maximum of DG integration, but they rely on a communication infrastructure which is able to provide real time measurements from the grid. Investing in communication infrastructure for coordinated voltage control brings the advantage that grid states become available which were estimated based on models in the past. On the other hand, grid operation based on coordinated control concepts increase complexity, because communication blackout scenarios and communication security issues have to be considered.

Framework Model and Basic Assumptions In this work different distributed and coordinated voltage control concepts were investigated, and their influence on grid losses, number of tap-changes, grid voltages and power flow was analysed. The assumptions that were made for these analyses are summarised here:

- Distribution grids are operated radially with a single connection point to the HV grid and no rings in topology
- Rural distribution grids are mostly built up of overhead lines that have a line's series inductance in the order of the line's series resistance
- At the TF a local AVC controls the OLTC's tap position based on a given voltage set value
- DGs are synchronous generators driven by a relatively constant primary energy source (water, biomass, ...)
- All synchronous generators are oversized and able to contribute reactive power in the order of half of their nominal active power
- The transport of grid measurement data over the communication infrastructure can be achieved within a few seconds, and a high update rate of measurement data (below 10s for every measurement) is available

- For distributed and coordinated voltage control the knowledge of a few voltages from selected grid nodes (CNs) is sufficient to safely operate all grid voltages within the given voltage limits (that contain safety margins)
- Coordinated voltage control concepts are based on the contribution matrix (CM) approach which linearises the CNs' voltage sensitivity on DGs' active- and reactive power changes
- Since the CM values depend on the network switching state, topology information has to be provided as well as different CMs for relevant topology changes

Investigated Control Concepts Based on these assumptions, a coordinated voltage control concept was described and implemented, which splits the task of voltage control into two separate control units that can work independently from each other. The level controller calculates the voltage set value for the TF's AVC and operates the voltages of the grid with one of the strategies 'upper-limit', 'centered', 'lower-limit' or 'minimum-tapping'. The range controller calculates the reactive power set values for the DGs to limit CNs' voltage range, which helps the level controller to keep all CN voltages within the valid voltage band. This is done by solving a non-linear optimisation problem under linear constraints. The constraints are calculated with the help of the CM, and the objective function of the problem can be chosen to follow arbitrarily strategies - in this work the following strategies are proposed:

- Use as little reactive power as possible (*mode G*)
- Minimise the sum of requested reactive power to minimise the impact of reactive power voltage control to the HV grid (*mode J*)
- Minimise the reactive power flow over the TF (*mode K*)
- Minimise the reactive power flow over selected grid lines (*mode L*)
- Minimise the voltage range (*mode I*)
- Minimise the voltage deviation from nominal voltage at every CN (*mode H*)

Simulation Details The impact of these control strategies on the grid is analysed based on simulations performed for two Austrian distribution grids. Simulation details are summarised here:

- Simulations were performed for one year based on 15min-average load and generation profiles
- Generation profiles and some load profiles base upon measured values, the rest of the load profiles base upon generated data
- Simulations were executed in a three minute time step with linear interpolated profile data
- HV grid voltage was set constant for simulations
- Communication delay was not simulated, so all measurement information was immediately available for the controller and all control results were set immediately
- Grids were simulated in the normal switching state without topology changes
- Power flow in the HV grid and within the generators was not simulated, so grid losses are only calculated for grid lines and transformers

Simulation Results The following listing summarises the simulation results for both grids in the basic and the growth scenarios:

- Operating the MV in distributed voltage control without utilising DGs' reactive power control (*mode A* and *B*) leads to voltage violations in SS 'Lungau' basic scenario, which get severe in SS 'Lungau' growth scenario. SS 'Nenzing' does not need reactive power control in basic scenario, but in the realistic growth scenario voltage violations will occur if reactive power control is not applied.
- The extension of the level control functionality for times with high ranges (*mode B*) improves the amount of time the conventional level control mode (*mode A*) can keep grid voltages within the given voltage limits for about 1-2% during the year in all four simulated scenarios (the effectiveness of this extension depends on the relation between the nominal tap-change height to the AVC's deadband as well as on the variation of the HV grid voltage).
- Operating all DGs in the grid in local control with $cos\varphi = 0.9$ (*mode C*) significantly increases grid losses by 8 to 25%, but in all four simulated scenarios grid voltages were successfully held within the valid voltage band.
- An operation of all DGs in local Q(P) control (*mode D*) halves the increase of grid losses of $cos\varphi = 0.9$ to 4-13%, but this control mode leaded to off-limit conditions in SS 'Lungau' growth scenario in 6% of the year.
- Having a local Q(U) control mode implemented at all DGs in the grid (*mode E* and *F*) increases grid losses only 1-9% and the number of tap-changes can be decreased significantly, but voltage limits in SS 'Lungau' get violated up to 10% of the year.
- All coordinated voltage control modes (*mode G* to *L*) were able to fully avoid voltage violations, because the first primary objective was the limitation of high voltage ranges. During times where reactive power was not constrained due to range limitations, different voltage control strategies were performed:
- The minimisation of the DGs' reactive power that is necessary to solve voltage range violations (*mode G*) increases grid losses by 10% for SS 'Lungau' growth scenario and 1% in maximum for all other scenarios while the number of necessary tap-changes slightly increases in the order of 10% (in SS 'Nenzing' growth scenario tap-changes decreased by 7% compared to the uncontrolled growth scenario).
- If it is required to compensate the reactive power requested by the controller by utilising DGs that are actually not required for voltage range control (*mode J*), losses and number of tap-changes are very similar to the values arising by simply minimising the requested reactive power (*mode G*).
- Optimising all grid voltages (*mode H*) or only minimising the voltage range (*mode I*) generates higher grid losses up to 20%, because a lot of reactive power is needed to achieve the objective. Operating one of these modes (*H* or *I*), tap-changes are significantly reduced in SS 'Lungau' while they are significantly increased in SS 'Nenzing'.
- In all four scenarios minimising the reactive power flow over the transformer (*mode K*) is not optimal because grid losses are 1 to 5% above the losses of the control mode that uses as little reactive power as possible (*mode G*). Again, tap-changes are reduced in SS 'Lungau' while they are increased in SS 'Nenzing'.
- The control mode that minimises the reactive power flow over selected grid lines (*mode L*) is able to reduce losses compared to the control mode that uses as little reactive power as possible (*mode G*), and in the basic scenarios losses were about 1% below the reference mode that operates DGs at $cos\varphi = 1$ (*mode A*). Furthermore the number of tap-changes could be decreased significantly compared to the distributed control mode.

- The integration of nearly 8MW generation in SS 'Lungau' increases annual grid losses by 75% from 1570MWh to 2752MWh in reference *mode A*, which is caused due to adverse locations of the new DGs (all additional DGs are connected to a feeder where generation share is already high). The additional integration of nearly 16MW generation in SS 'Nenzing' increased annual grid losses by 29% from 2562MWh to 3316MWh in reference *mode A*.
- The analysis of the simulation results showed that the CM approach (that linearises the impact of DGs' (re-)active power changes to the CNs' voltage) achieves good results in both scenarios of SS 'Lungau' and basic scenario of SS 'Nenzing'. But there are some indications that in the growth scenario of SS 'Nenzing' the total amount of 23MW controllable reactive power leads to inaccuracies in the control behaviour.

7.2 Conclusion

Voltage control concepts in rural medium voltage (MW) grids based on actual grid measurement data offer possibilities to enable a high share of distributed generation (DG) while voltage quality can be maintained. While local and distributed voltage control concepts offer robust and simple ways to increase the amount of DG in MV grids, existing infrastructure can only be optimally utilised with coordinated voltage control concepts. These concepts increase grid operation complexity, because communication infrastructure has to be retrofitted and communication blackout and security issues have to be considered additionally to conventional power system planning aspects. Whether coordinated voltage control concepts can be competitive with classical grid reinforcement depends on many different parameters, e.g. age of grid lines and the scheduled time grid lines will be renewed, the amount of projected DG connection in future, operational expenses of communication and controller infrastructure and last but not least the applicability and effectiveness of coordinated control concepts.

Usefulness of coordinated voltage control can be increased if the appliance of a coordinated control concept makes a reduction of grid operation costs possible by reducing grid losses and the amount of necessary tap-changes. Of course the additional integration of DG brings revenues for the distribution system operator (DSO), but in some cases grid losses or the usage of the transfomer's on-load-tap-changer (TF's OLTC) can increase significantly. In this work several distributed and coordinated voltage control concepts were simulated and the results were analysed and compared. Local voltage control concepts generally produce higher grid losses than coordinated concepts, because the knowledge of the state of the grid enables the specific utilisation of available resources. Simple coordinated voltage control strategies like minimising TF's reactive power flow (*mode K*) or minimising the sum of the reactive power requested by the controller (*mode J*) were not able to reduce grid losses. A (regrettably insignificant) reduction in grid losses and a significant decrease in the number of tap-changes was achieved by minimising the reactive power flow over selected grid lines (*mode L*), but the decision at which grid line the reactive power measurements are placed was not optimised. Therefore no statement can be made about the maximal amount of grid losses that can be saved by operating such a 'line optimised' coordinated voltage control strategy.

In the scope of this work grid losses were evaluated only for the MV grid lines and the MV grid TF, so grid losses in the high voltage (HV) network and the increase of losses in generators contributing reactive power were not considered. Therefore statements about loss increase or reduction have to be carefully interpreted. From the DSO's point of view the statements of this work concerning grid losses might be relevant, but the global optimum of grid loss reduction can only be found if grids are simulated in a wider scope. The savings that are relevant for the DSO (that were achieved by minimising grid line reactive power flow) are below 1% of total grid losses - in total numbers in the order of 20MWh annual.

Savings in necessary tap-changes are more significant, because in some simulation modes up to 90% of tap-changes could be avoided, but it has to be considered that simulations were performed with constant HV grid voltage. Nevertheless the DG control strategy can significantly influence the number of necessary tap-changes, especially when the share of DGs is high. Since OLTCs have to be maintained

cost-intensively after around 50.000 tap-changes, the OLTC maintenance intervals can be considerably extended.

The conclusion of this work is that coordinated voltage control concepts offer various possibilities to keep grid line losses and the number of tap-changes low in contrast to distributed or local voltage control concepts which can partially significantly increase grid losses and the number of tap-changes. The more information about the actual state of the grid is available, the more the grid losses can be optimised. Simulation results show that the coordinated control strategies proposed and simulated in this work were able to achieve their control objective while producing stable and continuous set values. This demonstrates that coordinated voltage control concepts are able to perform much more than only voltage control. To which extent coordinated voltage control concepts are reasonable and applicable for the individual DS depends on several parameters and influencing factors making general predictions about the amount of additionally connectable DGs and the influence to system operation costs difficult. In any case DS have to be simulated based on detailed network models to analyse the individual characteristics of the grid.

7.3 Outlook

Further investigations in the selection of the optimal number and placement of grid line measurements should be done to give a concrete answer to the question: To which extend grid losses can be decreased when applying a coordinated voltage control concept that optimises reactive power flow over selected grid lines? In this context it makes sense to replace the PQ-constant model of the generators with a detailed generator model to increase the scope of loss optimisation. On the other hand it makes sense to replace the constant voltage slack at the TF's HV side – at least by parts of the HV grid that contains adjacent elements to rate the loss reduction of a control concept that reduces the TF's reactive power flow.

Furthermore, the Q(U) local voltage control mode can be considered as a promising local control strategy that does not increase grid losses significantly and has a very positive impact on the number of necessary tap-changes. The simulations showed that in times where the operation of the Q(U) control concept caused voltage violations, the lowest grid voltages were below the voltage lower limit. The level controller did not realise that up-tapping would be possible, because if DG busbar voltage rises, local Q(U) control starts reactive power consumption to avoid overvoltage. An improvement of the level controller (which works as a distributed voltage controller with all DGs operating Q(U) control) in a way that such lower limits violations can be avoided would lead to a very flexible and simple alternative to coordinated voltage control concepts. Operating DGs in local voltage control modes has the advantage that they can be operated independently from grid topology and from communication system, which leads to a robust system that can react fast on grid state changes. Therefore it could be promising to improve the Q(U) control mode to offer a simple alternative to centralised operated coordinated voltage control concepts with a similar capability of voltage control.

For the general discussion of loss reduction provided by distributed or coordinated voltage control concepts it is necessary to replace the PQ-constant models of loads by more accurate models concerning voltage dependency of loads, so that the question can be answered which level controller strategy (upper-limit, lower-limit, centered, minimum-tapping) reduces grid losses best. With this information the reduction of grid losses can be opposed to the number of necessary tap-changes. This would answer the question if it is better to align the voltage range somewhere within the valid voltage band (optimising grid losses at the cost of tap-changes), or if it is better to perform tap-changes only to avoid voltage violations (optimising tap-changes at the cost of grid losses).

When it comes to a market launch of coordinated voltage control concepts that utilise the DGs' capability of contributing reactive power, the consecutive next step will be to implement an appropriate active power curtailment control concept. This can significantly increase the share of DGs in MV grids while the income of DGs' holder is not reduced significantly, because active power curtailment will only be necessary very seldom.

Bibliography

[1] Nicholas Jenkins. *Embedded generation*, volume 31 of *IET Power and Energy Series*. IET - The Institution of Engineering and Technology, 2000.

[2] W. Pruggler, F. Kupzog, B. Bletterie, and B. Helfried. Active grid integration of distributed generation utilizing existing infrastructure more efficiently - an austrian case study. In *Electricity Market, 2008. EEM 2008. 5th International Conference on European*, May 2008.

[3] A. Bonhomme, D. Cortinas, F. Boulanger, and J.-L. Fraisse. A new voltage control system to facilitate the connection of dispersed generation to distribution networks. In *Electricity Distribution, 2001. Part 1: Contributions. CIRED. 16th International Conference and Exhibition on (IEE Conf. Publ No. 482)*, volume April, 2001.

[4] M. Stifter, B. Bletterie, H. Brunner, D. Burnier, H. Sawsan, F. Andren, R. Schwalbe, A. Abart, R. Nenning, F. Herb, and R. Pointner. DG DemoNet validation: Voltage control from simulation to field test. In *Innovative Smart Grid Technologies (ISGT Europe), 2011 2nd IEEE PES International Conference and Exhibition on*, December 2011.

[5] Adolf J. Schwab. *Elektroenergiesysteme*. Springer, 2012.

[6] Prabha Kundur. *Power System Stability and Control*. McGraw-Hill Companies,Incorporated, January 1994.

[7] Dietrich Oeding and Bernd Rüdiger Oswald. *Elektrische Kraftwerke und Netze*. Springer Berlin Heidelberg, 2011.

[8] Fabio Saccomanno. *Electric power systems: analysis and control*. IEEE Press, February 2003.

[9] S.K. Joshi K.S. Pandya. A survey of optimal power flow methods. *Journal of Theoretical and Applied Information Technology*, 4(5):450–458, May 2008.

[10] A. Eberle GmbH & Co. KG. Spannungsregler REG-D™ Bedienungsanleitung. `http://www.a-eberle.de/download-center/spannungsregler/dokumente/bedienungsanleitungen/ba-reg-d-d-pdf/download.html`, December 2009.

[11] Milan Calovic. Modeling and analysis of under-load tap-changing transformer control systems. *IEEE Transactions on Power Apparatus and Systems*, PAS-103(7):1909–1915, July 1984.

[12] Joon-Ho Choi and Jae-Chul Kim. Advanced voltage regulation method at the power distribution systems interconnected with dispersed storage and generation systems. *IEEE Transactions on Power Delivery*, 15(2):691–696, April 2000.

[13] E-Control. Technische und organisatorische Regeln für Betreiber und Benutzer von Netzen - Parallelbetrieb von Erzeugungsanlagen mit Verteilernetzen - D4. `e-control.at/de/marktteilnehmer/strom/marktregeln/tor`, December 2008.

[14] BDEW - Bundesverband der Energie- und Wasserwirtschaft. BDEW-Richtlinie "Erzeugungsanlagen am Mittelspannungsnetz". www.vde.com/de/fnn/dokumente/documents/rl_ea-am-ms-netz_bdew2008-06.pdf, June 2008.

[15] Tampere University of Technology. Specification of coordinated voltage control application, ADINE Project Deliverable 17. http://www.hermia.fi/@Bin/746408/ADINE_D17_31122008_rev1.1.pdf, December 2008.

[16] R. Caldon, R. Turri, V. Prandoni, and S. Spelta. Control issues in mv distribution systems with large-scale integration of distributed generation. In *Proc. Bulk Power System Dynamics and Control - VI*, Cortina d'Ampezzo, Italy, August 2004.

[17] Roberto Caldon, Silvano Spelta, Valter Prandoni, and Roberto Turri. Co-ordinated voltage regulation in distribution networks with embedded generation. In *18th International Conference and Exhibition on Electricity Distribution, 2005. CIRED 2005*, June 2005.

[18] S. Conti and A. M. Greco. Innovative voltage regulation method for distribution networks with distributed generation. In *Proc. 9th. Int. Conf. on Electricity Distribution*, Vienna, Austria, May 2007.

[19] T. Pfajfar, I. Papic, B. Bletterie, and H. Brunner. Improving power quality with coordinated voltage control in networks with dispersed generation. In *9th International Conference on Electrical Power Quality and Utilisation, 2007. EPQU 2007*, October 2007.

[20] S.N. Liew and G. Strbac. Maximising penetration of wind generation in existing distribution networks. *Generation, Transmission and Distribution, IEE Proceedings-*, 149(3):256 –262, May 2002.

[21] Ahmed Shafiu, Vincent Thornley, Nick Jenkins, Goran Strbac, and Adam Maloyd. Control of active networks. In *18th International Conference and Exhibition on Electricity Distribution, 2005. CIRED 2005*, June 2005.

[22] T. Senjyu, Y. Miyazato, A. Yona, N. Urasaki, and T. Funabashi. Optimal distribution voltage control and coordination with distributed generation. *IEEE Transactions on Power Delivery*, 23(2):1236 –1242, April 2008.

[23] N. Nimpitiwan and C. Chaiyabut. Centralized control of system Voltage/Reactive power using genetic algorithm. In *International Conference on Intelligent Systems Applications to Power Systems, 2007. ISAP 2007*, November 2007.

[24] T. Niknam, A.M. Ranjbar, and A.R. Shirani. Impact of distributed generation on volt/Var control in distribution networks. In *Power Tech Conference Proceedings, 2003 IEEE Bologna*, volume 3, page 7 pp. Vol.3, June 2003.

[25] D. Villacci, G. Bontempi, and A. Vaccaro. An adaptive local learning-based methodology for voltage regulation in distribution networks with dispersed generation. *IEEE Transactions on Power Systems*, 21(3):1131 –1140, August 2006.

[26] Joon-Ho Choi and Jae-Chul Kim. Advanced voltage regulation method of power distribution systems interconnected with dispersed storage and generation systems. *IEEE Transactions on Power Delivery*, 16(2):329–334, April 2001.

[27] H. Hatta, S. Uemura, and H. Kobayashi. Demonstrative study of control system for distribution system with distributed generation. In *Power Systems Conference and Exposition, 2009. PSCE '09. IEEE/PES*, March 2009.

[28] F.A. Viawan and D. Karlsson. Coordinated voltage and reactive power control in the presence of distributed generation. In *Power and Energy Society General Meeting - Conversion and Delivery of Electrical Energy in the 21st Century, 2008 IEEE*, July 2008.

[29] L.F. Ochoa, A. Keane, and G.P. Harrison. Minimizing the reactive support for distributed generation: Enhanced passive operation and smart distribution networks. *IEEE Transactions on Power Systems*, 26(4):2134–2142, November 2011.

[30] A. Keane, L.F. Ochoa, E. Vittal, C.J. Dent, and G.P. Harrison. Enhanced utilization of voltage control resources with distributed generation. *IEEE Transactions on Power Systems*, 26(1):252–260, February 2011.

[31] Stephen P. Boyd and Lieven Vandenberghe. *Convex optimization*. Cambridge University Press, 2004.

[32] Adi Ben-Israel and Thomas N. E. Greville. *Generalized Inverses: Theory and Applications*. Springer, June 2003.

[33] EN 50160. Voltage characteristics of electricity supplied by public electricity networks. (OVE: `www.as-search.at`), 2010.

[34] Wolfgang Prüggler. *Business models for active distribution grid management - development and economic impact analysis*. Dissertation, Vienna University of Techology, March 2010.